NTNU – Trondheim
Norwegian University of
Science and Technology

Fundamentals of natural gas processing - hydrocarbon dew point meter modelling

Kathrine Michalsen

Helene Sire Nævdal

NTNU
Norwegian University
of Science and Technology

Department of Energy
and Process Engineering

EPT-M-2014-71

MASTER THESIS

for

Students Kathrine Michalsen and Helene Sire Nævdal

Spring 2014

Fundamentals of natural gas processing - hydrocarbon dew point meter modelling
Modellering av hydrokarbonduggpunktsmåler

Background and objective

Norway is the second largest supplier of gas to the European market. Gas production is also often tied to oil production. Furthermore, natural gas has low impact to the environment compared to other hydrocarbon resources. Statoil's Subsea Separation Technologies department addresses new ideas and problems related with separators in natural gas production systems.

Scrubbers are gas liquid separators used for removing liquid from a gas phase in every gas production plant. The performance of these units have an impact on the specifications for the gas, e.g. low separation performance is giving poor gas quality increasing the risk for hydrate formation. Dew point testers can be used both for controlling gas specification and assessing separator performance.

It is the purpose of this work is to achieve a deeper understanding on the flow pattern, heat and mass transfer and thermodynamic phenomena in a dew point test unit. This will decrease the uncertainties associated with the dew point test method. A better understanding on these phenomena will lead to future improvements. This insight will be obtained by modelling of the dew point unit. The ambition is to model the coupled effects of fluid flow, heat and mass transfer and thermodynamics for a simple dew point unit.

Comsol tool will be preferred as it is well suited for simple fluid simulations and heat transfer in fluids and solids. It also presents the possibility of coupling with a NeqSim as a thermodynamic package. Support on the simulation tools (NeqSim and Comsol) will be given by Statoil Research Centre. Student can also contact local Comsol support in Trondheim if needed.

The scope of the work is to model a standard Bureau Mines Dew Point Tester. The model comprises:

The following tasks are to be considered:
1. Review literature on dew point testers
2. Calculate heat transport considering cooling medium, natural gas temperature, walls, and heat transport in the solid matrix. Implement thermodynamics based on NeqSim.
3. Study the need for modelling mass transfer and compositional gradients
4. Assess errors from real dew point and dew point determined by the technique.
5. Suggest future modelling improvements

Within 14 days of receiving the written text on the master thesis, the candidate shall submit a research plan for his project to the department.

When the thesis is evaluated, emphasis is put on processing of the results, and that they are presented in tabular and/or graphic form in a clear manner, and that they are analyzed carefully.

The thesis should be formulated as a research report with summary both in English and Norwegian, conclusion, literature references, table of contents etc. During the preparation of the text, the candidate should make an effort to produce a well-structured and easily readable report. In order to ease the evaluation of the thesis, it is important that the cross-references are correct. In the making of the report, strong emphasis should be placed on both a thorough discussion of the results and an orderly presentation.

The candidate is requested to initiate and keep close contact with his/her academic supervisor(s) throughout the working period. The candidate must follow the rules and regulations of NTNU as well as passive directions given by the Department of Energy and Process Engineering.
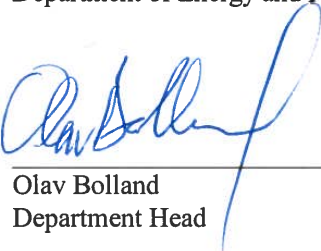
Risk assessment of the candidate's work shall be carried out according to the department's procedures. The risk assessment must be documented and included as part of the final report. Events related to the candidate's work adversely affecting the health, safety or security, must be documented and included as part of the final report. If the documentation on risk assessment represents a large number of pages, the full version is to be submitted electronically to the supervisor and an excerpt is included in the report.

Pursuant to "Regulations concerning the supplementary provisions to the technology study program/Master of Science" at NTNU §20, the Department reserves the permission to utilize all the results and data for teaching and research purposes as well as in future publications.

The final report is to be submitted digitally in DAIM. An executive summary of the thesis including title, student's name, supervisor's name, year, department name, and NTNU's logo and name, shall be submitted to the department as a separate pdf file. Based on an agreement with the supervisor, the final report and other material and documents may be given to the supervisor in digital format.

☐ Work to be done in lab (Water power lab, Fluids engineering lab, Thermal engineering lab)
☐ Field work

Department of Energy and Process Engineering, 14. January 2014

Olav Bolland
Department Head

Even Solbraa
Academic Supervisor

Research Advisor: Pablo Matias Dupuy (Statoil)

Preface

This thesis was written as a collaboration project between the Department of Energy and Process Engineering at the Norwegian University of Science and Technology (NTNU) and the Statoil Research and Development Centre at Rotvoll, Trondheim.
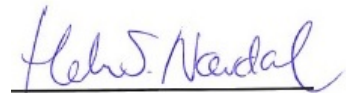
The thesis counts for 30 ECTS credits and is written in the 10th semester of the 5-year Mechanical Engineering degree at NTNU.

The thesis was proposed and supervised by Adjunct Professor Even Solbraa and Pablo Matias Dupuy at the Statoil Research and Development Centre.

Trondheim, 10.06.2014

Kathrine Michalsen   Helene Sire Nævdal

Acknowledgment

We would like to thank our supervisors Even Solbraa and Pablo Matias Dupuy for their insight, guidance and support during the work on this thesis.

We would also like to thank Efstathios Skouras-Iliopoulos, Eirini Skylogianni and Oddbjørn Rekaa Nilssen at Statoil Rotvoll for their knowledge and input.

<div align="right">

K.M, H.S.N

</div>

Abstract

When natural gas is taken from the reservoir it needs to be refined by removing liquid and other impurities in order to prevent hydrate formation in the pipelines and to keep the gas within sales specifications. Scrubbers, vertical separators, are used to remove the liquid and the efficiency of the scrubber has a great impact on the quality of the gas. To control the gas specifications and the efficiency of the scrubber, a dew point meter can be used. This tool will ideally provide the real dew point curve of the gas, which can prevent poor gas quality and damage on the equipment.

In this thesis, a manual chilled mirror dew point unit developed by the Bureau of Mines is thermally analysed using the simulation software COMSOL Multiphysics. The dew point meter is operated by circulating a gas sample past a cold mirror to identify the temperature where condensate forms. The reason for this study is to get a deeper understanding on the thermal and thermodynamic phenomena in the unit and to study the need for modeling mass transfer and compositional gradients. The objective of this thesis is to improve fundamental understanding of the unit, decrease the uncertainties associated with the dew point test method and to provide results that can lead to future improvements.

A simplified 3D model of the dew point unit has been used for the simulations. The parameters used are based on the experimental test rig at Statoil in Trondheim. Six different cases have been studied, where one or more parameters have been changed for each case to see how the changes affect the temperature in the unit. The simulations confirm that the coldest temperature is in the center of the mirror, and this is where the dew first will appear. The actual temperature at the center of the mirror surface has been found to be between 0.15 to 1.62 K higher than the temperature measured by the thermometer, depending on pressure, difference in chamber temperature and the velocity of the gas. Effects of compositional gradients due to thermal diffusion have shown to be present. New dew point temperatures have been calculated based on the new composition at the cold mirror. These results show dew point temperatures 0.31-1.11 K above the dew points calculated for the initial composition.

Sammendrag

Når naturgass hentes fra reservoaret må væske og andre urenheter fjernes for å unngå hydrat-dannelse i rørene og for å holde gassen innenfor salgsspesifikasjonene. Væskeutskillere ("scrub-bere") blir brukt for å fjerne væske fra gassen og effekten av disse har dermed stor påvirkning på gasskvaliteten. For å kontrollere gasspesifikasjonen og virkningsgraden til separatorene kan man benytte en duggpunktsmåler. Dette instrumentet gir optimalt den ideelle duggpunktskur-ven til den aktuelle gassen og kan dermed bidra til å motvirke dårlig gasskvalitet og ødeleggelse av utstyr.

I denne oppgaven har en manuell duggpunktsmåler fra the Bureau of Mines blitt termisk analy-sert ved å bruke simuleringsprogrammet COMSOL Multiphysics. I duggpunktsmåleren sirkuleres en gassprøve forbi et kaldt speil for å identifisere temperaturen hvor kondensat dannes. Bak-grunnen for dette studiet er å få en dypere forståelse av de termiske og termodynamiske fenomenene i enheten og å undersøke behovet for modellering av massetransport. Målet med denne opp-gaven er å øke grunnleggende forståelse av måleren, minimere usikkerhetene rundt duggpunk-tsmåleren og metoden og å finne resultater som kan føre til fremtidige forbedringer.

En forenklet 3D modell av duggpunktsenheten har blitt brukt i simuleringene og parameterene er hentet fra Statoils testrigg i Trondheim. Seks forskjellige tilfeller har blitt undersøkt, hvor en eller flere parametere har blitt endret i hvert tilfelle for å se hvordan dette påvirker tempera-turen i enheten. Simuleringene bekrefter at den kaldeste temperaturen er i midten av speilet, og at det dermed er her dugg først vil dannes. Noen feil har blitt avdekket mellom temperaturen målt av termometeret og den faktiske temperaturen i midten av speilet. Speiltemperaturen er mellom 0.15 og 1.62 K høyere enn hva som måles av termometeret, avhengig av trykk, temper-tureforskjell i kammeret og gasshastighet. Effekten av komposisjonsgradienter grunnet termisk diffusjon har blitt påvist og utifra dette har nye duggpunktstemperaturer blitt beregnet for den nye gassammensetningen på speilet. Disse duggpunktstemperaturene er 0.31-1.11 K høyere enn hva som er beregnet for den opprinnelige sammensetningen.

Contents

List of Figures

List of Tables

Nomenclature

Latin letters

M Molar weight [kg/mol]

I Unity tensor [-]

S Strain rate tensor [$1/s$]

$\boldsymbol{F}$ Body force vector [N/m^3]

T Temperature [K]

Q Heat source/sink [W/m^3]

C Turbulence modelling constant [-]

N Combined mass flux vector [$kg/m^2 \cdot s$]

Pr Prandtl number [-]

Re Reynolds number [-]

C_p Heat capacity [$J/kg \cdot K$]

P_k Production of turbulent kinetic energy [W/kg]

D_{AB} Binary diffusion coefficient [m^2/s]

D^T Thermal diffusion coefficient [$m^2/s \cdot K$]

$\tilde{D}_{ik}$ Multicomponent Fick diffusivity [m^2/s]

q Heat flux [W/m^2]

u Velocity [m/s]

$\boldsymbol{u}$ Velocity field [m/s]

p Pressure [bar]

k Thermal conductivity [$W/m \cdot K$]

l Dimensionless distance [-]

d Diameter [m]

m Mass [kg]

n Number of species [-]

c Concentration [mol/m^3]

g External force [m/s^2]

x Mole fraction [-]

v Atomic diffusion volume [-]

j_i Mass flux relative to the mass average velocity [$kg/m^2 \cdot s$]

$\boldsymbol{j}_i$ Mass flux vector [$kg/m^2 \cdot s$]

$\boldsymbol{d}_k$ Diffusional driving force [$1/m$]

s_T Soret coefficient [$1/K$]

k_T Thermal diffusion ratio [-]

u_τ Friction velocity [m/s]

Greek letters

Π Pressure tensor [-]

κ Turbulent kinetic energy [J/kg]

ρ Density [kg/m^3]

ε Dissipation rate of turbulent energy [$J/kg \cdot s$]

λ Thermal conductivity [$W/m \cdot K$]

σ Turbulent diffusion coefficient [-]

δ Unit tensor [-]

μ Dynamic viscosity [$Pa \cdot s$]

τ Laminar, viscous stress tensor [-]

ω Mass fraction [-]

μ_T Turbulent dynamic viscosity [$Pa \cdot s$]

λ_T Turbulent thermal conductivity [$W/m \cdot K$]

δ_w Distance from the wall to the computional domain [-]

δ_w^+ Wall lift-off in viscous units [-]

Subscripts

m Mean

w Wall

f Fluid

∞ Infinity

h Hydraulic

i Species i

Superscripts

+ Dimensionless

~ Favre average

¯ Reynolds average

Abbreviations

CFD Computational fluid dynamics

NCS Norwegian continental shelf

HCDP Hydrocarbon dew point

GC Gas chromatography

EoS Equation of state

MEMS Microelectromechanical system

PR The Peng-Robinson equation

SRK The Soave-Reidlich-Kwong equation

SNG Synthetic natural gas

RNG Real natural gas

UMR The Universal Mixing Rule

API The American Petroleum Institute

ASTM American Society for Testing and Materials

RANS Reynolds-averaged Navier-Stokes

HPC High-performance computing

Chapter 1

Introduction

Norway is the second largest supplier of natural gas, and covers around 20 per cent of the gas consumption in Europe (2012), mainly to Germany, the UK, Belgium and France. To make this possible, The Norwegian Continental Shelf (NCS) consists of a network of pipelines, with the total length of over 7995 km [10]. To prevent poor gas quality and the risk of hydrate formation in these pipelines, scrubbers are used to remove water content in the gas-phase. To control the performance of these scrubbers and the specifications of the gas, a dew point tester can be used.

The purpose of this study is to achieve a deeper understanding on the heat transfer and thermodynamic phenomena in a dew point test unit. This will decrease the uncertainties associated with the dew point test method and can lead to future improvements.

The scope of this work is to do a thermal and thermodynamic analysis of the dew point unit, especially looking at the solid material, the gas flowing in front of the mirror and also to look at the impact of mass transfer and compositional gradients in the unit. By doing this, discrepancies of the operating dew point meter can be revealed and measurement methods can be improved.

The cases that will be studied in this thesis are first a simulation with parameters used in the test rig today, then several cases where only one or two parameters are changed while the others

are kept constant. First, the inlet gas temperature, then the cooling temperature and last the velocity. This is to clearly see the effect of changing these parameters. The next case will include a study of mass transfer modelling and compositional gradients. The last case will assess errors from real dew point and dew point determined by the technique. The COMSOL Multiphysics computational tool will be used for simulations, and will make it possible to link several physical effects in one model and simulation.

The report consists of six main parts followed by the discussion, conclusion and recommendations for future work. Chapter 2 includes theory about natural gas processing and hydrocarbon dew point. Chapter 3 is a literature review on different techniques for measuring hydrocarbon dew point and also on different measuring methods used for the manual chilled mirror apparatus. Chapter 4 presents the hydrocarbon dew point unit used for this project as well as theory on condensation and thermal diffusion. Chapter 5 is theory about the COMSOL software and the interfaces used, which includes theory about heat and mass transfer and CFD. Chapter 6 presents the model used in this project and validation of the model and Chapter 7 includes all the simulations and results. Settings and parameters used in COMSOL can be found in the Appendix.

Chapter 2

Background

2.1 Introduction to natural gas processing

The production of natural gas is often tied up with oil production and has low impact on the environment compared to other hydrocarbon resources. The gas is found as a mixture containing mostly methane (70-90%), but also other heavier hydrocarbons such as ethane, propane and butane (together around 0-20%). The raw gas from the wellhead also contains non-hydrocarbons such as water and carbon dioxide. Since natural gas is combustible and gives off a great deal of energy while burned, the gas has a great area of utilization from domestic heating to energy demanding industries [11]. This chapter will give an introduction to natural gas processing, followed by a section on hydrocarbon dew point.

2.1.1 Processing objectives

When natural gas is extracted from the reservoir it needs to be refined by removing water, sand and other impurities in the gas. This operation is done to achieve the required quality of the gas and safe transportation in the pipes. If this is not performed properly it can cause hydrate formation in the pipes and break down in rotating equipment. Hydrates form when water con-

denses from the natural gas during transportation and a free water phase develops. Hydrates have an ice-like structure and can be a challenge in natural gas processing for instance by plugging the pipeline. It is therefore desirable to avoid the free water phase from forming. This can be achieved by keeping the temperature above the hydrate region or by injecting chemicals to reduce the hydrate region [12, 13]. Natural gas consists of unwanted compounds such as CO_2, N_2, Hg, He and H_2S in addition to hydrocarbons. In order for the gas to meet the sales specifications, the contaminates have to be removed from the gas. These impurities can also cause corrosion of pipeline and equipment and they present a major safety risk [1, 14]. Other reasons for removing water and other impurities are to protect burners and catalysts, for air pollution control and to prevent foaming in gas dryers and CO_2 removal units. [15]

2.1.2   Process modules

A typical natural gas processing plant, as can be seen in Figure 2.1, mainly consists of a gas oil separator, condensate separator, dehydrator, acid gas removal unit, nitrogen extractor or nitrogen rejection unit and a fractionator. [1]

There are many different processing system depending on the nature of the gas, the location of the plant etc. But the most common procedure is explained here. First, a slug catcher is in place to separate gas, hydrocarbon condensate and inlet water. The gas stream is then sent to the inlet separators where the gas, liquid hydrocarbons, liquid water and/or solids are separated. The liquids are sent to a three-phase separator where hydrocarbon condensate and water/methanol or water/glycol are outputs. Overhead gas from the three-phase separator is re-compressed, if needed, and used as fuel gas. The hydrocarbon condensate is stabilized to be safe for transportation, by removing the light fractions by distillation, before it is shipped. The next step in the process is acid gas treating, where the acid gases like CO_2 and H_2S are removed. If the pressure is not at the desired level, the next step is inlet compression. After that, dew point control and natural gas liquid recovery is executed. Water dew point control is required to meet the specifications and control hydrate formation. Preventing hydrate formation can either be done by lowering the hydrate formation temperature with chemical inhibition or remove the water by
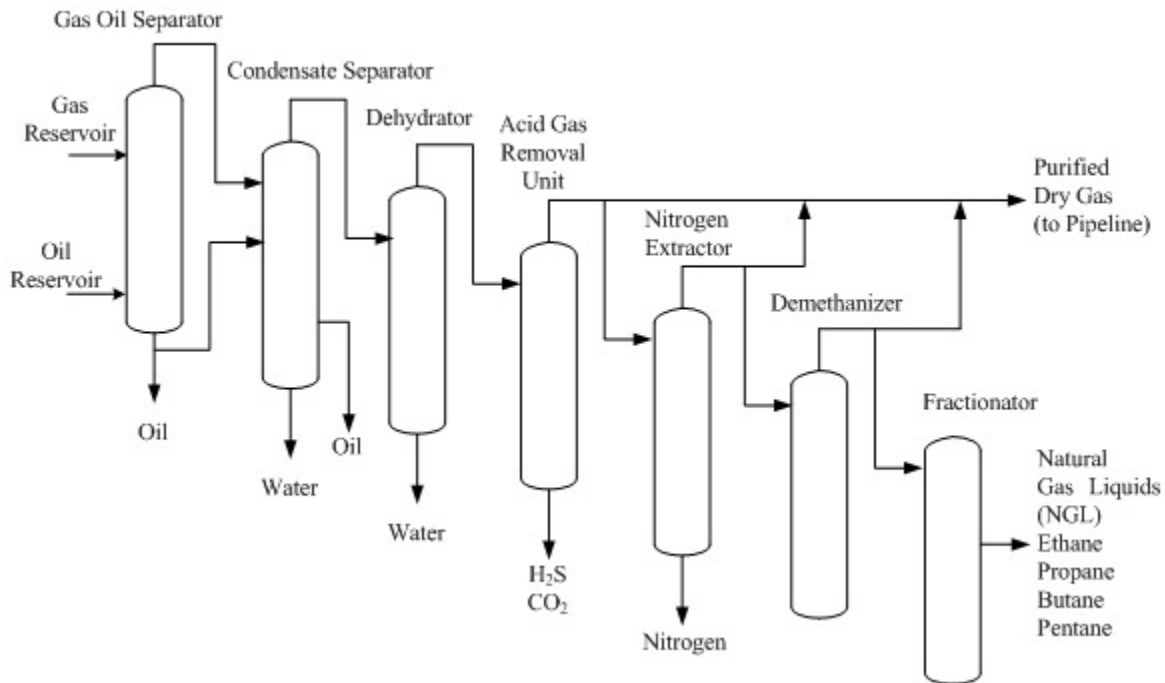
Figure 2.1: An example of a natural gas processing plant [1]

dehydration. Hydrocarbon dew point control or hydrocarbon liquid recovery is done by cooling the gas and condensing out the liquids. If the gas is produced at a pressure lower than sales pipeline pressure it is compressed to sales gas pressure. The gas is transported at high pressure in order to have a smaller pipe diameter. [14]

2.1.3   Scrubbers

There are two types of vessels for separating liquid and gas. Horizontal vessels called separators, mainly used for large amounts of liquid, and vertical vessels called scrubbers, mainly used for fluids with large gas to liquid ratio. An example of a scrubber is shown in Figure 2.2. A scrubber consists of different separation equipment installed in series inside the vertical shell. These can be divided into three main sections: the inlet section, the coalescing section and the demisting section. [15]

The inlet pipe is placed horizontally and the inlet arrangements are fitted in order to minimize gas and liquid momentum, to separate the bulk liquid, to prevent liquid shattering and to dis-

A - OIL AND GAS INLET
B - SEPARATOR SPACE
      OR CHAMBER
C - SWIRL CYLINDER
D - SWIRL CYLINDER
      INLET PORTS
E - DEFLECTION CODE
F - DRAIN TUBES
G - SCRUBBER DOME
      OR MIST EXTRACTOR
H - DRY-GAS CHAMBER
I - GAS OUTLET
J - OIL OUTLET
K - DRAIN CONNECTION
L - DRAIN-VALVE FLOAT
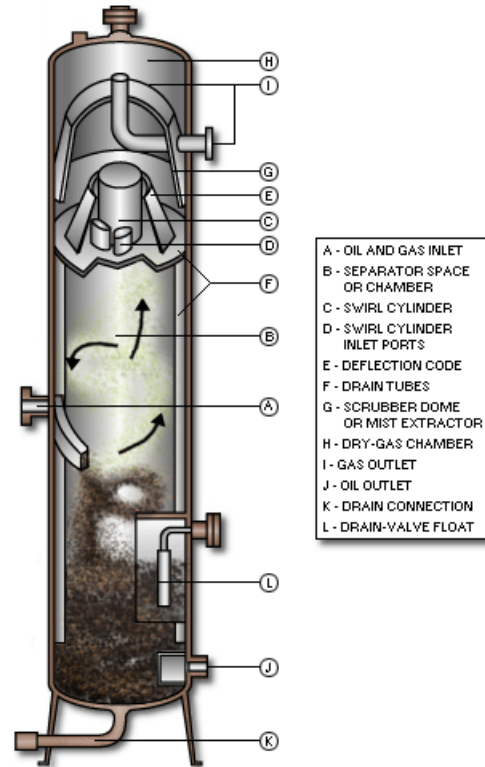
Figure 2.2: Example of a scrubber [2]

tribute the gas, liquid and sometimes the break-down foam over the scrubber cross section. The
inlet type that is most commonly used today consists of a series of vanes that gradually release
the gas and liquid into the scrubber. The inlet vane distributes the gas and liquid evenly with
a low pressure drop. In cases where foaming occurs, cylinder-on-cone cyclones are normally
used, since the centrifugal force can break down the foam. Figure 2.3 shows a scrubber with a
vane inlet at the bottom, a mist-mat in the middle and a cyclone deck at the top. Above the inlet,
the coalescing section is placed. The most common type of equipment used is either one or sev-
eral mesh pads or vane packs. The mesh pad consists of layers of knitted wires, while the vane
pack consists of plates formed in a zig-zag pattern. In cases where the vessel is quite large com-
pared to the gas volumes, the mesh or vane pack acts as a final demisting stage. However, when
the volumetric gas rate increases, the liquid can not be drained efficiently by gravity against the
gas flow. If that is the case the second stage agglomerates the liquid droplets so they can be sep-
arated more easily further downstream. The final demisting stage most often consists of a bank
of cyclones or a vane pack with channels that are shielded from the gas to allow unhindered

drainage of the liquid. The liquid is drained through drainpipes down to the liquid sump at the bottom of the scrubber. Axial flow cyclones are most commonly used because of lower pressure drop and more compact design compared to reverse flow type cyclones. [15]
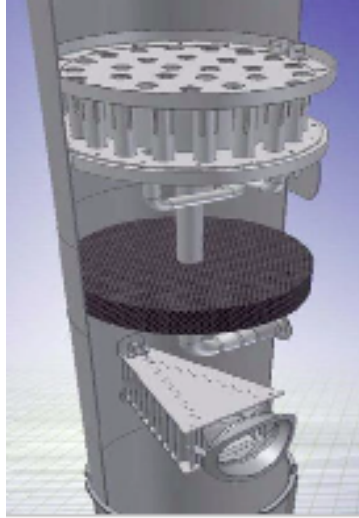
Figure 2.3: Scrubber with vane inlet, mist-mat and cyclone deck. [3]

Mal-functioning scrubbers and scrubber efficiency are often bottlenecks in the production and can lead to large costs. Scrubbers are used in every gas production plant and their performance has an effect on the specifications of the gas. Poor efficiency leaves more liquid in the gas when transported which can be crucial to the equipment. To test the efficiency of the scrubber a dew point tester can be used. This unit defines the real dew point in the gas and can therefore also be used to control specifications of the natural gas. Hydrocarbon dew point is further explained in the next section.

2.2   Hydrocarbon dew point

The hydrocarbon dew point in natural gas is where the first formation of liquid condensate occurs in the gas for a given temperature at a specified pressure. The dew point is dependent on pressure, temperature and the composition of the gas [16]. A specification made on hydrocarbon dew point is related to the cricondenbar, and the main aim is to manipulate the phase envelope to increase the area of single-phase flow. A phase envelope for the gas shows how

the temperature and pressure affects the gas sample. The cricondentherm point is the maximum temperature and the cricondenbar point is the maximum pressure on the hydrocarbon dew point curve [16], i.e. the highest temperature and pressure where the fluid can be in the two-phase region. Figure 2.4 shows a typical phase envelope for natural gas and water. The dew point of natural gas is also highly dependent of the heavy hydrocarbons present in the gas. Reducing or increasing the amount of heavy hydrocarbons in the gas mixture is the only way of changing the hydrocarbon dew point. [13]
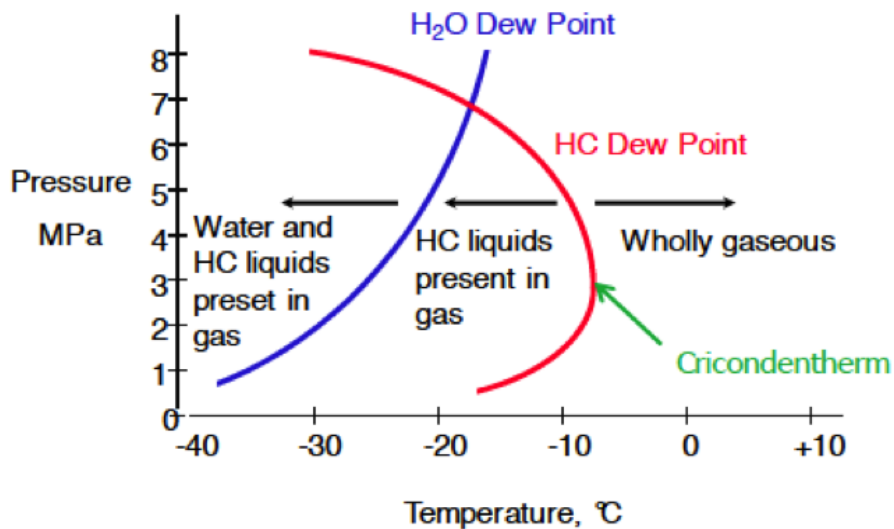
Figure 2.4: Typical phase envelope for northern european natural gas by Michell Instruments

Because of the complexity of the hydrocarbon condensation process, the hydrocarbon dew point has several definitions. The ISO 14532:2005 standard define it as "The temperature above which no detectable condensation of hydrocarbons occurs at a specified pressure". Since this is not possible to measure in practice when the dew needs to be visible to the operator, the API Manual of Petroleum Measurement Standards Chapter 14.1 define it as: "The temperature at which hydrocarbon condensates first begin to form a visible deposit of droplets on a surface, when the gas is cooled at a constant pressure." [17]

Chapter 3

Literature Review

3.1 Hydrocarbon dew point measurement methods

Methods for measuring the hydrocarbon dew point can be classified as direct or indirect methods. The direct methods are performed by observation of the forming dew while the indirect methods use data from measurements to calculate when the dew will occur [4]. Further in this section will the most widely used methods for measuring the hydrocarbon dew point be presented.

Equation of state method using gas cromotography analysis

Gas chromatography (GC) analysis is used as a basis in all indirect methods. A GC analysis determines the composition of the gas and then applies the equations of state (EoSs) to this data to determine the HCDP. [4] Of the validated equations of state, are the Peng-Robinson (PR) and the Soave-Redlich-Kwong (SRK) the most widely used. The equations exists in several variations, but the basis is the use of critical temperature and pressure and an acentric factor to describe the pure components. Mixtures need additional interaction parameters. [18]

Several standards have been published to assure that the results are acceptable, and further research on this method is currently being done in order to improve the method. GC analysis is also used to determine the heating value of the gas, which is normally used as a sales basis. [19]

Manual visual dew point method

The manual visual dew point method is a direct method developed by the Bureau of Mines in the 1930's. It is the most widely used technique for HCDP measurement and requires the simplest hardware and a low capital investment. The sample gas is sent trough a chamber with a mirror in one end, while a coolant is conducted across the back of the mirror. The cooling has to be done slowly, so that the operator can detect the first sign of condensation. This can be seen when very small droplets of hydrocarbon condensate appears on the mirror. When this happens, the operator notes the temperature. This method is very subjective, as the operator has to determine the dew point visually. It is also a labour intensive method resulting in high personnel costs. [19]

This is the method that will be studied in this thesis and it will be presented more thoroughly in Chapter 4.

Automatic optical condensation method

Another direct method that has been in commercial use for over 20 years is the automatic optical condensation HCDP analyser. An optical detector is chilled until a thin layer of condensate is formed on the surface. The instrument measures a light dispersed from a light-emitting diode to detect the forming layer of dew on a concave mirror [4]. The instrument is designed to find the same dew point temperatures as the manual chilled mirror instrument, and can detect a condensate film of 70 mg/m^3 depending on the sensitivity settings of the instrument [20]. The automatic chilled mirror has better than ±0.6 K accuracy according to independent laboratory tests and can provide the user with up to six measurement cycles per hour. This method requires a high initial investment, but has low operating costs and does not require specialized training

for the operator. [19]

Dew point testing in other areas

On a side note it is interesting to see that dew point meters can also be used in entirely different fields. In medical science a similar method to the manual visual dew point method is used to look at humidity changes inside the human nose and throat and also for the evaluation of water loss rate of human skin. The difference with this type of application is that the dew point meter has to be able to read fast humidity changes. R.S. Jachowicz et al. (2009) [21] have researched a dew point meter for this application. A response time of less than 0.5 seconds is required and they have found that a silicon MEMS sensor can control the condensation/evaporation process with a time constant of less than a second.

3.2 Review of accuracy of existing methods

D. L. George et al. (2005) [22] was part of a research program to identify the most accurate analytical method for predicting HCDP. The test apparatus used was built around a Bureau of Mines chilled mirror dew point tester. They found that the agreement between the measured dew points and the dew points calculated using the EoS's depended both on the composition of the gas and on the pressure used for the experiments. The Peng-Robinson (PR) EoS was in good agreement with the actual dew points, whereas the SRK EoS gave dew points that were 5.6-8.3 K higher than what was measured experimentally. For richer gas mixtures, both PR and SRK predicted dew points of up to 14 K lower than the actual dew points.

V. Louli et al. (2012) [23] performed dew point measurements on six synthetic natural gas (SNG) mixtures using a chilled mirror apparatus with temperatures between 253 and 285 K and pressures between 3 and 105 bar. The UMR-PRU model (the PR EoS coupled with UNIFAC through the Universal Mixing Rule (UMR)) was used and the results were compared to the PR EoS. 17 SNG's and 2 real natural gases (RNG) taken from literature were also used for comparison. The

results showed that the UMR-PRU model was sufficiently accurate for predicting dew point, especially at pressures near the cricondenbar point.

Several studies on comparison of the existing methods have been carried out. When comparing the direct methods, manual and automatic chilled mirror instrument, the National Physical Laboratory [20] reports a discrepancy of 1-5 K, while A. S. Brown et al. (2008) [4] experienced an error of 3.2-7.7 K. In both cases the dew point temperature measured with the manual instrument is grater than the automatic instrument. Brown suggests possible errors for the discrepancy as difference in the cooling rate and sensitivity of the instruments.

3.3   Review of literature on heavy hydrocarbons

Several articles have been published explaining the difficulties of accurately measuring dew point of natural gas when heavy hydrocarbons are present.

B. H. Rusten et al. (2008) [24] observed a high deviation between the measured and calculated dew points for gas mixtures with hydrocarbons up to C5. All the EoS models used gave a dew point temperature lower than what was observed in the laboratory. Tests were also done on light synthetic gases with an added C7 component, namely n-heptane, cyclohexane and benzene. For these gases the models predicted too high cricondentherm and too low cricondenbar. They found the same tendency for real natural gases. For pressures up to 20 bar, all the models gave results in accordance with experimental data, but for higher pressures they predict a too low HCDP. They also found that for higher pressures, the SRK model gives a more accurate result than the PR model.

To illustrate the dew points dependence of the heavier hydrocarbons present in the gas A. S. Brown et al. (2008) [4] tested the dew points of a series of mixtures containing from 1 nmol/mol to 10 μmol/mol of single straight-chain hydrocarbons in methane at 27 bar. As indicated in Figure 3.1 the hydrocarbon dew points increase significantly in the mixtures containing six or more carbon atoms, and the gas with the highest carbon number has measured the highest

hydrocarbon dew point temperature.
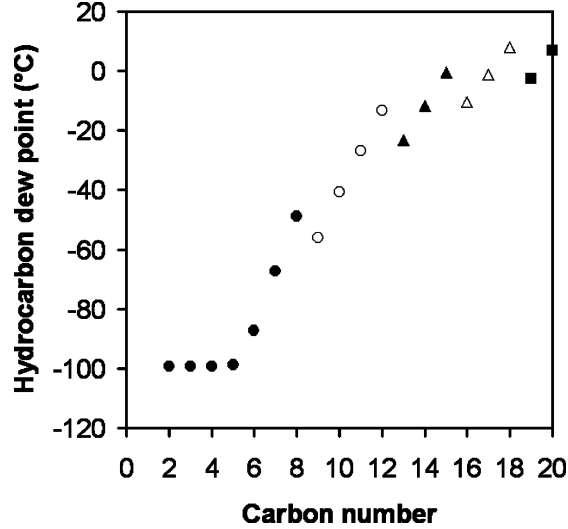
Figure 3.1: The hydrocarbon dew points dependents of carbon numbers in the gas mixture [4]

3.4 Measuring methods of the manual chilled mirror instrument

D. L. George (2006) [7] presented causes of measurement errors in gas quality analysis. He emphasised the importance of being aware that the results are subjective to the operator and in order to minimize this error the pressure and temperature instruments should be calibrated regularly. George describes how Warner (2001) [25] performed a study where the dew point temperature found by different operators on the same gas stream was ±1.3 K. He also presents a study done by Cowper (2002) [26] discussing how long it takes from a thin film forms on the mirror until it is visible to the operator. The study showed that the temperature at which condensation first occurs could be underestimated by 0.2-1.5 K. The ASTM standard (1995) [6] specifies a cooling rate on the mirror of 0.6 K per minute for good accuracy. George stated that a higher cooling rate may cause the measured dew point to be too high because of a time lag between the mirror temperature and the instrument measuring the dew point temperature. He recommended following the manufacturer's specifications using a flow rate of 5 scfh (0.1314 m^3/h) or lower if the valves cause large pressure drops and create a potential of condensation before the gas reaches the mirror surface. In order to minimize the errors that can be caused by the operator, automated chilled mirror devices were introduced to the market in 2006. At the time George

published his article there was no research available comparing the manual and the automated dew point meters.

E. Skylogianni (2013) [8] found, using a GERG rig, that a difference in the chamber temperature of 10 K (from 308.15 to 318.15 K) had an effect on the measured dew point of about 0.9 K. Measurements at 318.15 K were more accurate than at 308.15 K due to adsorption phenomena being more pronounced at lower temperatures. This effect was higher in gases containing higher hydrocarbons. The volume effect was also investigated for 300 cc and 600 cc, but the deviations found were within the experimental uncertainty. So the volume effect was found to be non-existent. The effect of sample conditioning on the accuracy of the measurements was also tested, but this was also found to not affect the results.

Chapter 4

The Hydrocarbon Dew Point Unit

4.1 The manual chilled mirror instrument

This chapter will present the dew point unit used in this thesis and give an introduction to condensation and thermal diffusion theory. The hydrocarbon dew point unit used for this thesis is a standard Bureau of Mines dew point meter by Chandler Engineering shown in Figure 4.1. The unit is used both in the lab to test gas samples and in the field. A detailed drawing of the hydrocarbon dew point meter can be found in Appendix A.5.

Figure 4.1: The Bureau of Mines dew point meter [5]
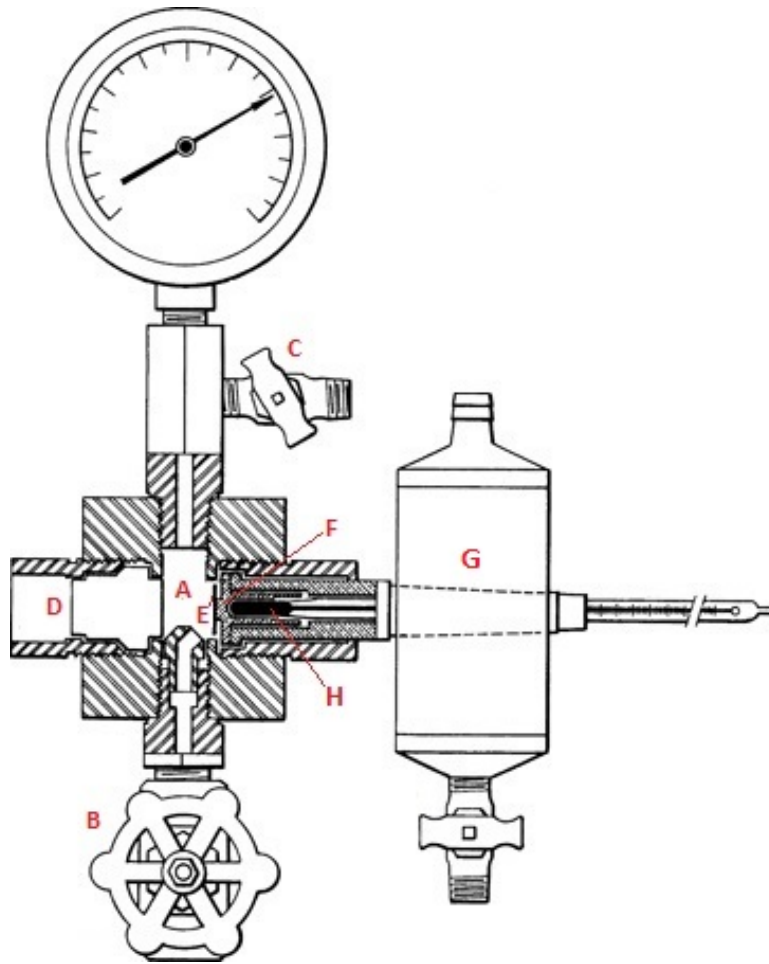
Figure 4.2: Explanatory drawing of the Bureau of mines dew point meter [6]

The unit, that can be seen in Figure 4.2, comprises of a pressure-tight chamber, A, containing the gas sample and valves, B and C, that control the flow of the gas through the chamber. At one end of the chamber there is a small window, D, where the operator can observe the inside of the chamber and the mirror at the opposite end. The mirror, E, is made of polished stainless steel. The backside of the mirror is connected to the copper rod by a tap, F, placed at the center of the mirror. The copper thermowell is attached to a chiller, G, which controls the expansion of the refrigerant and thereby controlling the temperature of the mirror. A hand-regulated valve allows the operator to increase the flow rate of the liquid CO_2, which lowers the temperature of the mirror. A thermometer, H, is placed inside the thermowell so the operator can read the temperature of the mirror. This instrument gives the dew point with an accuracy of ±0.1 K if used correctly. [27]
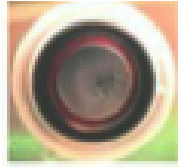
Figure 4.3: Example of dew formation on the mirror, from hydrocarbon condensation [7]

Measurements are done by circulating a gas sample through the chamber, while slowly cooling the mirror with CO_2 at a rate of 2 K/min. In the field, the gas only flows once through the chamber, whereas in the lab the gas sample is circulated back and forth in a closed loop. The temperature when the first dew is detected is noted and the gas is slowly heated, to move the gas out of the two-phase region, until the dew disappears. This temperature is also noted and the average of the two temperatures is reported as the dew point. The temperature difference of the two measurements can not be more than 1 K [24]. When the gas condenses on the cold mirror, the dew appears as a light grey to grey shadow at the centre of the mirror, as can be seen in Figure 4.3. The dew point measurements for the gas sample are based on isobaric cooling, which means that the pressure is kept constant while the measurements are performed. In order to obtain the phase envelope for the gas the experiment is carried out at different pressures. An example can be seen in Figure 4.4. [8]
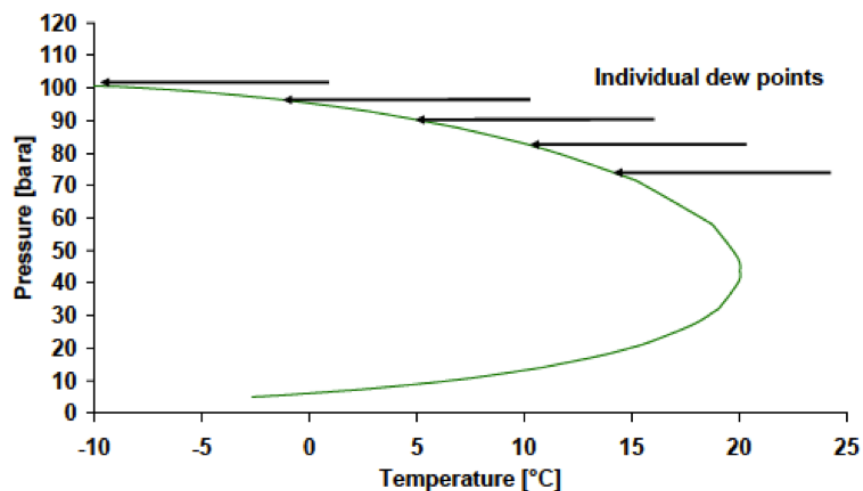
Figure 4.4: Example of isobaric cooling [8]

4.2   Condensation

As explained in 2.2, when the gas reaches its critical temperature the medium will experience a phase change. If the temperature is below the cricondentherm, liquefied natural gas condensate will form. In the manual hydrocarbon dew point unit this physical phenomenon will occur at the boundary layer connecting the cold mirror and the warmer gas. At the surface of the colder mirror, the gas will optimally adapt to the same temperature as the surface. When this temperature moves below the mixture's cricondentherm at one specific pressure, small droplets of liquid will form on the mirror. This process is called nucleation.

Nucleation is a physical process where a change of state occurs in the material around a nucleus. This happens when an initially stable substance moves into an unstable phase as a controlling parameter, such as temperature or pressure, changes. Heterogeneous nucleation happens when there are nuclei present in the substance, and homogeneous nucleation happens when there are no such contaminants present in the material. In this case, the material has to create its own nuclei. This happens when the perturbation in the fluid is so small that the system moves into a metastable condition, rather than an unstable one. Since the system aims for a more stable state, heterogeneous fluctuations appear and droplets form. Homogeneous nucleation is less common than heterogeneous nucleation. In the dew point unit the mirror will work as a nucleation site where the nucleation can occur, and when the pressure and temperature allows it, droplets will form on the mirror surface. [28, 29]

Natural gas exists as a composition of a variation of different hydrocarbons. Heavier hydrocarbons have higher dew points than lighter hydrocarbons and because of this, natural gas composition with heavy hydrocarbons condense at a higher temperature. This becomes a problem when the condensation of heavy hydrocarbons contaminates the surface of the mirror making a bigger nucleation surface. This can contribute to discrepancies in the results. Another issue is that if the mirror is not properly cleaned, or contains scratches, it can work as an additional nucleation site which can also cause condensation to happen earlier at a higher temperature. [7]

Hydrocarbon condensate has low surface tension, and because of this is the film of dew difficult for the human eye to catch. In addition to this, the hydrocarbon condensate consists of a mixture of several components which makes it complicated to predict the behavior of the gas. [19]

Since the gas experiences a temperature difference in the unit, it is of interest to know more about the molecular diffusion in the gas mixture due to the warm gas meeting the colder mirror.

4.3 Thermal diffusion

The Soret effect, also known as thermal diffusion, explains how the components in a mixture separate and transport molecules that are driven by temperature gradients. The effect was first explained in detail by Charles Soret in 1879 when he experienced that the heavier components in a salt solution gathered at the coldest end of a tube. To understand the diffusion one of the chemical compounds in the mixture needs to be used as a reference in order to find the mass flux. This can be found by using Equation 4.1 which represent the mass flux in the x direction. The first term indicates Fick's law of diffusion where the diffusion is dependent on concentration. D is the isothermal diffusion coefficient. The second term includes the thermal diffusion coefficient that represent the diffusion due to the temperature gradients and ω_0 is the mass fraction of the reference component. [30]

$$J_x = -\rho D \frac{\partial c}{\partial x} - \rho D^T \omega_0 (1 - \omega_0) \frac{\partial T}{\partial x} \tag{4.1}$$

There are several methods for calculating the diffusion coefficients. The Maxwell-Stefan diffusivity is the most comprehensive model, and Fick´s diffusion is a simplification of this model. For multicomponent diffusion in gases with low density, the Maxwell-Stefan diffusion coefficient can be replaced by the binary diffusion coefficient, D_{AB}. The empirical Equation 4.2 derived by Fuller et al. [31] has been used to calculate this value. This coefficient indicates the

concentration dependent diffusion in a mixture.

$$D_{AB} = \frac{0.000143\,T^{1.75}}{p M_{AB}^{1/2}[(\sum v)_A^{1/3} + (\sum v)_B^{1/3}]^2} \tag{4.2}$$

T is temperature, p is pressure, M_A and M_B is the molar weight of component A and B and gives $M_{AB} = 2[(1/M_A) + (1/M_B)]^{-1}$. $\sum v$ is found for each of the components by summing the atomic diffusion volumes found in the table by Fuller et al. [31]

The Soret coefficient, s_T, gives the ratio between the thermal diffusion coefficient and the binary diffusion coefficient. When the system is in steady state, and the chemical potential is constant, an approximation to the Soret coefficient can be derived as given in Equation 4.3 presented in literature by Kjelstrup et al. [32]. The coefficient has the unit K^{-1}.

$$s_T \equiv -\left(\frac{\partial c_1/\partial x}{c_1 \partial T/\partial x}\right)_{J=0} \approx \frac{0.35(m_B - m_A)}{T(m_B + m_A)} \tag{4.3}$$

J is the molar flux and $m_{A,B}$ is the mass of the components. Which component is defined as A or B depends on which is the reference species. When s_T is estimated, the thermal diffusion coefficient, D_i^T can be found by using Equation 4.6 that is derived from Equation 4.4 and 4.5 for the thermal diffusion ratio, k_T. When k_T is positive the species moves towards the colder region, and when negative it moves to the warmer region [33]. D^T indicates the diffusion that is dependent on the temperature gradients in the system and has the property $\sum_i^n D_i^T = 0$. n is the number of species.

$$k_T = s_T x_A x_B T \tag{4.4}$$

$$k_T = \frac{D_A^T}{\rho D_{AB}} \frac{x_A x_B}{\omega_A \omega_B} \tag{4.5}$$

$$D_A^T = s_T T \rho D_{AB} \omega_A \omega_B \qquad (4.6)$$

The reference temperature used in the equations about diffusion in the unit, is the mean temperature between the cooling and the natural gas, denoted as 1 and 2 in Equation 4.7. The recommended calculation of the mean temperature, T_m is [33]

$$T_m = \frac{T_1 T_2}{T_2 - T_1} ln(\frac{T_2}{T_1}) \qquad (4.7)$$

The Soret effect is a well known irreversible thermodynamic phenomena. If the effect is considerable the composition of the gas will change on its path travelling from the inlet towards the mirror because of the temperature gradients present in the system.

Chapter 5

COMSOL Theory

5.1 Introduction

COMSOL Multiphysics is a simulation software that enables the user to combine several physical effects in the same model. It is also possible for the user to customize the software by adding other physical effects or formulas needed for their specific model [34]. The Heat Transfer module and the Chemical Reaction Engineering module have been used for this thesis. The Non-Isothermal Flow user interface was used to combine fluid flow and heat transfer and the Transport of Concentrated Species user interface was used to determine thermal diffusion. Theory about the interfaces and the equations used in the software will be described in this section, but calculations and basis for the choice of interfaces will be presented in Chapter 6 and 7. Most of the information given in this chapter is taken from the COMSOL user guides and other available information about the software. Some of the information presented may be insufficient because of limited information available from COMSOL.

5.2 The Non-Isothermal Flow user interface

The Non-Isothermal Flow interface is found under the fluid flow physics group in COMSOL. This interface is a predefined multiphysics coupling consisting of a single-phase flow interface. It uses the fully compressible formulation of the continuity equation and momentum equations, in combination with the Heat Transfer interface. [35]

5.2.1 CFD

Computational fluid dynamics (CFD) is a method to solve and analyse fluid flow problems with numerical methods and algorithms. A computer is used to calculate the flow of liquid and gases over surfaces defined by boundary conditions. Almost every CFD analysis is based on the Navier-Stokes equations, with a small range of simplifications depending on the desired results.

The Navier-Stokes equations

The Navier-Stokes equations can be derived from Newton's second law of motion. They consist of the three momentum equations in the x-,y- and z-direction. In addition, the mass conservation, or continuity, equation is used to get four equations to solve the four unknowns. The Navier-Stokes equations express the conditions of equilibrium between surface-, body- and inertia forces. The equations are very complex and different computer software is available in order to solve these equations more easily. Equation 5.1 and 5.2 show the continuity and momentum equation, respectively, as they are used in COMSOL for a fully compressible flow. [36, 37]

$$\frac{\partial \rho}{\partial t} + \nabla \cdot (\rho \boldsymbol{u}) = 0 \tag{5.1}$$

$$\rho \frac{\partial \boldsymbol{u}}{\partial t} + \rho \boldsymbol{u} \cdot \nabla \boldsymbol{u} = -\nabla p + \nabla \cdot \left(\mu \left(\nabla \boldsymbol{u} + (\nabla \boldsymbol{u})^T \right) - \frac{2}{3} \mu (\nabla \cdot \boldsymbol{u}) \boldsymbol{I} \right) + \boldsymbol{F} \tag{5.2}$$

ρ is the density, $\boldsymbol{u}$ is the velocity vector, p is the pressure [Pa], $\boldsymbol{I}$ is the unity tensor, μ is the dynamic viscosity, k is the thermal conductivity and $\boldsymbol{F}$ is the body force vector.

Flow patterns

In order to check if a flow is turbulent or laminar, the Reynolds number can be calculated. The Reynolds number is a dimensionless quantity that is used to predict the flow pattern. The flow is considered laminar if Re < 2300, transient when 2300 < Re < 4000 and turbulent when Re > 4000. The Reynolds number for a pipe or a duct is calculated by Equation 5.3. [38]

$$Re = \frac{\rho u d_h}{\mu} \tag{5.3}$$

d_h is the hydraulic diameter and u is the velocity.

Laminar flow is easier to predict than turbulent flow. For turbulent flow is the particle path completely irregular and it is very difficult to analyze mathematically, whereas for laminar flow the particles move in straight lines. CFD analysis of laminar flow is a lot more straight forward than for the complex turbulent flow. The Navier-Stokes equations are the only equations used for laminar flow in COMSOL.

Turbulent flow

Turbulence is a flow that is recognized as chaotic and highly unsteady as the flow is three-dimensional and contains a great number of vortexes. The turbulence diffusion contributes to the mixing of conserved properties [39]. Because of the complexity of the flow, several turbulence models have been made to make the computations possible and each model is adjusted to different flow cases. RANS, Reynolds-averaged Navier-Stokes, is a group of models where the small local oscillations are being treated in a time-averaged manner. As a consequence, additional unknowns are added to the system and approximations of the flow field at the walls are introduced [9]. This causes the solution given by the simulation of turbulent flow to be only an approximation of the reality. The RANS models available in COMSOL are the κ-ε, κ-ω, low Reynolds number κ-ε, SST and Spalart-Allmaras. The difference between these models is their use of wall functions, number of additional variables and what these variables represent. Wall functions ignore flow in the buffer zone, where the flow begins to transition into turbulent flow,

as can be seen in Figure 5.1, and analytically compute a non-zero velocity at the wall [9].
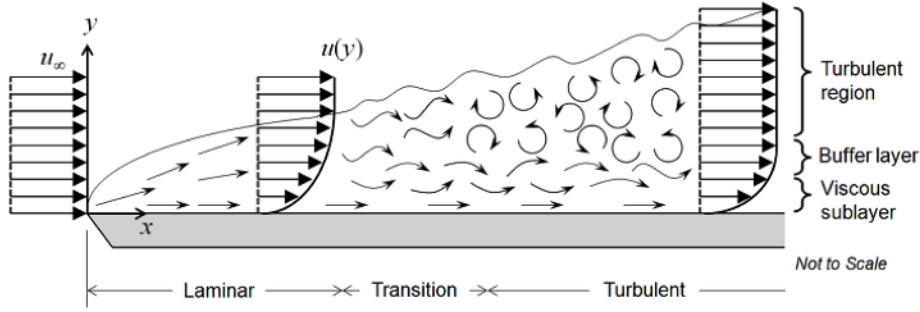
Figure 5.1: Turbulence modelling. Fluid flow over a flat plate [9]

The κ-ε turbulence model is a good compromise between convergence and requirement for computational memory. This model solves for the two variables: κ, the turbulent kinetic energy, and ε, the dissipation rate of turbulent energy. It uses wall functions, so the buffer region is not simulated. The transport equations used in COMSOL for κ and ε are presented in Equation 5.4 and 5.5 respectively.

$$\rho(u \cdot \nabla)\kappa = \nabla \cdot \left[\left(\mu + \frac{\mu_T}{\sigma_\kappa} \right) \nabla \kappa \right] + P_\kappa - \rho \varepsilon \tag{5.4}$$

$$\rho(u \cdot \nabla)\varepsilon = \nabla \cdot \left[\left(\mu + \frac{\mu_T}{\sigma_\varepsilon} \right) \nabla \varepsilon \right] + C_{\varepsilon 1} \frac{\varepsilon}{\kappa} P_\kappa - C_{\varepsilon 2} \rho \frac{\varepsilon^2}{\kappa} \tag{5.5}$$

σ_κ and σ_ε are the turbulent diffusion coefficients, μ_T is the turbulent viscosity, C_ε is a modelling constant and P_κ is the production of turbulent kinetic energy. For the low Reynolds number κ-ε turbulence model is the term $f_\varepsilon(\rho, \mu, \kappa, \varepsilon, l_w)$ multiplied with the last term in Equation 5.5. l_w is the dimensionless distance to the closest wall. [37]

The turbulent viscosity is presented in Equation 5.6.

$$\mu_T = \rho C_\mu \frac{k^2}{\varepsilon} \tag{5.6}$$

C_μ is a model constant.

The production of turbulent kinetic energy is expressed by Equation 5.7.

$$P_k = \mu_T\left(\nabla\boldsymbol{u} : \left(\nabla\boldsymbol{u} + (\nabla\boldsymbol{u})^T\right) - \frac{2}{3}(\nabla\cdot\boldsymbol{u})^2\right) - \frac{2}{3}\rho k\nabla\cdot\boldsymbol{u} \tag{5.7}$$

In the dew point tester the gas flowing past the mirror is non-isothermal and there is heat trans-fer on the solid-gas interface. Because of the wall functions, the κ-ε model is not as accurate close to the walls as the low Reynolds number κ-ε model. The low Reynolds number κ-ε model, hereafter named low-Re κ-ε, is an extension of the κ-ε model. It does not use wall functions but calculates the entire domain, assuming laminar flow close to the walls. This way the solution becomes much more accurate [9, 40].

The model constants used in COMSOL are determined by experimental data and are listed in Table 5.1 below.

Table 5.1: Turbulence model constants

Constant	Value,low-Re κ-ε	Value,κ-ε
$C_{\epsilon 1}$	1.5	1.44
$C_{\epsilon 2}$	1.9	1.92
C_μ	0.09	0.09
σ_κ	1.4	1.0
σ_ϵ	1.5	1.3
κ_v	0.41	-

5.2.2 Heat transfer

The heat equation for a fluid is solved in the Non-Isothermal Flow user interface by Equation 5.8. All the equations in this section are taken from the COMSOL CFD user guide [37].

$$\rho Cp\left(\frac{\partial T}{\partial t} + (\boldsymbol{u}\cdot\nabla)T\right) = -(\nabla\cdot\boldsymbol{q}) + \boldsymbol{\tau}:\boldsymbol{S} - \frac{T}{\rho}\frac{\partial\rho}{\partial T}\Big|_{\bar{p}}\left(\frac{\partial p}{\partial t} + (\boldsymbol{u}\cdot\nabla)p\right) + Q \tag{5.8}$$

Cp is the specific heat capacity at constant pressure [J/kg·K], $\boldsymbol{q}$ is the heat flux by conduction. For the stationary simulations the $\frac{\partial}{\partial t}$ terms disappear. The pressure work term $\frac{T}{\rho}\frac{\partial\rho}{\partial T}\Big|_{\bar{p}}\left(\frac{\partial p}{\partial t} + (\boldsymbol{u}\cdot\right.$

$\nabla)p\Big)$ and the viscous heating term $\boldsymbol{\tau} : \boldsymbol{S}$ are not included by default, but can be added as subnodes. They have not been used for the simulations in this thesis.

The heat transfer in solids node can be added to the model. This has been used for the heat transfer between the copper, the seal and the mirror. COMSOL uses Equation 5.9, based on energy conservation, as the mathematical model for heat transfer in solids.

$$\rho C_P \frac{\partial T}{\partial t} = -(\nabla \cdot \boldsymbol{q}) + Q \tag{5.9}$$

$\frac{\partial T}{\partial t}$ is the temperature variation over time and Q is the heat source or sink. When the model of the dew point unit is simulated as steady state the temperature does not vary over time and the first term disappears.

Heat transfer in turbulent flow

The temperature equation solved in the turbulent Non-Isothermal Flow interface is presented in Equation 5.10. It is derived from the equation for total internal energy using the Favre average and the Boussinesq approximation.

$$\bar{\rho} C_P \Big(\frac{\partial T}{\partial t} + \tilde{u}_j \frac{\partial T}{\partial x_j} \Big) = \frac{\partial}{\partial x_j} \Big((\lambda + \lambda_T) \frac{\partial \tau}{\partial x_j} \Big) + \tilde{\tau}_{ij} \tilde{S}_{ij} - \frac{\tau}{\bar{\rho}} \frac{\partial \bar{\rho}}{\partial \tau} \Big|_{\bar{p}} \Big(\frac{\partial \bar{p}}{\partial t} + \tilde{u}_j \frac{\partial \bar{p}}{\partial x_j} \Big) \tag{5.10}$$

$\bar{\rho}$ is the Reynolds averaged density, $\tilde{T}$ is the Favre average of a variable T, $\tilde{\tau}_{ij}$ is the Favre averaged laminar, viscous stress tensor $\tilde{S}_{ij}$ is the Favre averaged strain-rate tensor, $\bar{p}$ is the Reynolds averaged pressure and λ_T is the turbulent thermal conductivity.

The heat transport turbulence models available in COMSOL are Kays-Crawford, extended Kays-Crawford and user-defined turbulent Prandtl number. The Kays-Crawford is known to give good results for most turbulent wall-bounded flows, except for liquid metal, and is set as default in COMSOL. The extended Kays-Crawford is mainly used for liquid metals. The Kays-Crawford

model is given by Equation 5.11.

$$Pr_T = \left(\frac{1}{2Pr_{T\infty}} + \frac{0.3}{\sqrt{Pr_{T\infty}}} \frac{C_p \mu_T}{\lambda} - \left(0.3 \frac{C_p \mu_T}{\lambda} \right)^2 \left(1 - e^{-\frac{\lambda}{0.3 C_p \mu_r \sqrt{Pr_{T\infty}}}} \right) \right)^{-1} \tag{5.11}$$

Pr_T is the turbulent Prandtl number, $Pr_{T\infty} = 0.85$, λ is the conductivity and μ_T is the turbulent dynamic viscosity.

There is a theoretical gap for the temperature field between the solid wall and the computational domain of the fluid, in the same way as the wall functions for the wall boundary condition described in Section 5.2.1. The heat flux between the fluid and the wall is given by Equation 5.12.

$$q_{wf} = \frac{\rho C_p C_\mu^{\frac{1}{4}} \kappa^{\frac{1}{2}} (T_w - T_f)}{T^+} \tag{5.12}$$

T_w is the wall temperature, T_f is the temperature of the fluid, C_μ is a modelling constant, κ is the turbulent kinetic energy and T^+ is the dimensionless temperature.

5.3   The Transport of Concentrated Species user interface

The Transport of Concentrated Species user interface employs mass fractions to model the transport of chemical species in a mixture. It models transport by diffusion, convection and migration in mixtures where transport properties, such as diffusion, depend on the composition of the mixture. This interface is utilized to model the thermal diffusion in the chamber containing the gas. The simulation will indicate if the temperature difference between the gas and the mirror can cause compositional gradients in the mixture. The equations used by COMSOL presented in this section are taken from the COMSOL documentation for the chemical species transport user interface [41] and the equations of change can be found in Transport Phenomena by Bird et al [33].

To calculate the transportation of mass, one can choose from three diffusion models imple-

mented in COMSOL. These models are the Maxwell-Stefan, Mixture-averaged and Fick's law. What separates these models is their use of diffusion coefficients, complexity and computational power required.

The Maxwell-Stefan model is chosen because it is the most detailed diffusion model. However, it also requires the most computational power out of the three models. The equation for the relative mass flux vector, $\boldsymbol{j}_i$, when using the Maxwell-Stefan model, is presented in Equation 5.13.

$$\boldsymbol{j}_i = -\rho w_i \sum_{k=1}^{Q} \tilde{D}_{ik} \boldsymbol{d}_k - \frac{D_i^T}{T} \nabla T \tag{5.13}$$

$\tilde{D}_{ik}$ are the multicomponent Fick diffusivities, $\boldsymbol{d}_k$ is the diffusional driving force, D_i^T is the thermal diffusion coefficient and w_i is the mass fraction for species i.

Equation 5.14 shows the equation for the diffusional driving force.

$$\boldsymbol{d}_k = \nabla x_k + \frac{1}{p}\left[(x_k - w_k)\nabla p - \rho w_k g_k + w_k \sum_{l=1}^{Q} \rho w_i g_i\right] \tag{5.14}$$

The species that the interface is solving for, using the mass constraint Equation 5.15, is selected. In order to avoid numerical errors, the species with the highest concentration is chosen. The sum of all mass fractions is equal to 1.

$$w_Q = 1 - \sum_{i=1}^{Q=1} w_i \tag{5.15}$$

When using the Maxwell-Stefan diffusion model, the diffusion coefficient and the thermal diffusion coefficients for each of the species have to be specified. In a multicomponent mixture is the sum of the thermal diffusion coefficients zero. The Convection and Diffusion node is the default transport mechanism for this interface.

The multicomponent equations of change in terms of the fluxes

The Navier-Stokes equations presented at the start of this chapter were given for a pure fluid. The velocity field in the Navier-Stokes equations is affected by the flux. For a non-isothermal multicomponent fluid of n chemical species are the equations of change modified to the equations presented below. [33]

The mass transport equation with a reference point that is stationary to the flow is shown in Equation 5.16.

$$N_i = j_i + \rho u w_i \tag{5.16}$$

The equation of continuity for each component is described by Equation 5.17.

$$\nabla \cdot j_i + \rho(u \cdot \nabla) w_i = 0 \tag{5.17}$$

Equation 5.18 is the momentum equation,

$$-(\nabla \cdot \Pi) + \sum_{i=1}^{n} \rho_i g_i = 0 \tag{5.18}$$

where Π is the pressure tensor, $\Pi = \tau + p\delta\tau$ is the viscous part of the momentum flux (shear stress tensor), p is the static pressure and δ is the unit tensor. The last term, $\sum \rho_i g_i$, represents that each of the species present may be acted on by a different external force per unit mass.

The energy equation becomes Equation 5.19,

$$-(\nabla \cdot q) - \left(\nabla \cdot (\Pi \cdot u)\right) + \sum_{i=1}^{n} (n_i \cdot g_i) = 0 \tag{5.19}$$

where q is the multicomponent energy flux relative to the mass average velocity, u. Emission and absorption of radiant energy is neglected.

Chapter 6

Model and Geometry

This chapter presents the geometry of the model and the materials used for the simulations. It also includes a brief discussion on laminar vs. turbulent flow, the mesh selection process and the final mesh chosen for the simulations. Figure 6.1 shows the geometry of the 3D model.
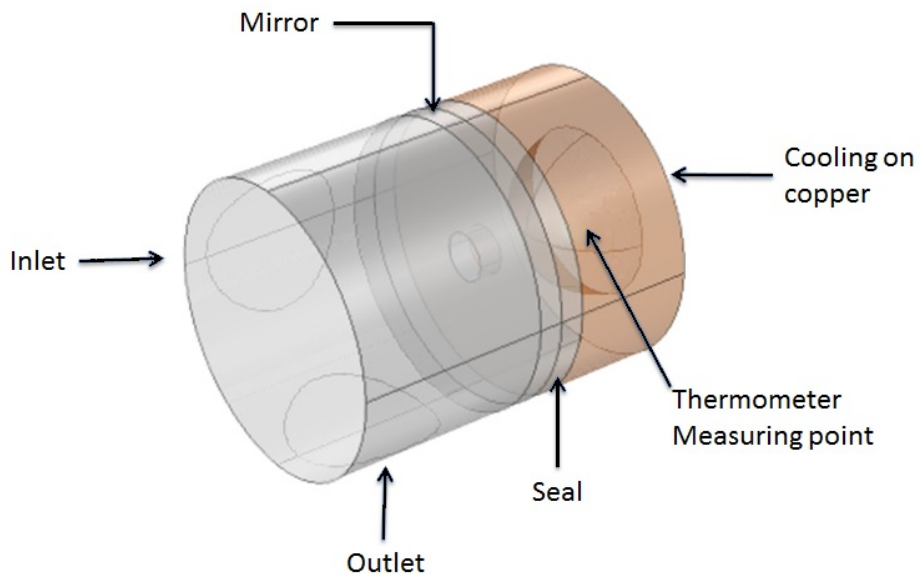
Figure 6.1: 3D geometry

6.1 Model geometry

The natural gas enters at the inlet and exits at the outlet. The cooling is placed at the back of the copper rod, leading the low temperature through a copper tap to the back of the mirror. A seal is placed between the copper rod and the mirror, surrounding the copper tap to concentrate the cold temperature and the formation of the dew at the center of the mirror. The model is fully isolated and it is therefore no heat loss to the environment. More detailed drawings with dimensions can be found in Appendix A.5. Figure 6.2 shows the model used in this thesis placed on a drawing of the Bureau of mines dew point apparatus to show the connection between the model and the unit.
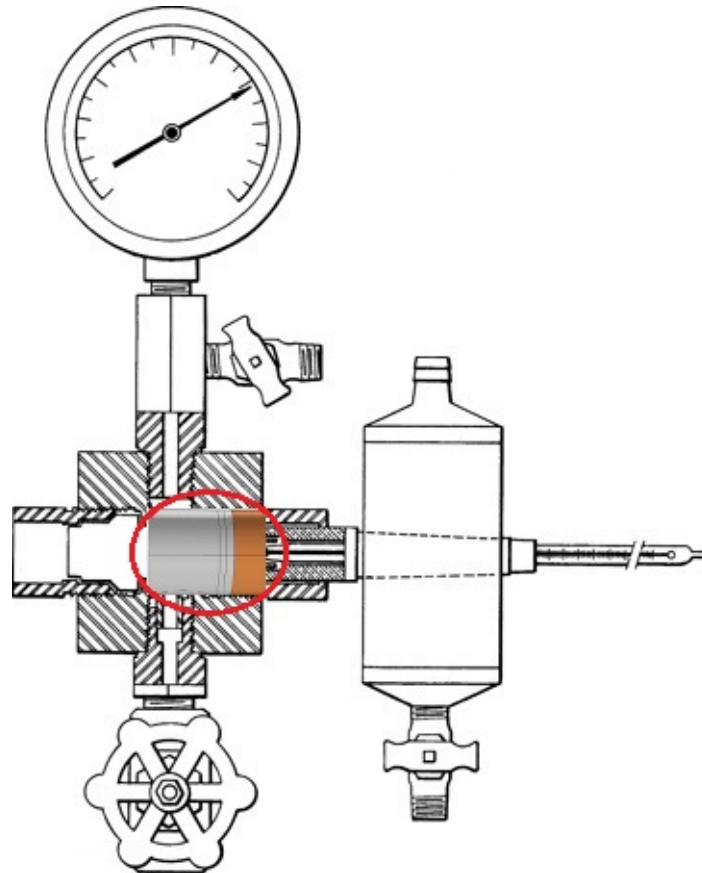
Figure 6.2: The model used in this thesis placed on the drawing of the Bureau of mines dew point meter

6.2 Materials

The open-source software Neqsim (non-equilibrium simulator) is a dynamic process simulator that has been developed at the Norwegian University of Science and Technology at the Department of Refrigeration and Air Conditioning [42]. It was desired to connect the thermodynamic package in Neqsim to COMSOL, so that the thermodynamic properties of natural gas could be implemented in the model. That way, COMSOL would continuously calculate properties for the natural gas, based on the changing temperature in the chamber. Unfortunately, this turned out not to be possible. However, observations during simulations showed that the temperature of the gas close to the mirror has approximately the same temperature as the mirror. Therefore, when focusing on that area, constant properties for the natural gas at that temperature have been used. The constant values taken from NeqSim are based on the SRK EoS model. Figure 6.3 shows an overview of the materials used on different parts of the model.
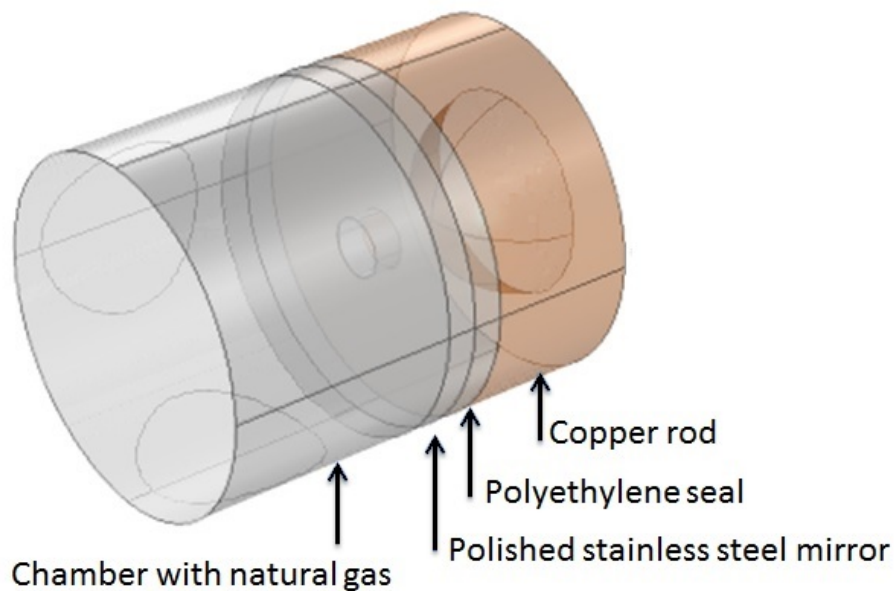
Figure 6.3: Materials

Two synthetic natural gases from a Statoil GC analysis from 2013 have been taken from the Master Thesis of Eirini Skylogianni [8]. In this thesis, they have been named Binary mixture and Natural gas. The composition of each component is presented in Table 6.1 and 6.2.

Table 6.1: Composition of Binary mixture

Component	mol%
Methane	99.90955
n-Heptane	0.09045

Table 6.2: Composition of Natural gas

Component	mol%
Carbon dioxide	0.27901
Nitrogen	5.77660
Methane	83.29466
Ethane	7.58345
Propane	2.00043
i-Butane	0.25648
n-Butane	0.49794
i-Pentane	0.10525
n-Pentane	0.12592
n-Hexane	0.05933
n-Heptane	0.01186
n-Octane	0.00905

The solid materials used in the model are copper for the thermowell, stainless steel on the mirror and polyethylene for the seal. The material of the seal is not known, but polyethylene has been chosen for its good heat resistant properties. The material properties used are presented in Appendix A.1. Copper and polyethylene are built-in materials in COMSOL and the properties for stainless steel were provided by Tibtech [43].

6.3 Laminar vs. turbulent flow

As the velocity of the gas flow increases, the flow may approach a change from laminar to turbulent flow depending on the significance of the Reynolds number. In the simulations carried out later in this thesis (Chapter 7) the velocity of 0.002 m/s is the most widely used value, while the highest velocity tested for is 0.03 m/s. Table 6.3 shows the constant properties used for calculating the Reynolds numbers for the flow and Table 6.4 shows the Reynolds numbers calculated for velocity 0.002 m/s (400 cc/h) and 0.03 m/s. The numbers have been calculated both at the inlet, where the gas enters the chamber and across the mirror as the gas flows in the chamber, using Equation 5.3. The first velocity, 0.002 m/s, is the one used as the standard velocity in this thesis and is also the one currently being used in the lab at Statoil Rotvoll for the dew point meter test rig. The Reynolds numbers are clearly laminar. Both 135 and 231 « 2300. For the other velocity, 0.03 m/s, the flow is in the transient area, which means that the flow is no longer laminar, but still not fully turbulent.

Table 6.3: Properties for calculating Reynolds number

Density	Viscosity	Inlet diameter	Mirror diameter
115.25 kg/m^3	0.014244 mPa·s	0.0085 m	0.0144 m

Table 6.4: Calculated Reynolds numbers

Velocity	0.002 m/s	0.03 m/s
Re, inlet	135	2063
Re, mirror	231	3495

A flow can become turbulent due to a high temperature gradient. This happens because of a thermal boundary layer. For low heating and cooling rates and temperature differences, the temperature can be treated as a passive scalar. However, when larger temperature differences are present, buoyancy forces may be non-negligible, and the thermal field directly affects the dynamic one. Buoyancy effects arise when the variation of density across the flow is not negligible. If the density changes are not too big, the Boussinesq approximation is often used, since it assumes that density changes may be ignored (except the ρg_i term) [44]. For most of the velocities used in this thesis, the flow has such a low Reynolds number that even though there is a

high temperature difference from the inlet to the mirror, it will not make the flow turbulent. The flow that is in the transient area, with a velocity of 0.03 m/s, can potentially be affected by this effect.

The low-Re κ-ε model vs. the κ-ε model

When running a simulation on a 3D model, compared to a 2D model, the simulation time increases drastically. The same happens when running the simulation using the low-Re κ-ε model instead of the simpler κ-ε model. In this thesis a 3D model is used, and it was therefore of interest to check the difference in accuracy between the two turbulence models, κ-ε and low-Re κ-ε, to see the possibility of using the less computer demanding model. To check this, a simplification of the 3D model was created in 2D, as illustrated in Figure 6.4, to see the difference between the two turbulence models. This model was used for simulation with both the κ-ε model and the low-Re κ-ε model using the parameters listen in Table 6.5.
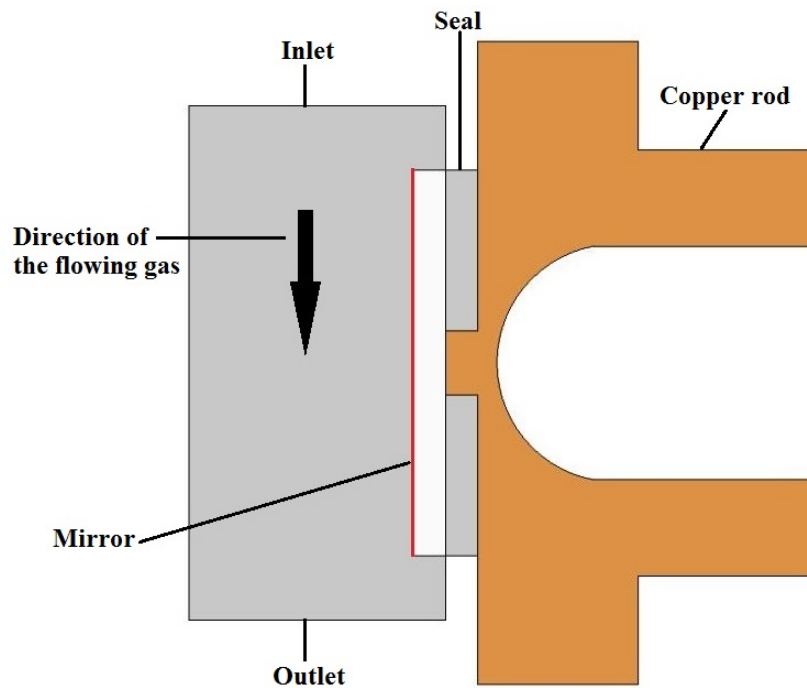
Figure 6.4: The 2D model. The red line represents the surface used for the graph presented in Figure 6.5.

Table 6.5: Low Reynolds number κ-ε turbulence model vs. κ-ε turbulence model

Constant	Value
T_{in}	313.15 K (40 °C)
T_{CO_2}	253.15 K (-20 °C)
p	80 bar
u_{in}	0.002 m/s

Figure 6.5 shows the distribution in temperature across the mirror from the inlet to the outlet, as illustrated by the red line in 6.4. As can be seen in the graph the two curves show the same temperature tendency. Both turbulence models experience a fall in temperature as the flow is cooled by the mirror. The difference of the two models is that the low-Re κ-ε model is adjusting more to the mirror temperature than the κ-ε model and therefore holds a lower temperature profile along the surface.
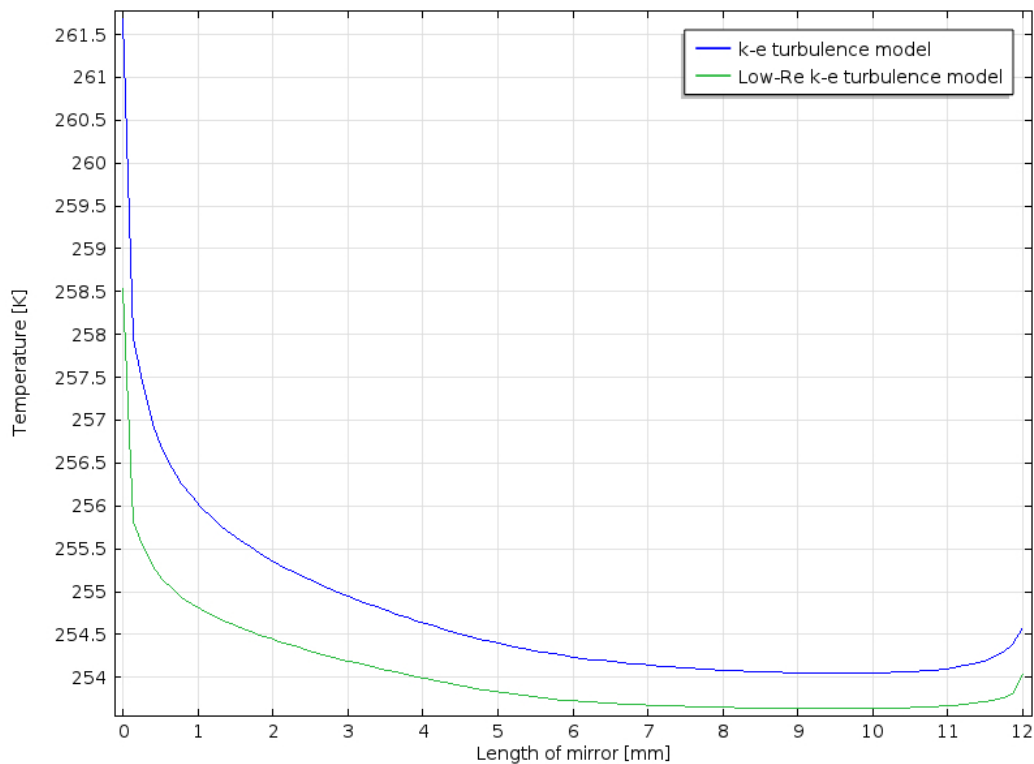
Figure 6.5: Simulation result comparing the low Reynolds κ-ε and the κ-ε turbulence model

The simulation resulted in a temperature difference of approximately 0.5 K at the coldest measuring point on the model, as can be seen in the graph. Because of the severe difference in time requirement for the two simulations, this temperature difference is noted as a part of the un-

certainty when modeling with the κ-ε turbulence model. This simulation was only performed to show the difference between the two turbulence models. The simulation results for the 3D model will be properly presented in Chapter 7.

6.4 Mesh

The physics-controlled mesh-selection in the mesh settings in COMSOL is a tool that automatically defines the grid depending on the geometry and the physics added to the simulation. The user selects the element size of the grid, ranging from extremely coarse to extremely fine. The walls have a boundary layer mesh that is smaller than the mesh elsewhere in the model. This is default in COMSOL [9]. The grid size needs to be small enough to give reliable results that are independent of the grid size, but at the same time will an unnecessary fine grid drastically increase the simulation time. The procedure for choosing the right mesh is explained in this section. The final mesh chosen can be seen in Figure 6.6.
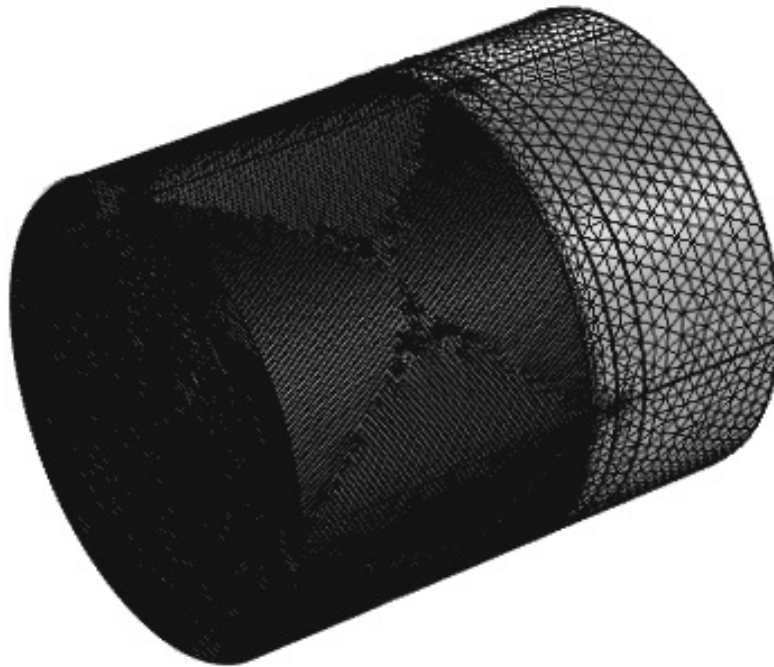
Figure 6.6: Final mesh

6.4.1 Mesh independency

In order to see the model's independency of the mesh, simulations were performed on finer and finer grids, while keeping all other parameters constant, and comparing the results. If two of the meshes give equal results, the simulation is mesh independent and the coarsest of the two meshes is chosen in order to reduce simulation time. The results presented in this section will be introduced later, and is here only used to illustrate the results' dependence or independence of the mesh. The element size of the physics-controlled grids can be seen in Table 6.6.

Table 6.6: Physics controlled grid element size

Grid element size	Domain elements	Boundary elements	Edge elements
Fine	356,549	20,226	803
Finer	1,464,498	58,066	1,286
Extra fine	1,843,453	61,514	1,414
Extremely fine	4,847,988	76,208	1,714

Figure 6.7 and Figure 6.8 show the variation in results when comparing the different physics-controlled meshes, in both the fluid- and solid part of the unit, ranging from fine to extremely fine. Figure 6.7 shows the temperature horizontally across the middle of the mirror for each of the meshes. Figure 6.8 shows the temperature through the solid from the mirror to the thermometer measuring point. Especially for the mirror part in Figure 6.8, from 0-1 mm, the graphs differ.

There was a small variation between the results when comparing the physics-controlled meshes which makes it difficult to decide which mesh to proceed with, since none of the meshes give equal results. Because of this, the user-controlled meshing was explored. Using this sequence type gives the user the opportunity to optimize the mesh by making the grid finer in the areas of focus, like the mirror, and coarser in other areas. This gives a mesh that is suitable for the model without using unnecessary simulation time. Many different meshing settings were investigated, for instance by changing the number of boundary layers around the mirror and changing the maximum element size. Based on the results from comparing the physics controlled meshes, the extra fine grid was chosen as the starting point for the user-controlled meshing.
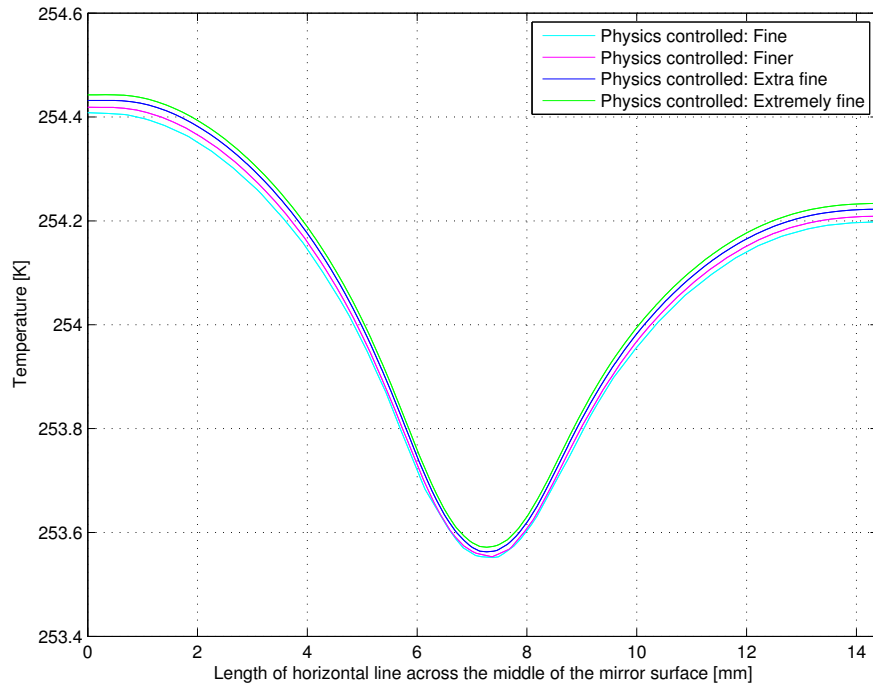
Figure 6.7: Comparison of results from physics controlled mesh ranging from fine to extremely fine, temperature measured horizontally across the middle of the mirror surface.
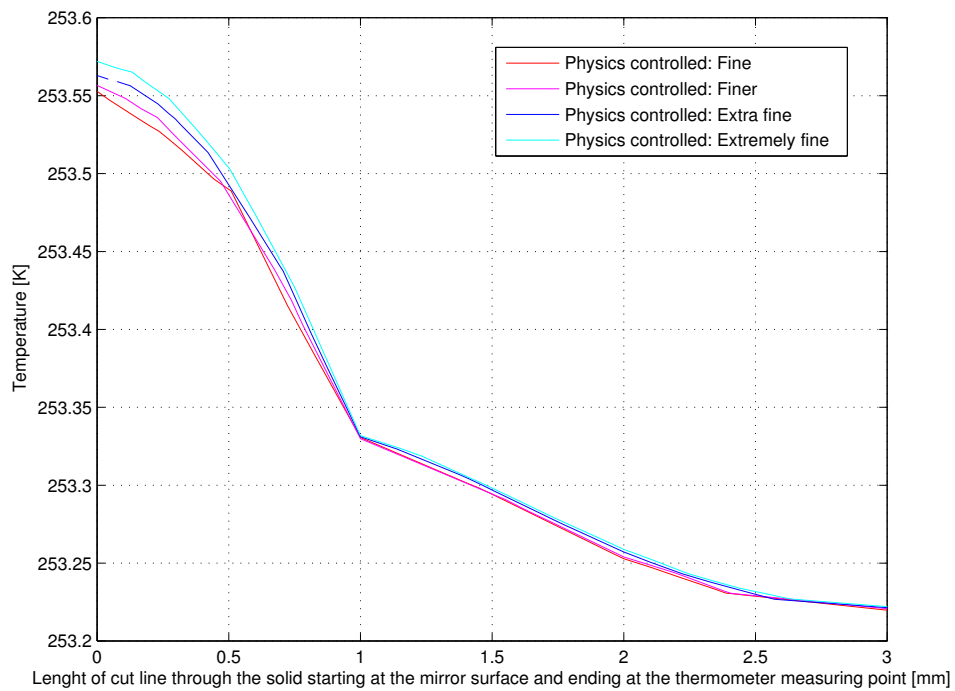
Figure 6.8: Comparison of results from physics controlled mesh ranging from fine to extremely fine, temperature measured through the solid from the middle of mirror surface to the thermometer measuring point further back.

Lift-off coefficient

For turbulent simulations with the κ-ε model, another consideration needing to be checked before relying on the mesh is to check the wall lift-off in viscous units when using wall functions. The wall resolution should be 11.06 on the walls surrounding the fluid, as shown in Figure 6.9. If the value is higher, it means the mesh is relatively coarse and the accuracy might be compromised. The wall lift-off in viscous units is calculated using Equation 6.1.

$$\delta_w^+ = \rho u_\tau \frac{\delta_w}{\mu} \tag{6.1}$$

$u_\tau = C_\mu^{1/4} \sqrt{k}$ is the friction velocity and δ_w is the distance from the wall to the computational domain and is automatically computed. It is limited from below so that it never becomes smaller than half of the height of the boundary mesh cell. [37]
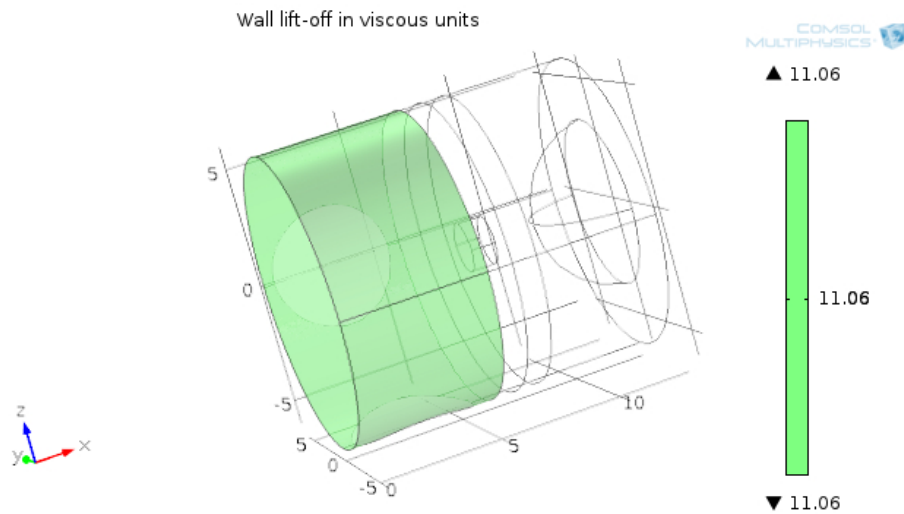
Figure 6.9: Wall lift-off in viscous units from κ-ε simulation

6.4.2 Final mesh

The final mesh was created using the settings in Table 6.7. This is the mesh used for all the simulations in this report. The grid element size of the final mesh can be seen in Table 6.8 and the final mesh can be seen in Figure 6.10.

Table 6.7: Mesh settings

Setting	Domain	Value
Grid size	Fluid	Extra fine
		Max. element size changed to 0.25
	Solid	Extra fine
	Chamber	Extremely fine
Corner refinement	Chamber	Min. angle between boundaries: 240 deg
		Element size scaling factor: 0.35
Free tethrahedral	Chamber	Extremely fine
		Max element size changed to 0.25
	Copper connection	Extremely fine
		Max element size changed to 0.09
	Remaining	
Boundary layers	Chamber	Number of boundary layers: 5
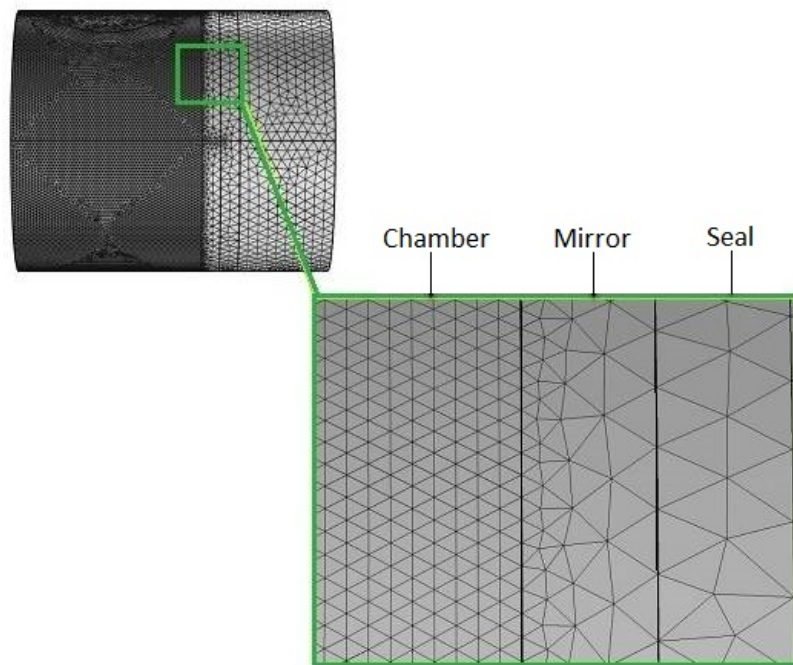
Figure 6.10: The mesh seen from the side

Table 6.8: User controlled grid element size of final mesh

Domain elements	Boundary elements	Edge elements
2,614,773	68,392	1,576

Mesh quality

The statistics function in COMSOL was used to check the quality of the mesh. This function pro-
vides information about the minimum and average mesh element quality and a mesh element
quality histogram. The histogram shows the relative frequency of mesh elements with different
quality values. Each domain was studied using this function, to see how good the mesh was in
that area. This is presented in Appendix A.2. Figure 6.11 shows that the 0.5% worst quality of the
mesh is mainly in the chamber and around the edges. But the solids and the mirror, which are
the main focus of this thesis, are all better quality.
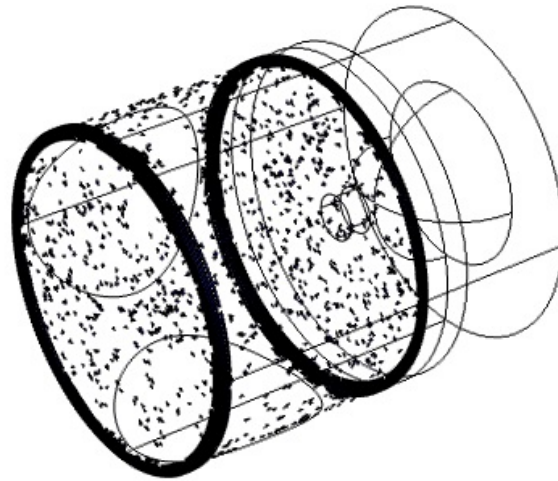
Figure 6.11: The 0.5 % worst quality of the mesh

6.5 Convergence

The process of finding a numerical solution is an iterative process, which means that the solution is changing from one iteration step to the next using values from the previous step. If the change between two preceding solutions is significant, the result will also change accordingly. When the difference between two consecutive results is within the tolerance specified, the solution is converged. All numerical solutions have some error, how much is acceptable is depending on the case. All the simulations in this report have converged to a solution with a relative error less than 10^{-4}. Figure 6.12 shows a typical convergence plot for the laminar simulations using the nonlinear solver. The Newton-Raphson iteration method is used by COMSOL.
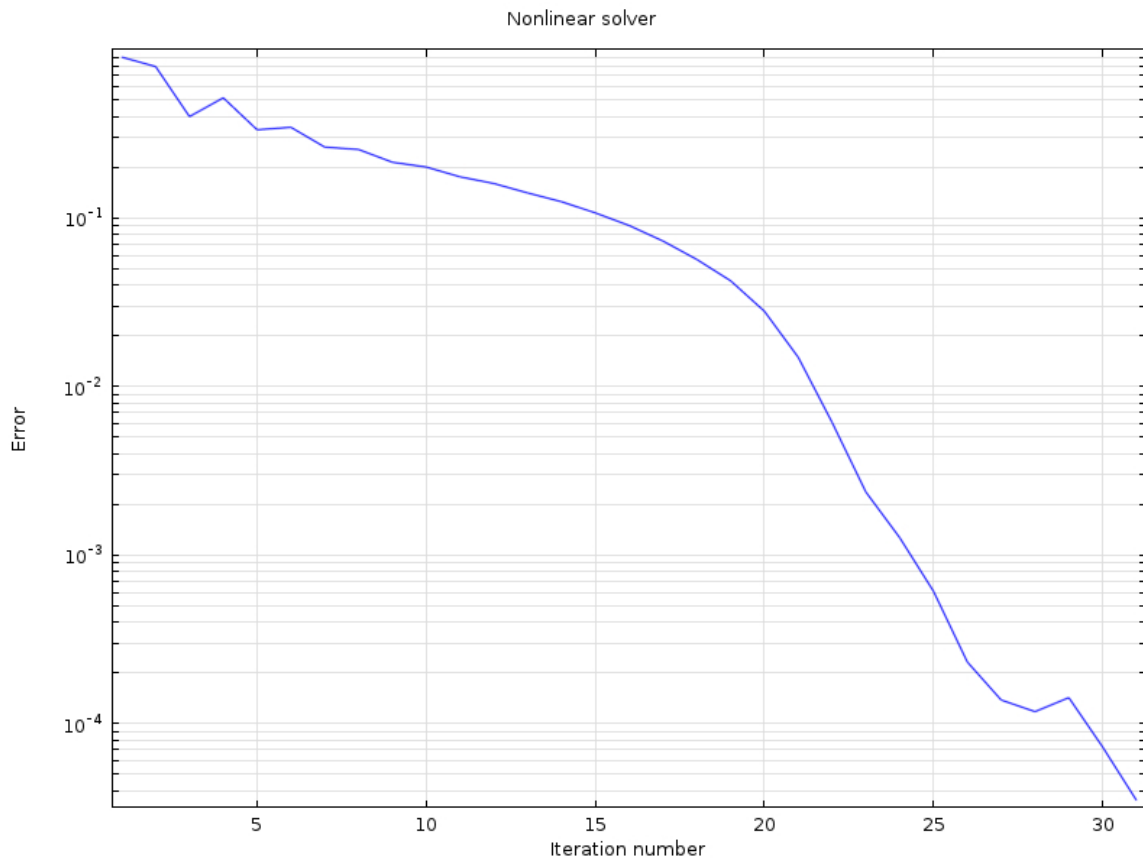
Figure 6.12: Convergence plot, nonlinear solver

Chapter 7

Simulations and Results

7.1 Simulations

The following cases have been simulated in order to improve the fundamental understanding of the unit, to decrease the uncertainties associated with the dew point test method and to provide results that can lead to future improvements. First, a case where typical parameters used in the test rig today are investigated. Then, one or two parameters are varied in each case, to see how this affects the results. Next, a case looking at mass transfer modelling and last, a case discussing possible errors in today's testing technique. A section about what have been tried, but that did not work, can be found at the end of the chapter.

- Case 1: Simulation using typical parameters for the test rig
- Case 2: Significance of different temperatures of the inlet gas
- Case 3: Significance of different cooling temperatures
- Case 4: Significance of different inlet velocities
- Case 5: Mass transfer modelling and compositional gradients
- Case 6: Assessing errors from real dew point and dew point determined by the technique

Basis for the simulations are parameters that are used for the test rig at Statoil Rotvoll. Experimental values from the Master Thesis of Eirini Skylogianni [8] have been used for information on which parameters are normally used in the test rig, e.g. an inlet velocity of 400 cc/h. The parameters used for the different cases are presented at the start of each case. Calculations can be found in Appendix A.4.

Case 1-4 is carried out using constant values for the density of the inlet gas. The reason for doing this rather than using ideal gas law, is the deviating value of the density when comparing the values calculated from ideal gas to the ones calculated by NeqSim. Because of the composition of the gas and the contribution of compressibility, the value calculated in NeqSim is significantly higher than what is calculated from ideal gas conditions. The compressibility factor, z, is the parameter indicating how a real gas deviates from ideal gas behavior. All cases used in this thesis have a compressibility factor less than 1, between 0.6 and 0.9, which indicate that the attractive forces between the molecules dominate and that the actual gas occupies a smaller volume than the ideal gas. This factor is mainly dependent of temperature and pressure which affects the spacing between molecules. At high pressures and low temperatures the intermolecular forces become of importance [45]. Based on the complex system beyond the calculations in NeqSim, this value is considered more credible. Therefore are the constant values based on the temperature of the mirror used in the following simulations. When performing simulations on the thermal diffusivity in the chamber, Case 5, a polynomial for density is used. Uncertainties associated with these methods are studied in Case 6.

7.2 Case 1: Simulation using typical parameters for the test rig

The first simulation was performed using parameters that are currently being used at the hydrocarbon dew point test rig at Statoil Rotvoll, see Table 7.1. The temperature distribution of the entire model can be seen in Figure 7.1. This will be examined in the following section, first looking at the mirror surface, then at the heat transfer through the solid parts of the unit and last looking at the accuracy of the measured temperatures.

Table 7.1: Case 1 parameters

Setting	Value
Inlet gas	Natural gas
Inlet temperature	318.15 K (45 °C)
CO_2 cooling temperature	253.15 K (-20 °C)
Gas inlet velocity	0.002 m/s (400 cc/h)
Constant pressure	85 bar
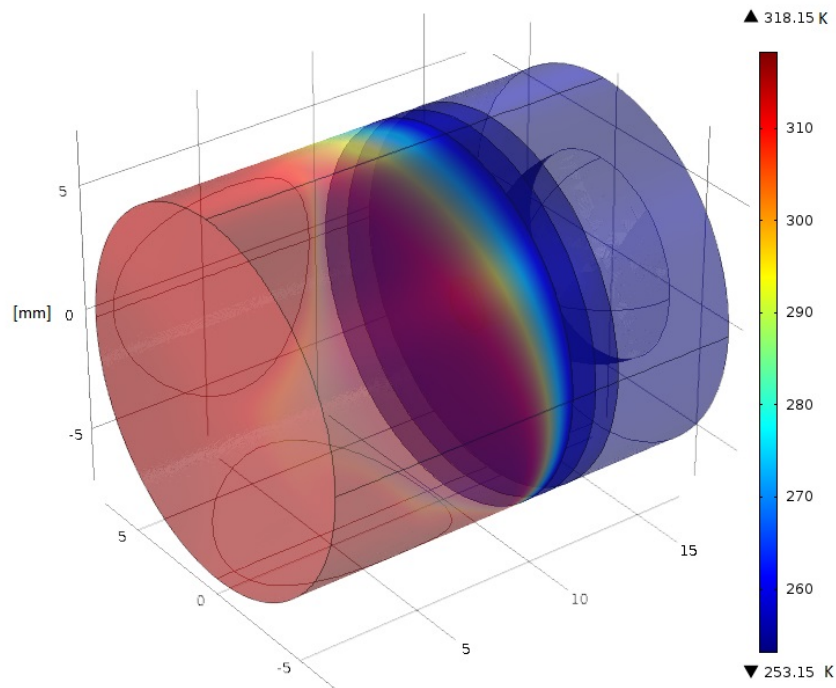
Figure 7.1: Temperature distribution in the entire model

7.2.1 Mirror surface

The mirror is cooled from the back by the copper tap connecting the mirror and the copper rod, while the warmer gas heats the mirror from the front. To show the temperature distribution on the mirror surface, a cut plane was placed as shown in Figure 7.2. As can be seen from the results presented in Figure 7.3, the temperature difference on the mirror is 1.73 K (from 253.73 K in the center of the mirror to 255.46 K at the inlet side).
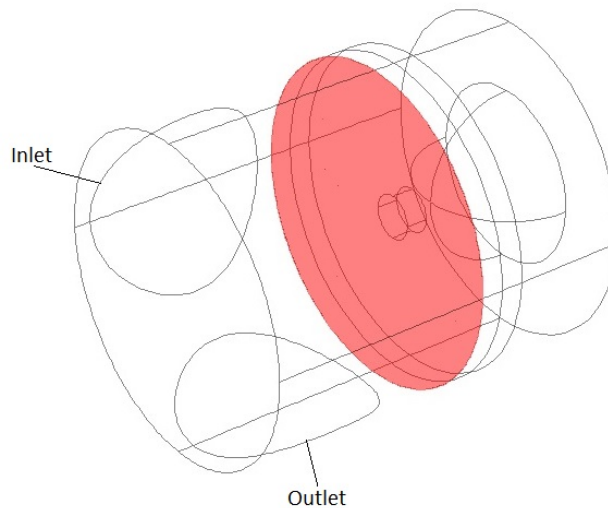
Figure 7.2: Illustration of the cut plane used to show the temperature distribution of the mirror surface

The warm gas enters the mirror from the left and this is therefore the warmest part of the mirror. The cooling led by the copper rod to the middle of the mirror is clearly visible. This is where the dew will appear. Most of the gas flows directly down towards the outlet pipe while some of the gas hits right above the exit and circulates inside the chamber. This flow follows the upper wall and then collides with the inflowing gas and follows its path, either on another circulation around the chamber or out through the outlet pipe. Because of this tendency of the flow pattern the surface of the mirror is generally warmer at the lower region and colder at the area above the middle. An overview of the flow pattern can be seen in Figure 7.4, and the circulation at the upper part of the chamber is evident.
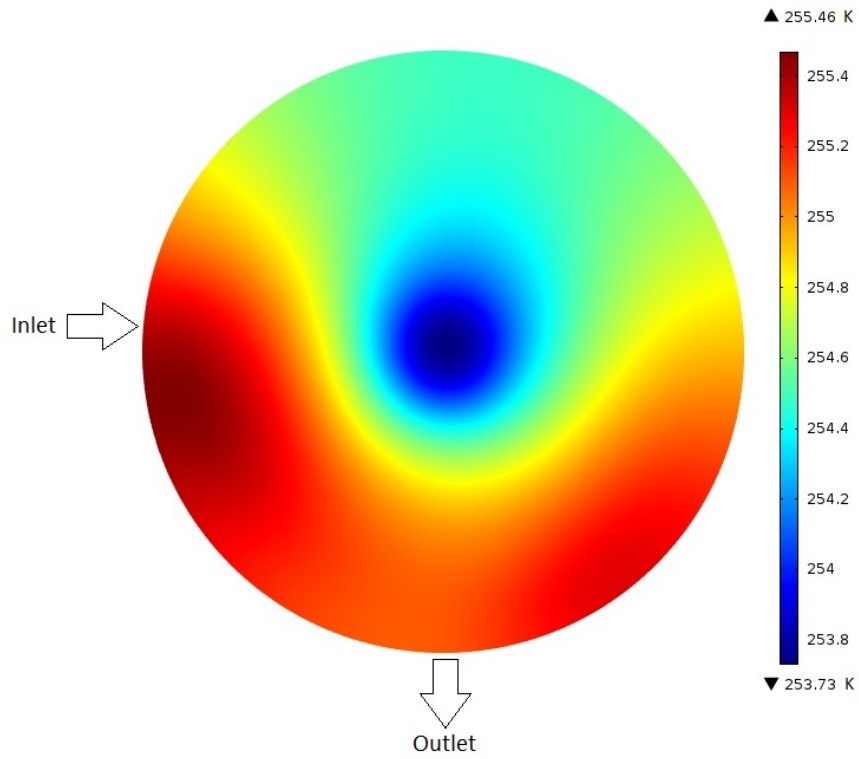
Figure 7.3: Temperature distribution on mirror surface
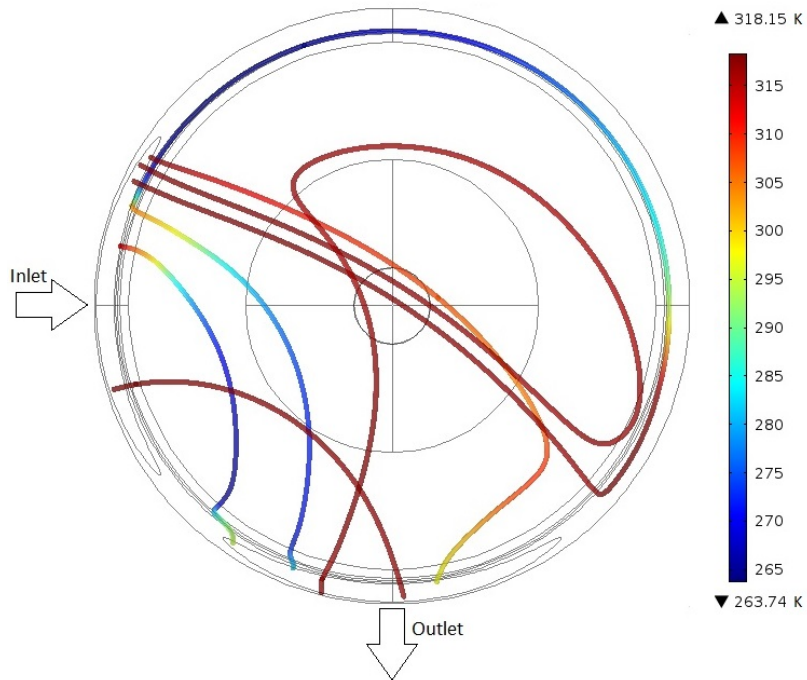
Figure 7.4: Streamlines showing the flow path of the gas in the chamber

In order to look more closely at the temperature distribution on the surface, a cut line was placed horizontally across the mirror, from the left to the right, as can be seen in Figure 7.5. The result is presented in Figure 7.6.
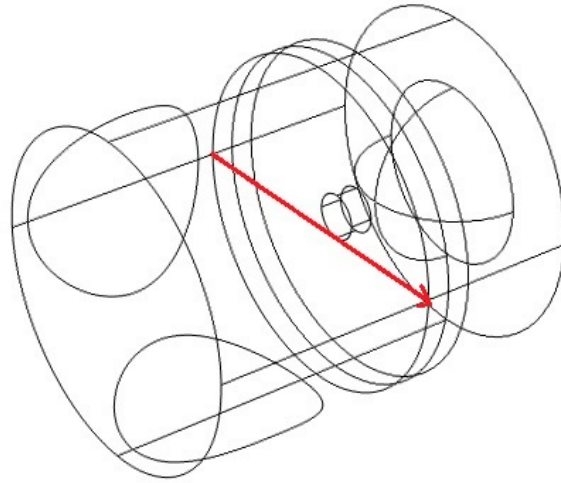
Figure 7.5: Horizontal cut line across the middle of the mirror surface
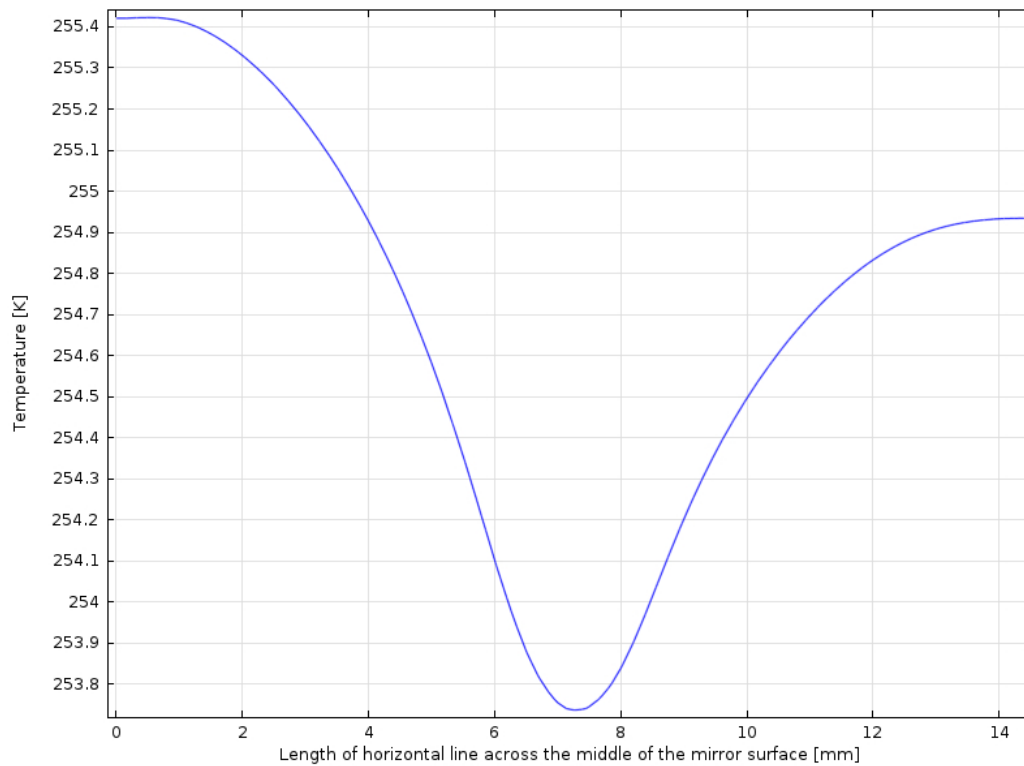
Figure 7.6: Result from the horizontal cut line across the mirror surface

The mirror is clearly coldest in the center, warmest at the inlet side of the mirror and a bit colder at the opposite end. The gas that enters the chamber holds a high temperature but is quickly chilled when passing the mirror. The inlet side (left side) is the area on the mirror surface where the gas is hottest, since it has not yet passed over the coldest part of the mirror. The coldest part is clearly visible as the dip in the center of the curve. The temperature here goes down to 253.74 K which is 0.59 K above the temperature of the CO_2 cooling. This is the point where the gas passes over the area on the mirror that is directly cooled through the copper rod attached to the back of the mirror. The temperature of the gas furthest to the right on the curve is a bit lower than on the left side. This is probably a mix of gas passing across the center, that has been cooled, and gas flowing below the center of the mirror that has not been that much affected by the colder center.

When placing the cut line vertically, from the top to bottom of the chamber as shown in Figure 7.7, the result shows that the area around the outlet is warmer than the area at the top of the chamber. This can be seen in Figure 7.8. Some of the gas is passing directly from the inlet to the outlet, just passing briefly over the mirror. This explains the temperature near the outlet to be just slightly lower than the temperature on the mirror near the inlet, as could be seen in Figure 7.6. The gas at the top of the mirror has been circulated around in the chamber, as could be seen in Figure 7.4, and is therefore slightly colder, both from being cooled down for a longer period of time and because a lot of the gas has passed directly over the coldest area on the mirror.
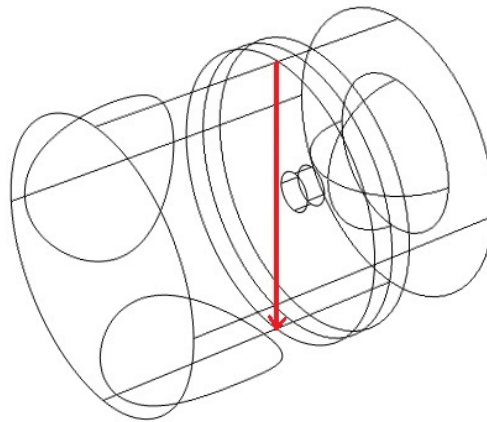
Figure 7.7: Vertical cut line across the middle of the mirror surface
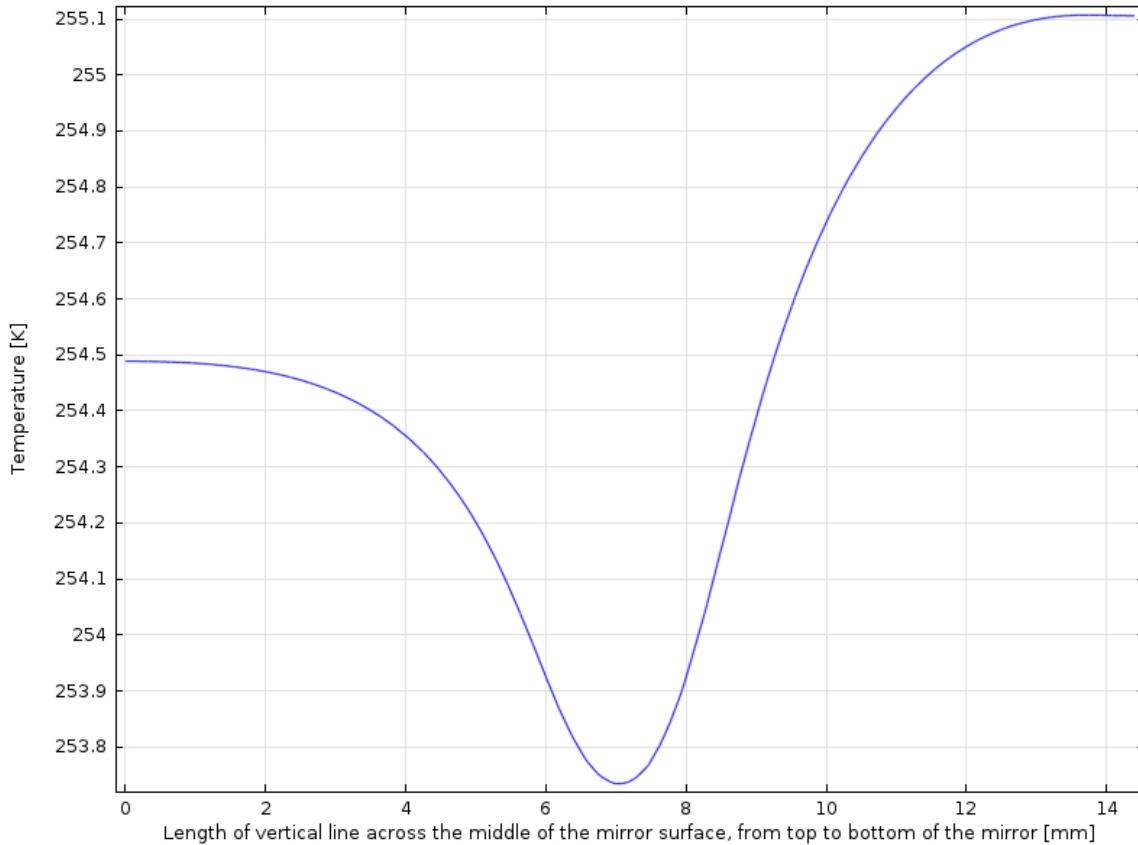
Figure 7.8: Result from the vertical cut line across the mirror surface

7.2.2   Solids

To see how efficiently the cooling is passing from the copper to the mirror, the temperature distribution in the solid parts of the model has been studied. Three cut lines were placed in the model as can be seen in Figure 7.9. One cut line going through the center of the model and one cut line on either side. The temperature along these lines is presented in the graph in Figure 7.10.

The left cut line goes through the part of the mirror that is closest to the inlet and holds a higher temperature than the right cut line placed at the opposite end of the mirror surface. There is not a major temperature difference between the three cut points on the mirror surface, but the cooling effect from the copper rod is quite clear when looking at the middle cut line compared to the left and right cut line. When looking at the part where all three cut lines go through the
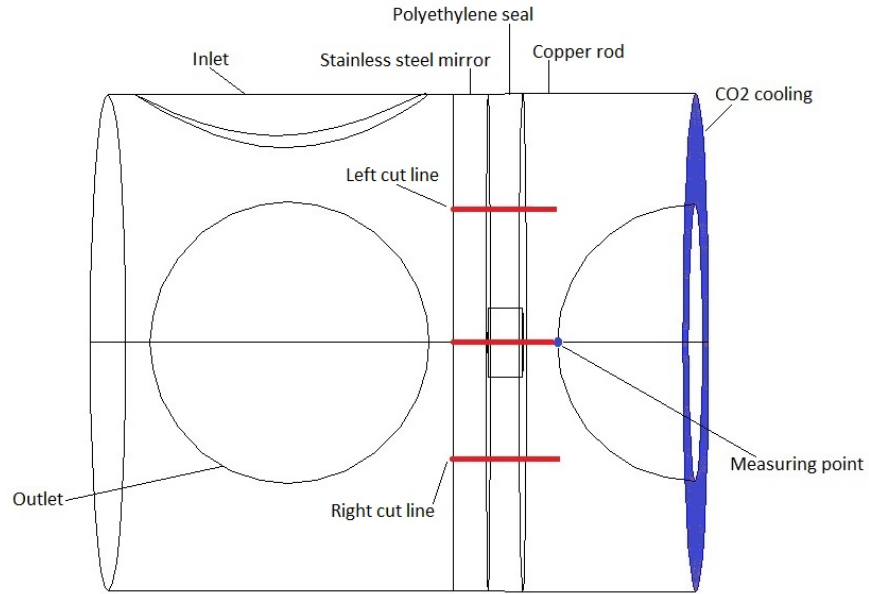
Figure 7.9: Cut lines in the solid (model seen from above).
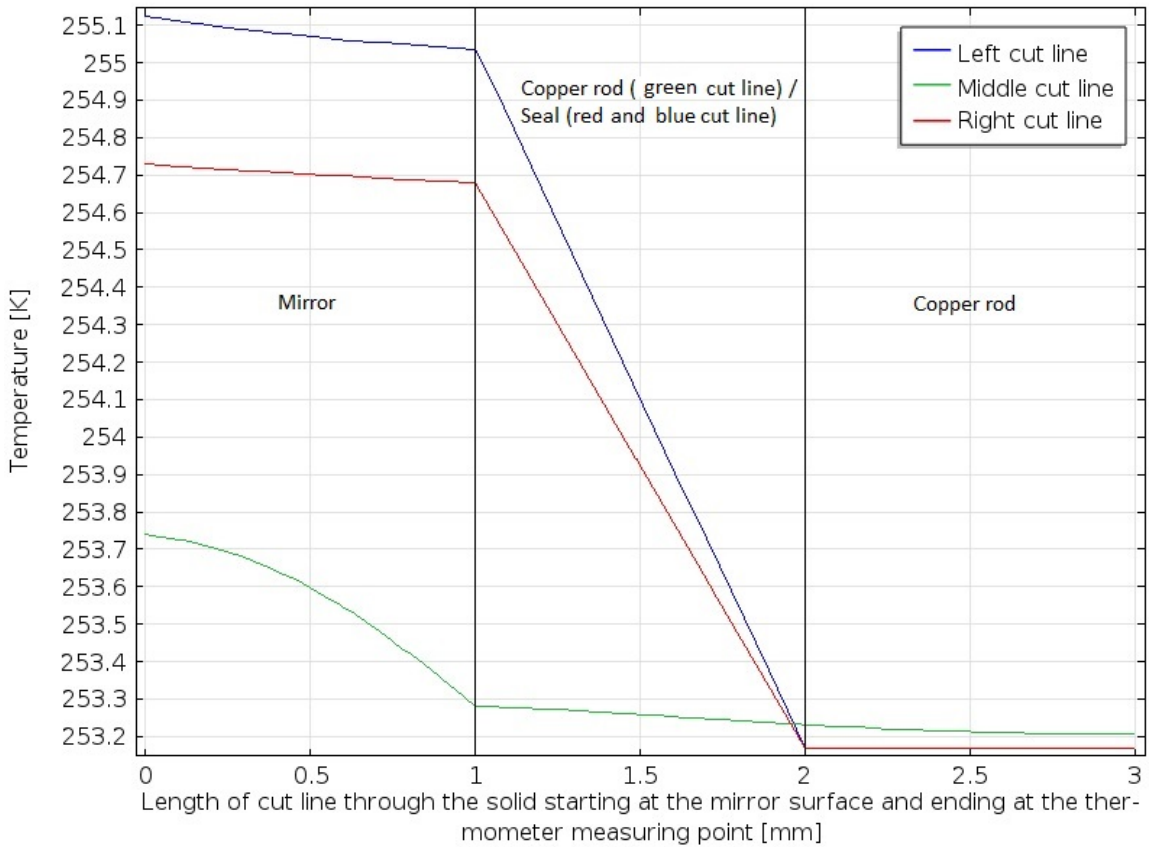
Figure 7.10: Results from the cut line through the solids

copper rod, the temperature has stabilized between the left and right cut line. This is because the cooling is equal on both sides, since the copper rod is uniformly cooled at the far end of the model. The center of the copper rod, at the point where the thermometer is placed, is not directly cooled but is cooled from the sides. This can also be seen in the graph, as the middle cut line holds a slightly higher temperature than the left and right cut line. The difference when passing to another material is clearly visible. The left and right cut lines go through three different materials, first the stainless steel mirror, then the polyethylene seal and last the copper rod. The middle cut line has only one material change, from the mirror directly to the copper rod.

Stainless steel is a relatively poor conductor with a thermal conductivity of 16.3 W/m·K. Copper on the other hand has a very high thermal conductivity, 400 W/m·K. Polyethylene has a relatively low thermal conductivity, 0.4 W/m·K, which means it only transfers small amounts of energy out to the environment. This means that the heat transfers is higher through copper than the other two materials. Heat capacity, Cp, says how much energy is needed to change the temperature of a certain material by a given amount. Polyethylene, with Cp = 1900 J/kg·K requires a lot of energy for the temperature to change, whereas copper, Cp = 385 J/kg·K and stainless steel, Cp = 500 J/kg·K require less energy. The reason the curve is not linear is probably due to radial heat transfer. Because of the constant conductivity for each material, there is probably some heat loss to the other parts of the unit. This can be seen especially for the middle cut line through the mirror and also through the copper. Since the model is isolated the heat is only transferring through the nearby materials.

7.2.3   Accuracy of the dew point measurements

When operating the dew point unit, the mirror temperature is read by a thermometer placed inside the copper rod a few millimeters behind the mirror. As indicated in Figure 7.10 there is a variation in temperature between these reference points. It was therefore of interest to find the exact difference in the measured temperature by the thermometer and the actual temperature of the mirror. To find this error the two points illustrated in Figure 7.11 was used to log the temperature during the simulation. The blue dot is the point on the middle of the mirror surface

and the red dot is the thermometer measuring point 3 mm behind the mirror surface.
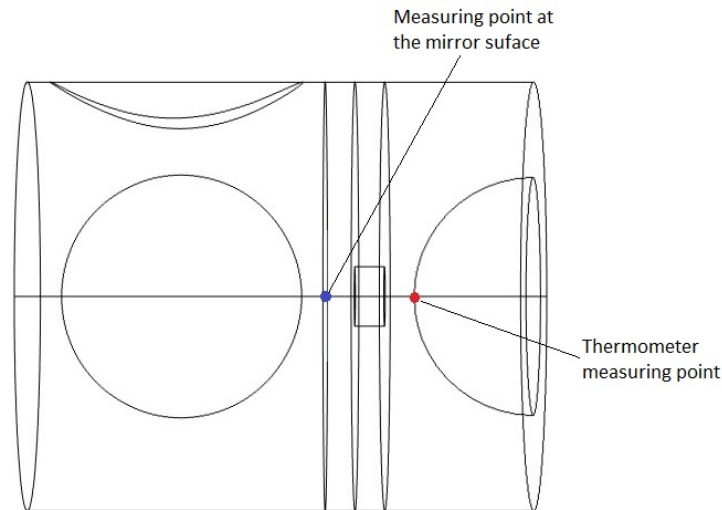
Figure 7.11: Measuring points (model seen from above).

The result can be seen in Table 7.2 and shows a temperature difference of 0.53 K. This difference is probably a result of heat loss and thermal resistance in the materials. Since the model is isolated, this result may differ from the real unit. If there exists heat transfer between the cooling copper rod and the surroundings, the measured temperature from the thermometer may have been higher, and the difference between the temperature on the mirror and the thermometer may have been less.

When looking at Figure 7.10 it is evident that most of the primary fall in temperature is through the mirror. As mentioned earlier the mirror consists of a different material and also provides a different conductivity and heat capacity. The copper provides a high conductivity of 400 W/m·K compared to 16.3 W/m·K for the mirror. In addition to the difference in the ability to transfer heat, the big temperature difference between the cold solid and the warm gas entering the chamber will also contribute to this error, especially since the mirror is the material on the boundary connecting these to substances. The error of 0.53 K occurs when running the simulation of these exact parameters. Further in this chapter, this error will be investigated in cohesion with inlet and cooling temperatures and the velocity of the inlet gas.

Table 7.2: Temperature at the center of the mirror compared to the temperature measured by the thermometer

T_{CO2}	$T_{thermometer}$	T_{mirror}	$\Delta T_{thermometer,mirror}$
353.15 K (-20 °C)	253.21 K	253.74 K	0.53

Time dependency

In this thesis, the main interest is to find out how the dew point meter performs when the system reaches its steady state condition. Literature discusses how fast the mirror temperature can decrease before it affects the accuracy of the measurements. To test this, a time dependent simulation has been carried out using the same parameters as previously (listed in Table 7.1). The result is illustrated in Figure 7.12 and shows that the temperature of the coldest point in the middle of the the mirror (illustrated by the blue dot in Figure 7.11) is 253.80 K after 60 seconds. This is only 0.1 K higher than steady state temperature of 253.70 K. The curve is starting off very steep the first 10 seconds, changes and then flattens until it reaches the steady temperature of the mirror. In this simulation all parameters is activated at time zero, and therefore start simultaneously.
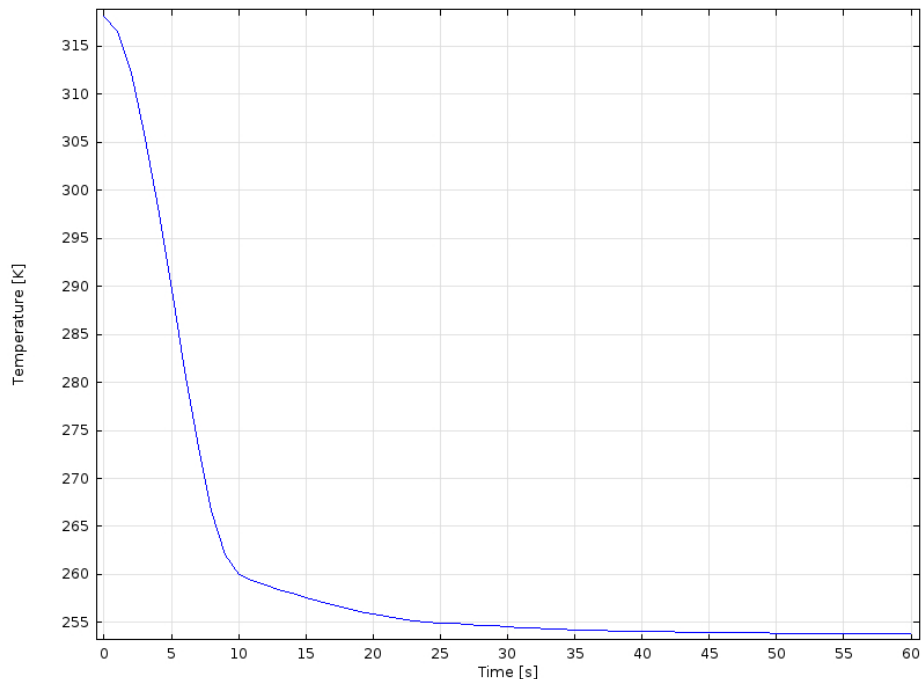
Figure 7.12: Temperature at the coldest point of the mirror surface due to time.

7.3 Case 2: Significance of different temperatures of the inlet gas

In the hydrocarbon dew point test rig operating at Statoil Rotvoll the gas is heated to a temperature of 318.15 K before it is cycled through the chamber and then cooled at the mirror until the dew starts to appear. When using the unit in the field, this temperature can be much higher. In this case, simulations have been carried out to see how much the gas with different inlet temperatures can be cooled within one circulation through the chamber. When the unit is used in field operations, the gas is circulated one time past the mirror, while using the unit in the lab, the gas is passed back and forth through the chamber until the gas condensates. Parameters used in the simulations are listed in Table 7.3 below.

Table 7.3: Case 2 parameters

Setting	Value
Inlet gas	Natural gas
Inlet temperature	298.15 K, 308.15 K, 318.15 K, 373.15 K
CO_2 cooling temperature	253.15 K
Gas inlet velocity	0.002 m/s (400 cc/h)
Constant pressure	85 bar

The results are presented in Figure 7.13, showing the temperature across the mirror, and Figure 7.14 showing the heat transfer through the solid parts of the unit. As expected, one can see from Figure 7.13 that the gas with a higher inlet temperature will not cool as much as the flow of a lower temperature. Still, the warmest gas entering at 373.15 K will, according to the simulations, manage to adapt to a temperature of 254.24 K. This gives a temperature change of 119.20 K on only one circulation inside the chamber. Especially using these temperatures, a varying density may have some effect on the heat transfer because of the high temperature difference in the chamber. This is studied later in this chapter, in Section 7.7. As for the other inlet temperatures, they all manage to cool down to a temperature between 253.56 K and 253.74 K. The difference of 10 K between the inlet gas temperatures results in a difference of only 0.09 K when the flow has reached the center of the mirror. For operations in the field, the possibly high temperature of the inlet gas may cause some errors and will not be as effective as for lower temperatures. Nev-

ertheless, the 55 K inlet temperature difference (between the inlet flow of 318.15 K and 373.15 K) results in a 0.5 K difference at the coldest point on the mirror.
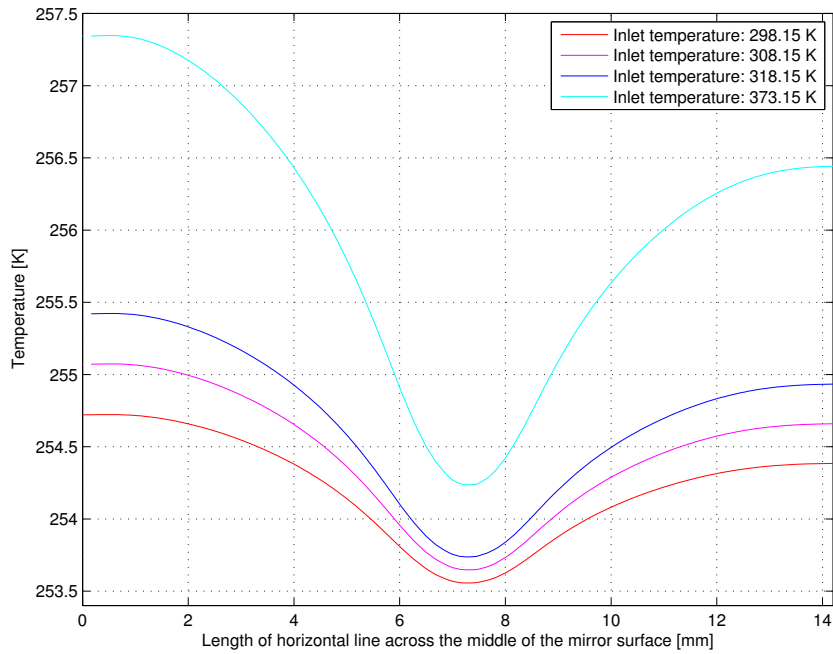
Figure 7.13: Temperature distribution horizontally across the mirror for change in inlet temperature.
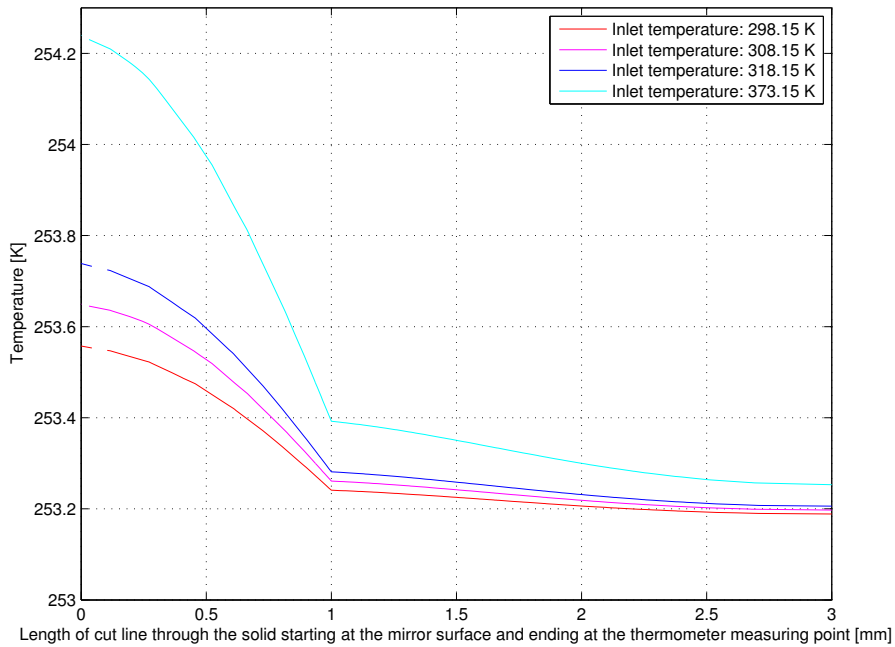
Figure 7.14: Heat transfer in the solid part of the unit for change in inlet temperature. The temperature along the middle cut line as presented in Figure 7.9

When looking at the temperature in the solid, see Figure 7.14, the lines start off at different temperatures and get closer as they approach the colder side of the solid. All four curves show a temperature difference within the solid, which indicates a certain deviation between the mirror temperature and the temperature measured by the thermometer.

Accuracy of the dew point measurements

The mirror temperature and the temperature measured by the thermometer is compared. Table 7.4 shows that the measured temperature is from 0.37 K to 0.99 K lower than the actual temperature of the mirror for the parameters used. The deviation is increasing with increasing inlet temperature. When bringing in a gas with a higher temperature while keeping the cooling temperature constant, the temperature difference between the cold mirror and warmer gas increases. This can be explained by Newton's law of cooling which says that the convective heat flux is a product of the convective heat transfer coefficient and the difference in temperature of the gas in the chamber and the mirror. When the heat flux is positive to the surface, the warm gas is heating the colder mirror. As the gas is getting colder and the mirror warmer, the error on the measured temperatures will increase. [46]

Table 7.4: Temperature at the center of the mirror compared to the temperature measured by the thermometer for different inlet temperatures

T_{inlet}	$T_{thermometer}$	T_{mirror}	$\Delta T_{thermometer,mirror}$
298.15 K (25°C)	253.19 K	253.56 K	0.37
308.15 K (35°C)	253.20 K	253.65 K	0.45
318.15 K (45°C)	253.21 K	253.74 K	0.53
373.15 K (100°C)	253.25 K	254.24 K	0.99

7.4 Case 3: Significance of different cooling temperatures

In this case several cooling temperatures have been tested while keeping the other parameters constant. This way the effect of the varying temperature will be visible in the presented graphs and tables. The cooling temperatures and pressures are selected based on the phase envelope for the natural gas, presented in Figure 7.15, since this is the area where the dew will appear.

The cooling temperatures and pressures selcted are shown in Table 7.5, along with the other parameters used for this case. When using different temperatures and pressures, new constant values for density, heat capacity and conductivity are implemented as material properties in COMSOL. These values are given in Appendix A.1.
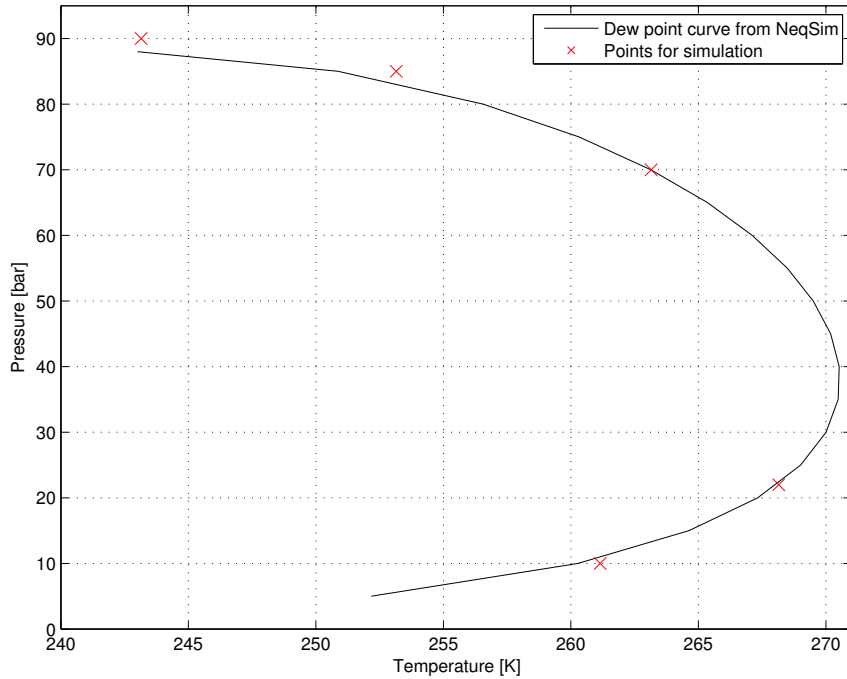
Figure 7.15: Dew point curve created from NeqSim for the natural gas. Selected points marked in red.

Table 7.5: Case 3 parameters

Setting	Value
Inlet gas	Natural gas
Inlet temperature	318.15 K (45 °C)
Gas inlet velocity	0.002 m/s (400 cc/h)
CO_2 cooling temperature and accompanying pressure	243.15 K(-30 °C), 90 bar
	253.15 K(-20 °C), 85 bar
	261.15 K(-12 °C), 10 bar
	263.15 K(-10 °C), 70 bar
	268.15 K(-5 °C), 22 bar

The tendencies and shapes of the graphs of the temperature across the mirror and through the solids are similar in this case as for the previous ones and are therefore not included in this section.

Accuracy of the dew point measurements

Also here is the difference between the temperature at the center of the mirror compared to the temperature at the point where the thermometer is placed. The results, presented in Table 7.6, show that a small temperature difference between the CO_2 cooling temperature and the temperature of the inlet gas gives more accurate results. The simulation of a 10 bar system and a cooling temperature of 261.15 K reveals that the cooling of the gas is not only dependent on the temperature difference in the chamber, but also on the pressure used. When moving from the top down on the phase envelope, the error of measured temperature decreases. This shows that the uncertainty when operating the dew point meter in the lab is higher at higher operating pressures.

Table 7.6: Temperature at the center of the mirror compared to the temperature measured by the thermometer for different cooling temperatures

P	T_{CO_2}	$T_{thermometer}$	T_{mirror}	$\Delta T_{thermometer,mirror}$
90 bar	243.15 K (-30 °C)	243.22 K	243.94 K	0.71
85 bar	253.15 K (-20 °C)	253.21 K	253.74 K	0.53
70 bar	263.15 K (-10 °C)	263.19 K	263.55 K	0.36
22 bar	268.15 K (-5 °C)	268.17 K	268.35 K	0.18
10 bar	261.15 K (-12 °C)	261.17 K	261.31 K	0.15

Changing the pressure affects the thermal conductivity of the gas by changing the density and the mean free path of the molecules. The mean free path is the average distance that a molecule can travel without colliding with another molecule. As the pressure increases, the density increases proportional to pressure and the mean free path decreases inverse of the pressure. In an ideal gas these values neutralize each other and the thermal conductivity is then independent of pressure. As for a real gas, taking the intermolecular forces into account, the pressure will affect the thermal conductivity. The dependency will increase with increasing deviation from the ideal gas behavior [47]. As mentioned in the beginning of this chapter the deviating factor between ideal and real gases, the compressibility factor, increases at higher pressure. As this factor increases, the system's thermal conductivity's dependence of pressure increases. When the hydrocarbon dew point unit operates at different pressures, the thermal conductivity in the gas will increase at higher pressures. This will result in higher heat transfer in the gas and between

the gas and the solid mirror, and may explain how the error in the measured temperature and the temperature on the surface of the mirror is dependent on pressure.

7.5   Case 4: Significance of different inlet velocities

To see the systems dependence of the inlet velocity of the gas, four different velocities were compared using the parameters in Table 7.7. Three laminar, 0.001 m/s, 0.002 m/s and 0.004 m/s and one turbulent, 0.03 m/s. The Reynolds numbers indicating the type of flow is presented in Section 6.3 and have been calculated using Equation 5.3.

Table 7.7: Case 4 parameters

Setting	Value
Inlet gas	Natural gas
Inlet temperature	318.15 K (45°C)
CO_2 cooling temperature	253.15 K (-20°C)
Gas inlet velocity	0.001, 0.002, 0.004, 0.03 m/s
Constant pressure	85 bar

Because of the limited computational power the κ-ε turbulence model was used to simulate the turbulence case. When first looking at the results, the values obtained from the turbulent simulation were unrealistic. The temperature at the mirror surface for the simulation at 0.03 m/s was almost at the inlet temperature of 318.15 K. The temperature at the start of the solid plot showed a massive drop in temperature over a distance of 0.05 mm and the temperature difference between the thermometer and the mirror was 55.52 K. These results would possibly have been different if the low-Re κ-ε model had been used instead of the κ-ε model, see Section 6.3. As mentioned previously, the κ-ε model uses wall-functions and is therefore not accurate close to the walls (i.e. the mirror surface), whereas the low-Re κ-ε model calculates for the entire domain by assuming laminar flow close to the walls. Because of this, the cut line was moved slightly into the mirror material for the turbulent simulation, at 0.03 m/s, in order to get a more realistic solution, this is the solution presented in the following graphs and table.

Figure 7.16 shows the difference in temperature across the middle of the mirror surface. As can be seen, the three laminar simulations with relatively low velocity have all been quickly cooled down to the mirror temperature. The turbulent flow, with a much higher velocity, holds a slightly higher temperature at the mirror surface. It is clearly visible that the simulation with the lowest velocity has the lowest temperature. When the velocity is increased, the cooling is not as effective. From the graph it is also clear that the temperature difference between the four different simulations is smaller at the cold center of the mirror. The turbulent simulation holds a slightly higher temperature than the three laminar simulations, but shows the same tendency.
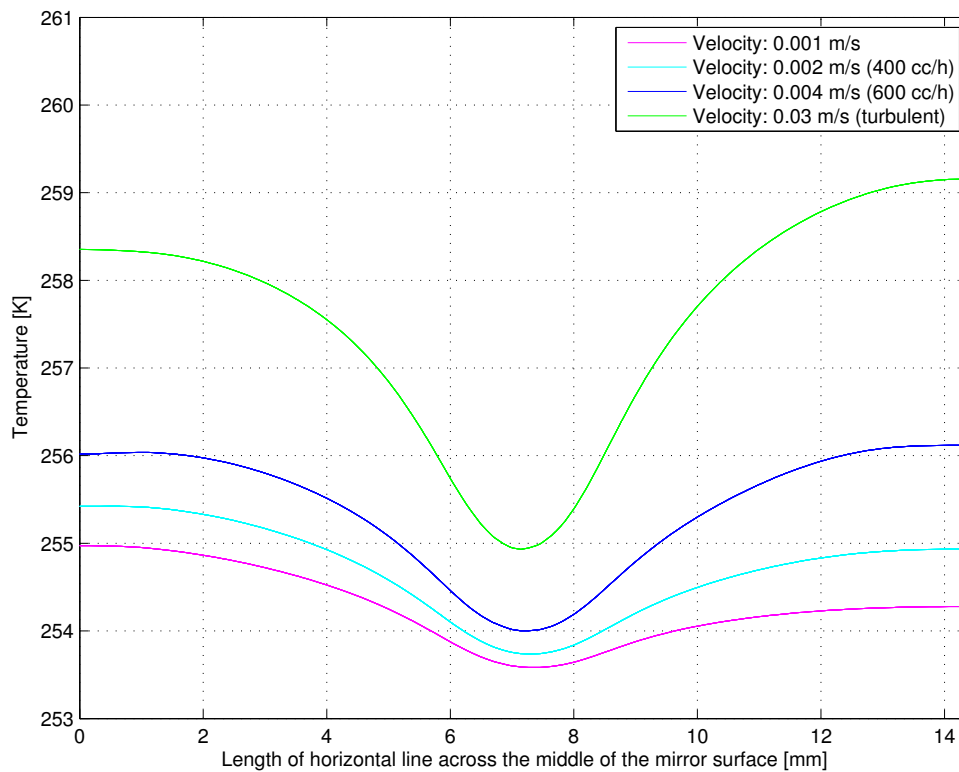
Figure 7.16: Comparison of the temperature distribution horizontally across the mirror surface when simulating with different velocities

Accuracy of the dew point measurements

Table 7.8 shows the difference between the temperature at the center of the mirror and the temperature measured by the thermometer, when using different velocities. The table shows that the temperature difference for the three laminar solutions is not massively affected by the

change in velocity. But for the highest velocity (0.03 m/s) there is a much higher temperature difference between the thermometer and the mirror. This can be explained by the Reynolds number increasing for increasing velocity, which in turn increases the Nusselt number and thereby increases the heat transfer coefficient.

Table 7.8: Temperature at the center of the mirror compared to the temperature measured by the thermometer for different velocities

Velocity	$T_{thermometer}$	T_{mirror}	$\Delta T_{thermometer, mirror}$
0.001 m/s	253.19 K	253.59 K	0.40
0.002 m/s (400 cc/h)	253.21 K	253.74 K	0.53
0.004 m/s (600 cc/h)	253.23 K	254.00 K	0.77
0.03 m/s (turbulent)	253.32 K	254.94 K	1.62

Velocity close to the mirror surface

Figure 7.17 shows the velocity close to the mirror surface for a laminar simulation, at $u_{in} = 0.002$ m/s. The values are taken 0.1 mm away from the mirror surface. As can be seen from the graph, the gas circulating close to the mirror surface holds a much lower velocity than when entering the chamber with a velocity of 0.002 m/s. At the upper section of the mirror the velocity is approximately zero. The gas has a slightly higher velocity with a maximum of $3.7 \cdot 10^{-9}$ m/s in the area parallel to the path where the gas flows directly from the inlet to the outlet, but it is still significantly slower than the inlet velocity of the gas. This also explains why the gas at the top of the mirror is colder than the gas at the bottom of the mirror, since the gas is basically stagnant in this area.

Figure 7.18 shows the velocity on the mirror surface for a turbulent simulation, at $u_{in} = 0.03$ m/s. The velocity on the mirror surface for this simulation is much higher than for the laminar simulation, as can be seen in the colour legend in the figure. Here the highest velocity is 0.034 m/s, which is higher than the velocity of the gas when it enters the chamber, whereas the lowest velocity is 0.0017 m/s. Also here is the gas circulating slower at the upper part of the mirror than the lower part, as it was for the laminar simulation discussed previously. But there is also a circulation at a higher velocity on the right side of the mirror, where the gas flowing from the inlet but that does not exit directly through the outlet, is circulated in the chamber.
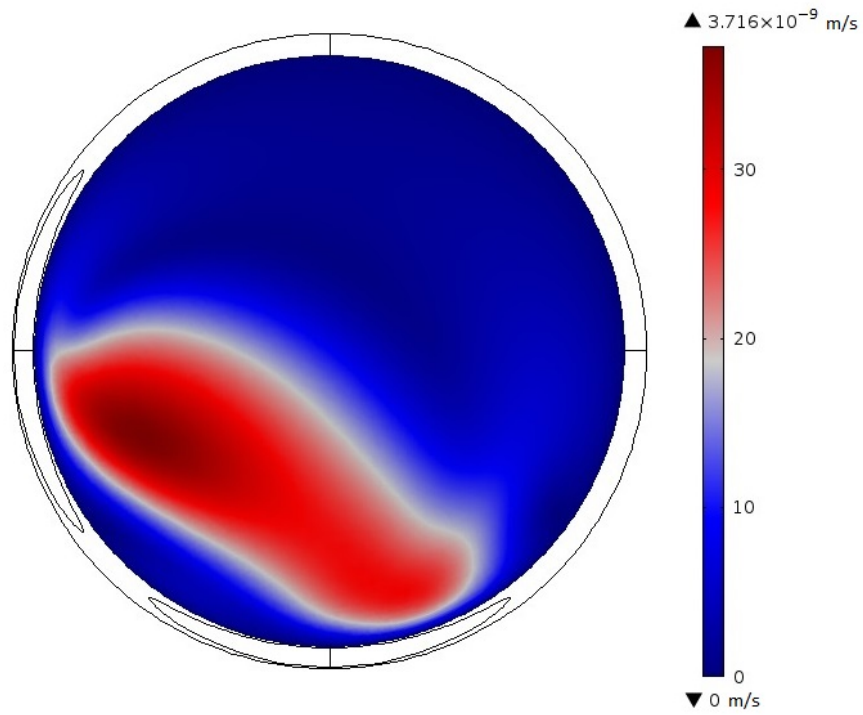
Figure 7.17: Velocity 0.1 mm from the mirror surface, $u_{in} = 0.002$ m/s
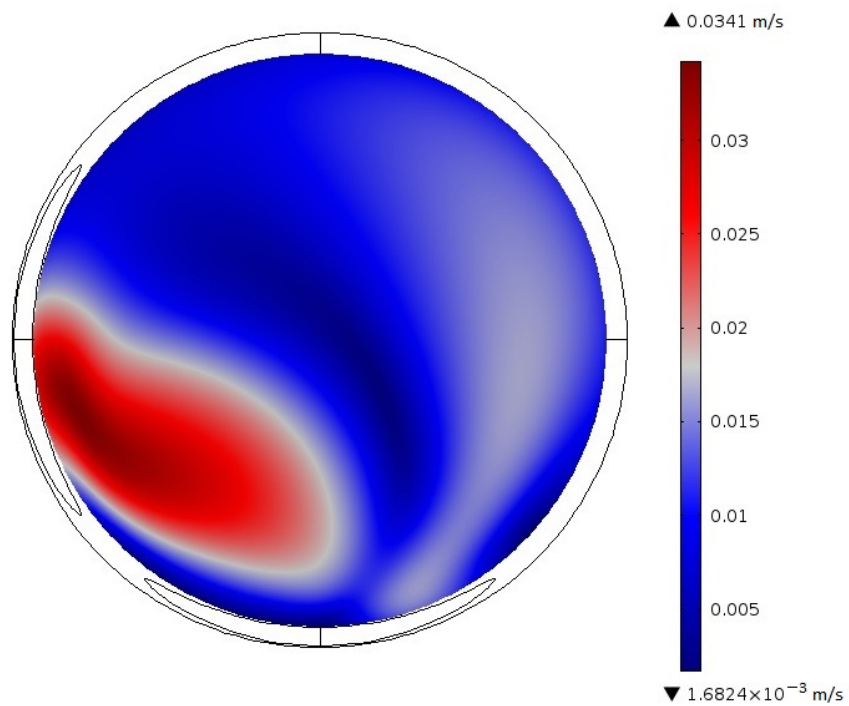
Figure 7.18: Velocity 0.1 mm from the mirror surface, $u_{in} = 0.03$ m/s

The results in this case are dependent on the depth of the chamber and the distance from the mirror to the inlet and outlet. The values used for the geometry in this thesis are based on approximate measurements, since the geometry of the unit made it difficult to do proper measurements inside the chamber.

7.6   Case 5: Mass transfer and compositional gradients

In this case it was desirable to find out if the temperature gradients in the unit would affect the composition of the gas as it reaches the mirror that holds a different temperature. When using the Transport of Concentrated Species user interface, the thermal diffusion coefficient is implemented in COMSOL as a reference to the contribution of the Soret effect. The theory behind the effect is studied in Section 4.3. As a recap, the effect will cause the heavier molecules to diffuse less rapidly than the lighter components and travel to the areas of a colder temperature. If this effect is of importance, the gas mixture will separate and the heavier components will gather in the colder areas of the unit. This way the composition will vary inside the chamber as it reaches the mirror and can give a different dew point temperature than expected.

For simplicity reasons a binary gas mixture has been used for this simulation. The binary gas has the composition presented in Table 6.1, and consists of methane and n-heptane. Because of the importance of density in this specific case, a polynomial value is used to calculate the density of the gas. This polynomial, compared to a constant value of density, will be discussed in Section 7.7. As an input to the Transport of Concentrated Species user interface in COMSOL, under the branch for Convection and Diffusion, both the binary- and thermal diffusion coefficients are calculated and implemented. Parameters used can be found in the following tables (see Table 7.9 to 7.11).

M represent the molar mass, x the mole fraction and ω the mass fraction, for species i. By using the equations presented in Section 4.3 about thermal diffusion, the diffusion coefficients have been calculated and are listed in Table 7.11. The reference temperature used is the mean temperature, T_m, calculated using Equation 4.7.

Table 7.9: Case 5 parameters

Setting	Value
Inlet gas	Binary mixture
Inlet temperature	45
CO_2 cooling temperature	Mean temperature of inlet and cooling temperature is given in Table 7.11
Gas inlet velocity	0.002 m/s (400 cc/h)
Constant pressure	Given in Table 7.11

Table 7.10: Values of the components present in the gas mixture at the inlet

Parameter	Methane	Heptane
M_i	0.01604 $\frac{kg}{mol}$	0.10021 $\frac{kg}{mol}$
x_i	0.999	0.001
ω_i	0.994	0.006

Table 7.11: Values of diffusion coefficients

$P[bar]$	$T_{CO_2}[K]$	$T_m[K]$	$D_{AB}[\frac{m^2}{s}]$	$D^T_{methane}[\frac{kg}{m \cdot s}]$	$D^T_{heptane}[\frac{kg}{m \cdot s}]$
10	258.15	286.06	$8.005 \cdot 10^{-7}$	$-8.373 \cdot 10^{-9}$	$8.373 \cdot 10^{-9}$
20	268.15	291.73	$4.142 \cdot 10^{-7}$	$-8.646 \cdot 10^{-9}$	$8.646 \cdot 10^{-9}$
40	268.15	291.73	$2.071 \cdot 10^{-7}$	$-8.972 \cdot 10^{-9}$	$8.972 \cdot 10^{-9}$
60	263.15	288.91	$1.357 \cdot 10^{-7}$	$-9.267 \cdot 10^{-9}$	$9.267 \cdot 10^{-9}$
70	253.15	283.18	$1.123 \cdot 10^{-7}$	$-9.404 \cdot 10^{-9}$	$9.404 \cdot 10^{-9}$
80	243.15	277.30	$9.475 \cdot 10^{-8}$	$-9.579 \cdot 10^{-9}$	$9.579 \cdot 10^{-9}$

When running the simulations with the parameters given in Table 7.11 it was of interest to see if the mixture had changed its composition when experiencing temperature gradients inside the chamber. To check this, the mole fraction of heptane at the inlet is compared to the mole fraction at the center of the mirror. The reason for using this point, is because this is where the dew appears and is therefore the point of interest. The change in composition and how this impacts the dew point temperature is given in Table 7.12 and illustrated in Figure 7.19. The dew point temperature is calculated in NeqSim and illustrates the magnitude of the Soret effect when using these specific parameters. Figure 7.19 shows the dew point curve based on the initial composition of the gas as it enters the chamber and the red crosses show the dew points affected by the compositional gradients.
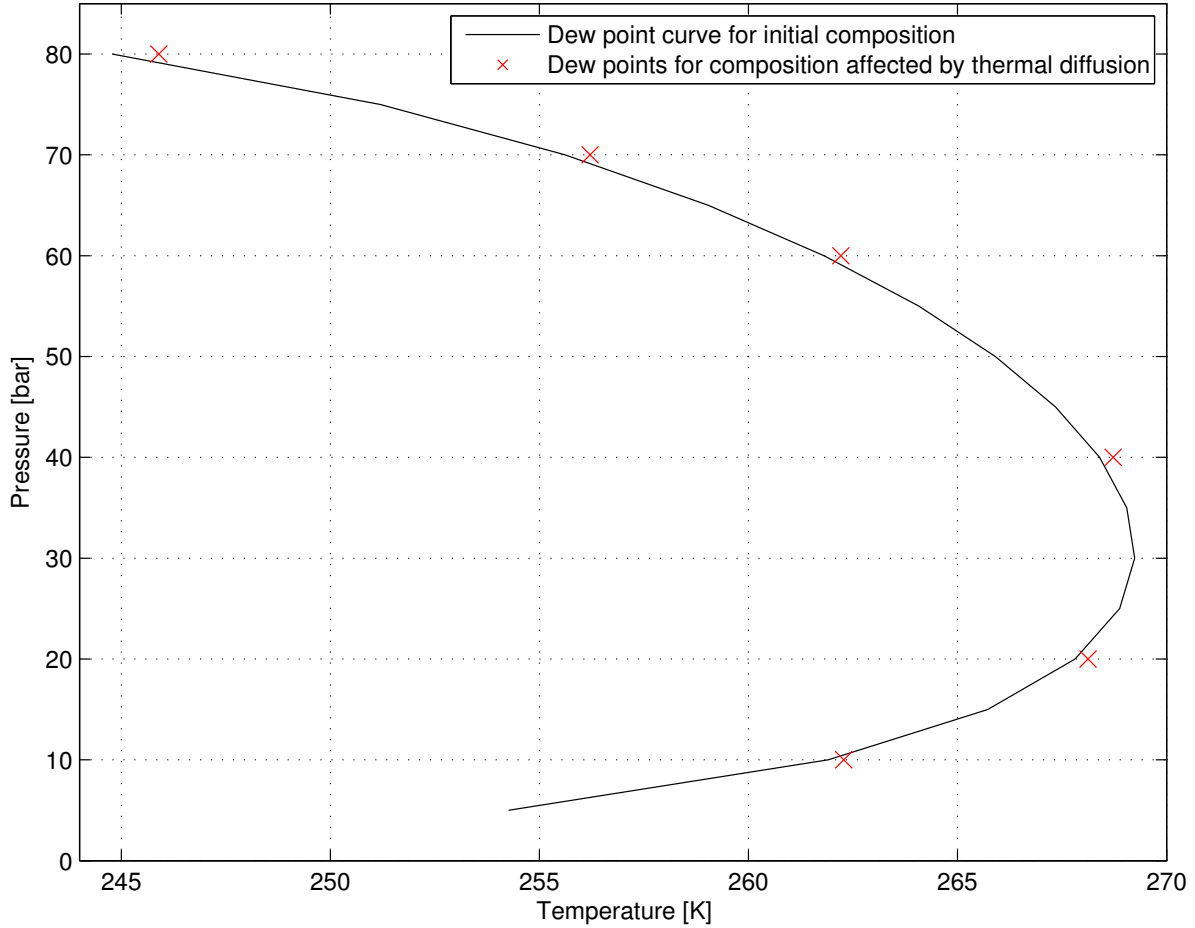
Figure 7.19: Initial dew point curve and dew points affected by compositional gradients

Table 7.12: New mole fractions of heptane and new dew point temperatures

$P[bar]$	$T_m[K]$	$x_{heptane,new}$	$\Delta x_{heptane}$ $(x_{hep,new} - x_{hep,old})$	$T_{dew,new}[K]$	$\Delta T_{dew}[K]$ $(T_{dew,new} - T_{dew,old})$
10	286.06	0.00102432	$2.5 \cdot 10^{-5}$	262.28	0.37
20	291.73	0.00101800	$1.8 \cdot 10^{-5}$	268.12	0.31
40	291.73	0.00101625	$1.6 \cdot 10^{-5}$	268.72	0.32
60	288.91	0.00101731	$1.7 \cdot 10^{-5}$	262.21	0.40
70	283.18	0.00102214	$2.2 \cdot 10^{-5}$	256.21	0.60
80	277.30	0.00102733	$2.7 \cdot 10^{-5}$	245.90	1.11

Some deviations were found when comparing the dew point temperatures calculated based on the new composition on the mirror to the dew point temperatures for the initial composition. The results from the 10 bar simulation deviates from the trend seen in the other results and deserves more study, but limited time did not make it possible to do a more thorough investiga-

tion. Disregarding the simulation with a pressure of 10 bar, Table 7.12 shows that an increase in pressure gives an increase in dew point uncertainty, here up to 1.11 K at 80 bar.

The dew point calculation in NeqSim can be sensitive to pressure, and can give some deviation for dew point temperatures at high pressures. Because of this, the 40 bar simulation has been used further in this case to see the compositional gradients at the surface of the mirror.
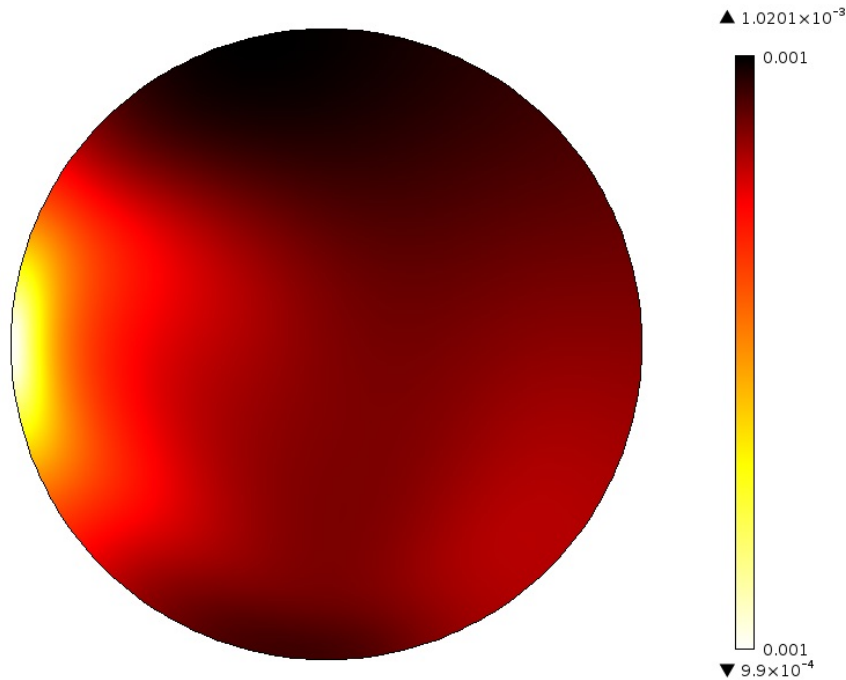
Figure 7.20: Mole fraction of heptane

Figure 7.20 shows the change in concentration of the heaviest component, heptane. As can be seen from the colour legend in the figure, the mole fraction of heptane has a change of $2.665 \cdot 10^{-5}$ across the surface when the mirror experiences a temperature difference of 0.9 K. According to the theory presented earlier in this section, it was expected that the heavier components would gather at the cold area in the center of the mirror. Instead, the bulk of heptane accumulates at the upper part of the surface and in the bottom just above the outlet. A possible reason for this might be that when using a velocity of 0.002 m/s the gas circulates at the upper area with a significantly lower velocity than the gas taking a 90 degree bend downwards moving straight to the exit. To see if the velocity and the flow pattern have an effect on this tendency of diffusion and separation of the mixture, the same simulation was carried out only changing the

velocity to nearly zero (10^{-7} m/s) . This low velocity will not give the same circulating motion in the upper part of the chamber as seen at higher velocities.
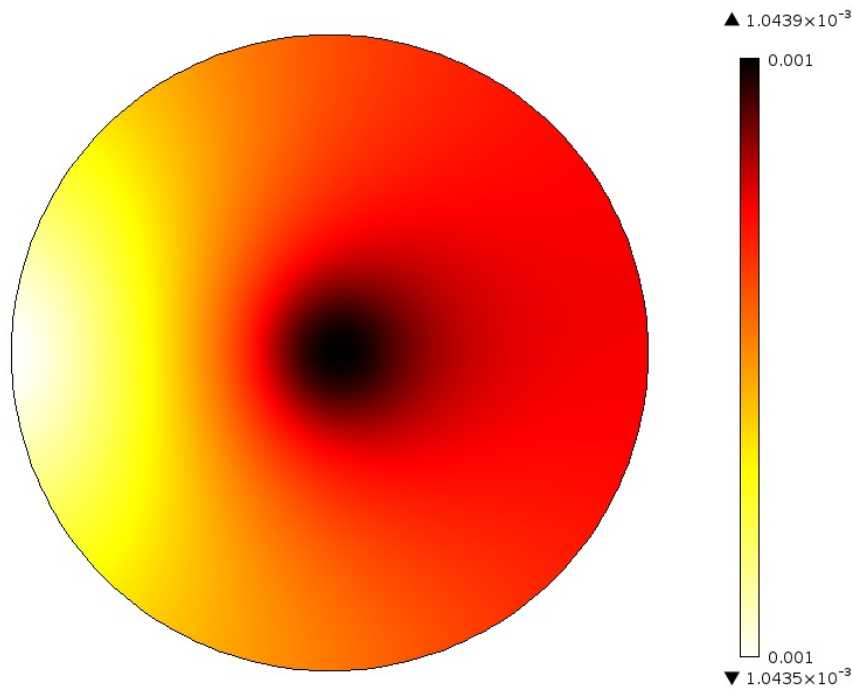
Figure 7.21: Mole fraction of heptane when using a very low gas velocity.

The diffusion on the surface presented in Figure 7.21 gives a result which is more in accordance with the theory of the Soret effect. The highest mole fraction of heptane is in the center of the mirror where the coldest point is located. It is generally higher on the right side, where the gas flow has been cooled, than the left side where the warmer gas flow enters the chamber. The accumulation of the heavier component, heptane, is clearly dependent on the temperature of the mirror, as can be seen in the corresponding temperature plot in Figure 7.22. Their similarities of their tendency of change can easily be seen when comparing the two figures.

The compositional gradients in these cases are not massive, but one can see some variation in the composition. Given the results from velocities of $2 \cdot 10^{-3}$ m/s and 10^{-7} m/s in a 40 bar system, the phenomena of thermal diffusion is clearly present in the dew point unit. The diffusion is dependent of temperature and also the velocity and direction of the flow. When using the velocity already in use in the rig at Statoil Rotvoll, the slower circulation in the upper part of the chamber results in accumulation of the heavier components in this area, and not only at the coldest point
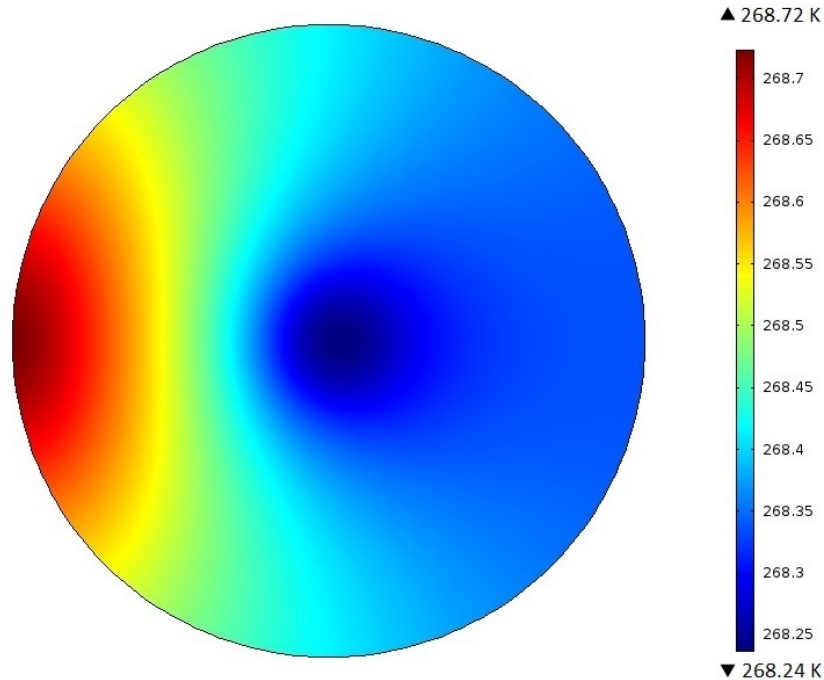
Figure 7.22: Temperature distribution on the surface of the mirror to the corresponding mole fraction of heptane when using a gas velocity close to zero.

in the middle of the mirror. The low velocity in the upper region causes longer detention time of the gas and thereby more time for it to cool and diffuse. A possible assumption for the high accumulation of heptane in the lower region of the mirror may be the phenomena which says that a suddenly cooled gas will fall due to the force of gravity. As the gas is getting colder, the density and weight of the gas will increase. When this happens, the particles may fall further down on the surface than the gas that has not yet been cooled properly. The high accumulation of heptane in the center of the mirror, at 40 bar, causes an increase in mole fraction of $4.4 \cdot 10^{-5}$. This results in a dew point temperature 0.86 K higher than for the initial composition and 0.5 K higher than when using a velocity of 0.002 m/s. Even though the low velocity causes the gas to cool closer to the cooling temperature, it also result in higher accumulation of the heavier components at the center of the mirror where the dew point is measured. Further studies on this topic has been recommended for future work, as limited time did not make it possible to investigate this topic further in this thesis.

7.7 Case 6: Assessing errors from real dew point and dew point determined by the technique.

In this case will both the errors found from the simulations related to the dew point apparatus and errors related to the simulations be discussed. Where it is possible these errors will be compared with values found in literature.

As mentioned in the literature review, Section 3.3, the SRK EoS provides a dew point lower than what is observed in the laboratory. For a light SNG with added n-heptane, like the binary mixture used in this thesis, the model predicted too high cricondentherm and too low cricondenbar. For pressures up to 20 bar, the results were in accordance with experimental results. But for higher pressures it predicted too low HCDP. Since all the parameters used in this thesis are based on the SRK EoS, this is an uncertainty in the results. In Section 3.2 the SRK EoS is said to give dew points that are 5.60-8.30 K higher than what is measured experimentally and for richer gas compositions, the predicted dew point is up to 14 K lower than the actual dew point.

When the apparatus is used the dew point temperature is measured both when the dew formes as the gas is cooled and when the dew evaporates as it is heated, the two temperatures can not vary more than 1 K for the measurement to be valid, as mentioned in Section 4.1. Also, as mentioned in Section 3.4, the measurements with the manual chilled mirror apparatus are very subjective and measurements performed by different operators on the same gas sample have been proved to give deviations of up to 2.60 K.

The variations in measurement errors found in the simulations are presented in Table 7.13. When looking at the highest velocity, inlet temperature, cooling temperature and pressure, the maximum error is 1.62 K. This shows that all the errors found in this thesis are smaller than the human errors and the errors from the SRK EoS model, and may therefore not to be noted when using the equipment.

Table 7.13: Summary of the measurement errors found by the simulations

Case	Error, min	Error, max	Comment
Case 2	0.37 K	0.99 K	Error increases for higher temperature difference
Case 3	0.15 K	0.71 K	Error increases for higher temperature difference and for higher pressures
Case 4	0.40 K	1.62 K	Error increases at higher velocities
Case 5	0.31 K	1.11 K	Error increases with increasing pressure

When simulating on an 85 bar system an inlet temperature difference of 10 K results in a temperature difference of 0.09 K at the coldest point on the mirror. This applies to the inlet temperatures of 298.15, 308.15 and 318.15 K. In the lab, the gas sample will be circulated back and forth, and because of this the difference of 0.09 K for one circulation is not substantial. When simulating for higher temperatures, as 373.15 K, the temperature at the center of the mirror is 0.5 K higher than for an inlet temperature of 318.15 K. There exists some errors between the measured temperature by the thermometer and the actual temperature on the mirror. This error ranges from 0.37 K to 0.99 K for the given parameters. What can be seen in the case study is that this error increases as the temperature difference in the chamber increases. The temperature difference between the mirror and the inlet gas varies from 45 K to 120 K. When raising the inlet temperature from 308.15 to 318.15 K, the error increases with 0.08 K.

By varying the cooling temperature and pressure, it is clear that the heat transfer in the unit is dependent on the pressure used during operation. Increasing the pressure will increase the uncertainty of the temperature measured by the thermometer. The errors found was 0.15 K at 10 bar and 261.15 K and 0.71 K at 90 bar and 243.15 K.

As mentioned in Section 3.4, the recommended flow rate by Chandler Engineering [27] is 0.01314 *cc/h* (0.643 *m/s*) or lower. The flow rates tested here are all within this specification, but a conclusion that can be drawn from the results in case 4 is that a velocity of 0.03 m/s is too high for the gas to cool down properly in a 85 bar system. Another factor that has to be kept in mind is that when using the κ-ε model instead of the low-Re κ-ε model the result has an error of approximately 0.50 K, as discussed in Section 6.3. When testing different velocities the result gives an error between the measuring points of 0.40 K at 0.001 m/s and 1.62 K at 0.03 m/s.

The diffusivity in the chamber causes compositional gradients as the temperature changes towards the mirror. When calculating dew points of the new gas composition at the center of the mirror, some variation is found. The new dew point temperatures compared to the ones calculated on the inlet composition is deviating by 0.31 K at 20 bar and 1.11 K at 80 bar. In this case, the error of dew point measurements increases as the pressure increases.

There may be some errors associated with the geometry of the model used for simulations and the thermodynamic restrictions added to the model. Especially the depth of the chamber and the isolation of the unit is worth mentioning. The depth of the chamber can affect the circulation and velocity of the gas. Blocking the heat transfer between the copper rod and the surroundings, may have caused too low temperature measured by the thermometer. This would have decreased the errors found by the measuring points.

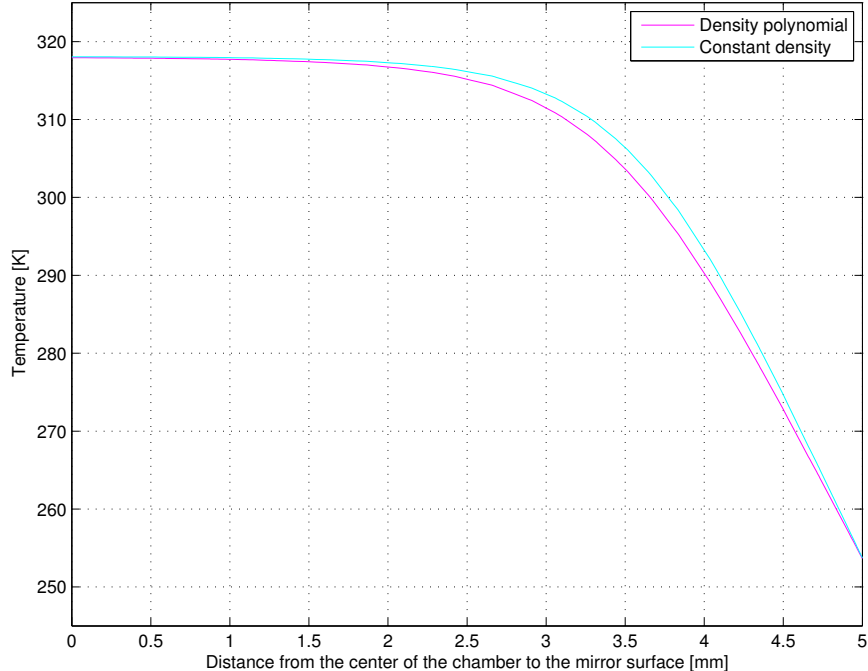**Error related to using constant density**

Figure 7.23: Comparing the constant density and the density polynomial, looking at the temperature change in the chamber for T_{in}=318.15 K, T_{CO2}=253.15 K and p=85 bar.

The density is dependent on temperature and pressure, and because of the significant temperature differences in the unit a varying density has been tested against a constant density value. Using constant values instead of continuously calculated values with NeqSim also gives a small error. Looking closer at the difference between using a constant density and using a density polynomial on the form $\rho(T) = \rho_m\left(\frac{T_m}{T}\right)$ gives the result that can be seen in Figure 7.23. The result shows a temperature difference of about 0.2 K at a distance 1.3-2 mm from the mirror surface. 0.5 mm from the mirror there is almost no difference, the same for more than 3 mm away from the mirror.

A simulation was carried out to compare the difference in mirror temperature due to a constant density and a changing density of the gas. In case 2, Section 7.3, a simulation was performed using an inlet temperature of 373.15 K and a mirror temperature of 318.15 K at 85 bar. Because of this significant temperature difference it was of interest to see if a changing density would affect the results. Two scenarios are investigated, Figure 7.24 shows a simulation of low pressure and a small difference in chamber temperature while Figure 7.25 shows the case using high pressure and a great difference in chamber temperature, as mentioned above. The result from this comparison show that there exists an uncertainty when using high pressures and large difference in inlet gas and mirror temperature. The use of constant values for density gives here an uncertainty between 0 and 0.22 K at the coldest point in the middle of the mirror. When using constant values for the density, the value is taken according to the temperature at the surface of the mirror. When the polynomial value is used, a mean temperature between the inlet gas and the chamber is used to estimate the density. This explains the significant difference in the temperatures at the inlet (left) side of the graph in Figure 7.25.

Figure 7.24: Comparing the temperature across the mirror for the polynomial and the constant density, for T_{in}=318.15 K, T_{CO2}=268.15 K and p=22 bar

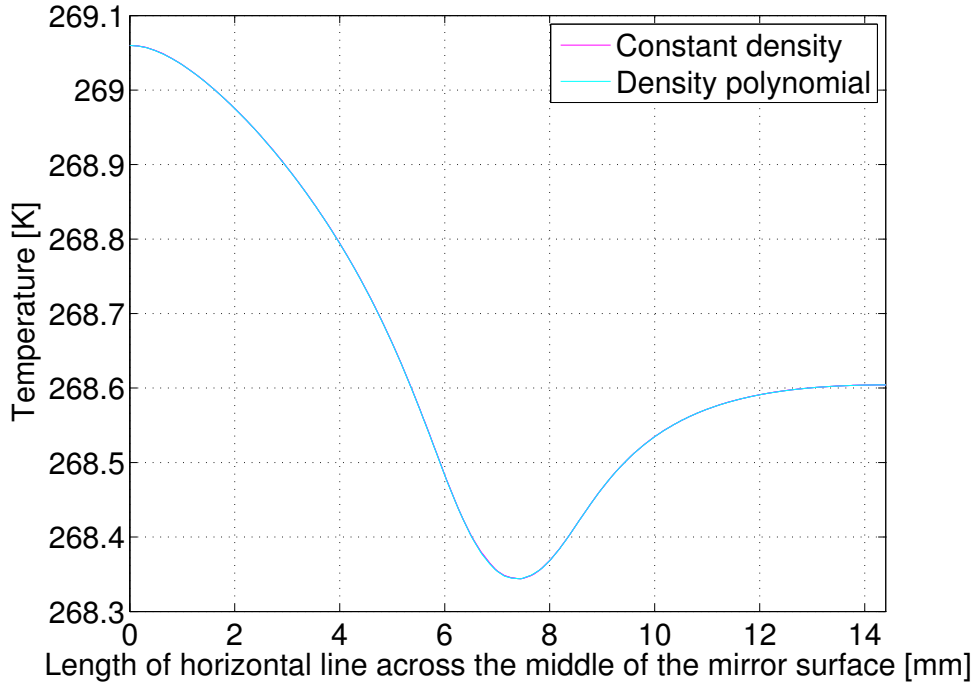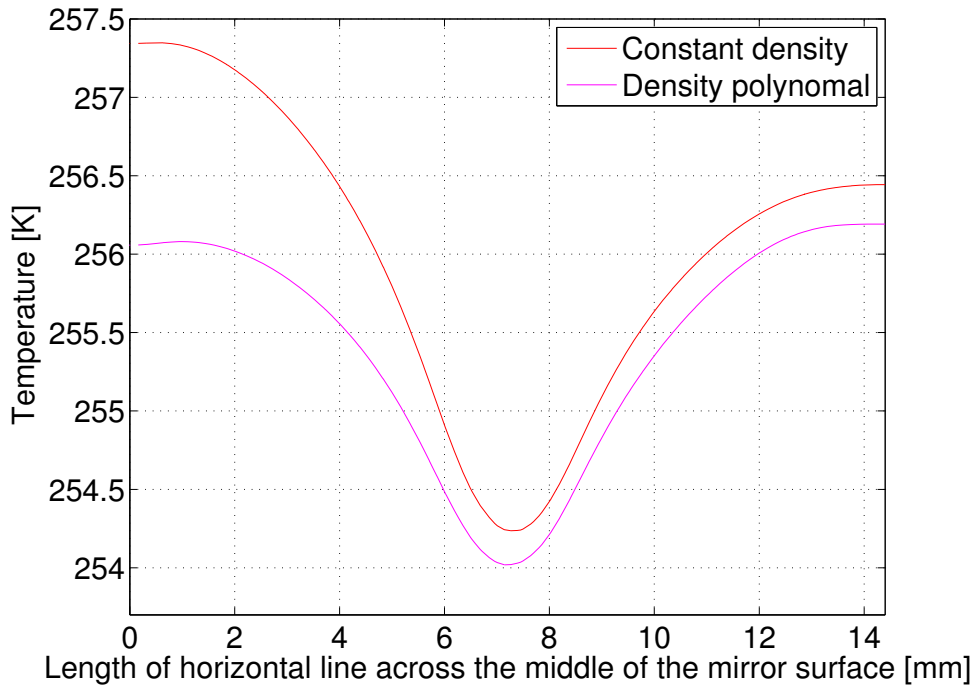Figure 7.25: Comparing the temperature across the mirror for the polynomial and the constant density, for T_{in}=373.15 K, T_{CO2}=253.15 K and p=85 bar.

7.8   Trial and error

Several weeks were spent on finding an optimal 3D representation of the model, to find the best modules and settings to use in COMSOL and to test many different meshes.

A lot of time was also spent on trying to implement NeqSim into COMSOL. It was assumed that this would eventually work, so not much time was spent on finding alternative material properties and polynomial values to use for the simulations. When it became clear that it would not be possible to implement NeqSim, material properties had to be chosen quickly in order to start getting results. Because of this, and because of test simulations showing that there was only a small variation in temperature across the mirror, it was decided to proceed with constant values provided by NeqSim. However, NeqSim is continually being developed, so for future work it is recommended to try to implement NeqSim.

Another issue was the low Reynolds number κ-ε turbulence model. This model increases the simulation time drastically. A HPC cluster at NTNU, called Kongull, was therefore used in order to reduce the simulation time. This worked very well using only the κ-ε model. But a problem that arose was when trying to run the simulation first with the κ-ε model, then using the result as a basis for the low-Re κ-ε model, as is needed when using that turbulence model. Trying many different approaches, Kongull would either just run the first or the second study or overwrite the first study with the second. This was eventually abandoned. After doing a test on the difference between the κ-ε model and the low-Re κ-ε model, as shown in 6.3, it was decided to proceed with only the κ-ε model, but keeping in mind that there exists a small variation.

Chapter 8

Summary

8.1 Discussion

Simulations have been carried out using both constant and varying parameters such as inlet temperature, cooling temperature, pressure and velocity. In addition has the magnitude and significance of the diffusion and the Soret effect in the unit been studied. All together have these cases provided results that increase the fundamental understanding of the dew point unit and uncover uncertainties associated with the use of the unit. Yet there are some uncertainties connected to the method and the results, that will be discussed in this section. The results from the simulations will be presented along with a discussion of the importance of these results.

Simulations confirm that the coldest point on the mirror is in the center where the back of the mirror is in direct contact with the cold copper. This is where the first dew will appear. The temperature at this point on the mirror is currently being measured with a thermometer a couple of millimeters behind the mirror. When comparing the measured temperature and the actual temperature on the center of the mirror surface there exists some differences. Errors ranging from 0.15 to 1.62 K are found. The lowest difference of 0.15 K is found at low constant pressure of 10 bar. High temperature difference in the chamber, i.e. high inlet temperature and low tempera-

ture of the cooling, gives an error of 0.99 K for the parameters used. The greatest error, of 1.62 K, is found as the flow pattern evolves to turbulence due to high velocity. As can be seen from the tendencies of the temperature differences in the presented cases, the pressure and the temperature difference in the chamber have an impact on this error. All the errors found in this thesis are smaller than possible human errors and the errors from the SRK EoS model, and therefore likely not to be noted when using the equipment. But it is still important to be aware that there exists a certain instrumental error related to the measurements.

Increasing the pressure in the unit will increase the thermal conductivity of the gas. The more the gas deviates from an ideal gas behavior, defined by the compressibility factor, the more is the conductivity dependent of pressure. Increasing the pressure will increase the compressibility factor, and also the conductivity's dependence on pressure. When the heat transfer in the unit is high, the heat from the warmer gas will contribute to a warmer mirror surface. The same happens as the difference in the chamber temperature increases. The difference between the temperature of the solid mirror and the temperature of the gas affects the convective heat flux as derived in Newton's law of cooling.

A possible source of error in these results may be that the model in COMSOL is isolated, and it is therefore no heat exchange to the environment, only within the unit itself. At the test rig at Statoil Rotvoll, the room around the unit holds a temperature of approximately 318 K. This means that the temperature difference inside the unit will then also exist outside the unit. The possibility of heat exchange from the cold cobber rod is not taken into account in these simulations. This would probably provide higher thermometer temperatures and thereby less errors associated with the measuring points.

The temperature of the gas close to the mirror is also affected by the flow pattern and the velocity of the gas. Most of the gas enters the chamber, takes a 90 degree bend, and exits at the bottom of the unit. The gas that hits the wall above the outlet, and has a high velocity, will mainly circulate at the upper area of the chamber before exiting. When the gas holds a high inlet velocity, the gas has shorter detention time in front of the mirror and is thereby not cooled as much as for lower

velocities. For the simulations with an inlet velocity of 0.002 m/s, providing a laminar flow, is the velocity at the top half of the mirror close to stagnant. This explains the colder temperature of the gas situated in this area. The velocity of the gas close to the mirror, at 0.1 mm distance, is significantly lower than at the inlet. The velocity close to the mirror varies between 0 and $3.72 \cdot 10^{-9}$ m/s. For a higher inlet velocity of 0.03 m/s, turbulent flow, the gas flow is also much slower at the top half of the mirror, but there is still a steady flow of gas circulating in this area. Here the velocity close to the mirror varies between 0.0017 m/s and 0.034 m/s. A problem related to the turbulent flow is the use of turbulence models for the simulations. Since the κ-ε model was used in this thesis, instead of the low-Re κ-ε model, some error is to be expected for the turbulent simulation. When comparing the two turbulence models on a simplified 2D model a difference of 0.5 K at the coldest point on the mirror was noted. Because of the simplified turbulence model, the laminar flow simulations provide more accurate results.

The flow pattern inside the chamber is highly affected by the geometry of the unit. Some of the measurements are assumed by observation of the unit because of difficulties to measure the dimensions inside the chamber. Documentation on the dimensions was not found. This applies mainly to the depth of the chamber, and also the length from the inlet to the mirror. This may be a possible source of error in the results.

The diffusion of the gas inside the chamber was studied to see if the Soret effect was visible, meaning that the heavier hydrocarbons migrate to the colder area in the chamber and the lighter components to the warmer area. This showed that there is an increase in the mole fraction of the heavier component, n-heptane, on the mirror surface. This resulted in an increase in dew point temperature between 0.31-1.11 K. When looking at where on the surface the n-heptane accumulates the result is not as expected according to the theory of the effect. The bulk of heptane accumulated at the upper and lower part of the mirror, instead of in the center of the mirror where the temperature is the lowest. The inlet velocity was then reduced to see if the effect could be seen more clearly at a lower velocity. When using an inlet velocity close to zero (10^{-7} m/s), the heptane accumulated in the coldest area at center of the mirror as previously expected. Here the circulation in the upper part is not present, and this is the reason for the different tenden-

cies of the the accumulation of heptane. The diffusion can therefore be said to be dependent on temperature, but also the detention time of the gas due to velocity and flow pattern. Close to due date, irregularities in the results at low pressures, namely 10 bar, was observed. Further studies should be done on this topic, as limited time did not make it possible to do a more thorough investigation in this thesis.

As for the simulations using different velocities, it may seem like the most credible velocity to use is the lowest at 0.001 m/s, since this gave the smallest measurement error. The case on thermal diffusion proves that this may not be the best option. As the velocity decreases, the Soret effect will be more dominated by temperature than the circulation of the gas in the chamber. When this happens, the accumulation of heptane will be at its maximum at the center of the mirror where the dew is formed. This will result in more deviating measurements of the dew point temperature. For instance will the dew point temperature for the simulation at 40 bar be 0.50 K higher with an inlet velocity close to zero than 0.002 m/s.

Case 1-4 was carried out using constant values for the density of the fluid. This may contribute to a certain error in the results. The density varies according to temperature, and because of big temperature differences in the unit it was of interest to find the magnitude of errors caused by this. Different methods have been tested to find a value for the uncertainty. Both the ideal gas law and a polynomial, as presented in Section 7.7, were tested. These values were compared to values given by NeqSim, which uses a far more complex system of equations to calculate the density. Results from these calculations showed that there exists an uncertainty between 0 and 0.22 K at the coldest point in the middle of the mirror, depending on the temperature difference in the chamber and the pressure used. When using constant values for the density, the value is calculated due to the cooling temperature. When the polynomial value is used, a mean temperature between the inlet gas and the chamber is used to estimate the density. Because of this is the magnitude of the error more significant at the inlet side of the mirror than at the coldest point in the center.

In addition to density are properties like heat capacity, conductivity and viscosity also kept con-

stant. The significance of this is not studied in this report but might have caused some devia-
tions in the results.

8.2   Conclusion

For this thesis, simulations were performed on a three dimensional model of a standard Bureau
of Mines dew point unit using the simulation software COMSOL Multiphysics. The aim of the
analysis was to improve the fundamental understanding of the dew point unit, to decrease un-
certainties related to the manual dew point test method and specifically to learn more about
heat transfer in the dew point unit and study the need for mass transfer modelling.

Simulations proved that the coldest point is the center of the mirror where the surface is directly
cooled by the copper rod. When varying the pressure, velocity, inlet and cooling temperatures
in the simulation a deviation between the measured temperature by the thermometer and the
actual temperature on the mirror is found. These errors range from 0.15 to 1.62 K depending on
the parameters used. Low pressure and smaller temperature difference in the chamber provide
more accurate results. The greatest error is found as the flow evolves to turbulence due to high
inlet velocity.

Using a high inlet velocity results in shorter detention time in front of the mirror and the gas is
thereby not cooled as much as for lower velocities. The geometry of the unit provides a circula-
tion of the gas in the upper area of the unit. For laminar flows, the velocity close to the mirror is
nearly stagnant in this region. This explains the low temperature in this area.

An increase in concentration of the heavier component at the cold mirror surface is observed
for a binary mixture of methane and n-heptane. This proves the Soret effect to be present and
shows that there are compositional gradients due to the change in temperature in the chamber.
The dew point temperatures calculated for the composition in the center of the mirror proved to
be 0.31-1.11 K higher than the dew point temperatures for the initial composition of the gas. The
bulk of the heavier component accumulates in the upper area of the mirror due to the low ve-

locity and low temperature. When testing for velocities close to zero the components migrate to the cold center of the mirror, which results in a higher deviation in the dew point temperatures.

8.3   Recommendations for future work

- It is recommended to implement NeqSim to get exact values for the simulations. If this does not work, polynomials should be used for the natural gas properties.
- Simulations implementing heat loss to the environment should be investigated to see if it influences the temperatures inside the unit.
- The Soret effect should be investigated further, by for instance following a streamline in COMSOL to see how the concentration of the natural gas changes in the chamber. An observation made when looking at the results from the simulations with the Transport of Concentrated Species interface was that the mole fraction of n-heptane accumulated differently on the mirror surface for different pressures and cooling temperatures. This should be studied further.
- Particle tracing in the chamber should be studied to see if this can be used to see where the particles accumulate.
- Compare photos taken of the dew on the mirror in the lab with the surface plot from the simulation, to see if, in the lab, the dew occurs in the same area that the simulations have said to be the coldest.
- Turbulent simulations should be run using the low-Re κ-ε model, if possible.
- Optimal geometry of the dew point unit should be studied. For instance by forcing the path of the gas from the inlet, past the mirror to the outlet.
- Optimal operating parameters (inlet velocity etc) should be found.
- The material of the seal should also be investigated, as well as the exact geometry and distance to the mirror from the tip of the copper rod where the thermometer is placed.

Bibliography

[1] B. Shimekit and H. Mukhtar, "Natural gas purification technologies–major advances for co2 separation and future directions," *Advances in Natural Gas Technology. Hamid, A.-M. ed. InTech China: In Tech*, pp. 235–270, 2012.

[2] A. Shaikh, "Oil and gas - vertical separator [internet]." Available from: `http://pipingdesigners.info/oil-and-gas-vertical-separator/`, 2012 Oct 30. [cited 2014 March 7].

[3] T. Austrheim, L. H. Gjertsen, and A. C. Hoffmann, "An experimental investigation of scrubber internals at conditions of low pressure," *Chemical Engineering Journal*, vol. 138, no. 1, pp. 95–102, 2008.

[4] A. S. Brown, M. J. Milton, G. M. Vargha, R. Mounce, C. J. Cowper, A. M. Stokes, A. J. Benton, D. F. Lander, A. Ridge, and A. P. Laughton, "Measurement of the hydrocarbon dew point of real and synthetic natural gas mixtures by direct and indirect methods," *Energy & Fuels*, vol. 23, no. 3, pp. 1640–1650, 2009.

[5] AMETEK, "Dew point testers [brochure]." AMETEK Inc, Pittsburgh, PA, 2009.

[6] ASTM Standard D1142, 1995 (2012), "Standard test method for water vapor content of gaseous fuels by measurement of dew point temperature," ASTM International, West Conshohocken, PA, 1995, DOI: 10.1520/D1142-95R12. http://www.astm.org.

[7] D. L. George, "Reducing measurement uncertainty in process gas quality measurements," *Proceedings of the 2006 International School of Hydrocarbon Measurement*, 2006.

[8] E. Skylogianni, "Measurements and modelling of hydrocarbon dew point of natural gases," [master thesis], NTNU, Trondheim, 2012.

[9] W. Frei, "Which turbulence model should i choose for my cfd application? [internet]." Available from: `http://www.comsol.com/blogs/which-turbulence-model-should-choose-cfd-application/.`, 2013. [cited 2014 Jan 17].

[10] Norwegian Petroleum Directorate, "Gas export from the norwegian shelf [internet]." Available from: `http://www.npd.no/en/Publications/Facts/Facts-2012/Chapter-7/.`, Apr 2012. [cited 2014 Jan 15].

[11] NaturalGas.Org, "Background [internet]." Available from: `http://naturalgas.org/overview/background.asp`, 2011. [cited 2014 Jan 15].

[12] A. Mert and A. Santiago, *Review on Natural Gas Thermophysical Property Measurement Techniques [open access chapter]*, ch. 3. Natural Gas - Extractions to End Use, InTech, 2012.

[13] A. Fredheim and E. Solbraa, "Gas processing [course material]," in *TEP4185: Natural Gas Technology*, NTNU, 2011.

[14] S. Mokhatab and W. A. Poe, *Handbook of natural gas transmission and processing*. Gulf Professional Publishing, 2012.

[15] T. Austrheim, *Experimental Characterization of High-Pressure Natural Gas Scrubbers*. Phd thesis, University of Bergen, 2006.

[16] J. Herring, "Finanical impact of accuarately measuring hydrocarbon dew point," in *90th Annual Convention of the Gas Processors Association*, 2011.

[17] A. Benton, "Dew point measurements in natural gas [internet]." Available from: `http://www.solversys.com/download/michell/CDII/Michell_HCDPMeas_en.pdf`, 2012. [cited 2014 April 29].

[18] J. A. Bullin, C. Fitz, and T. Dustman, "Practical hydrocarbon dew point specification for natural gas transmission lines,"

[19] J. Herring, "Hydrocarbon dew point is a critical consideration for pipeline operations," *Pipeline & Gas Journal*, vol. 237, no. 7, pp. 48–52, 2010.

[20] A. Brown, M. Milton, G. Vargha, R. Mounce, C. Cowper, A. Stokes, A. Benton, M. Bannister, A. Ridge, D. Lander, and A. Laughton, "Comparison of methods for the measurement of hydrocarbon dew point of natural gas," 2007.

[21] R. Jachowicz, J. Weremczuk, D. Paczesny, and G. Tarapata, "A mems-based super fast dew point hygrometer - construction and medical applications," *Measurement Science and Technology*, vol. 20, Oct 2009.

[22] D. L. George, A. M. Barajas, and R. C. Burkey, "The need for accurate hydrocarbon dew point determination," *Pipeline & Gas Journal*, Sept 2005.

[23] V. Louli, G. Pappa, C. Boukouvalas, S. Skouras, E. Solbraa, K. O. Christensen, and E. Voutsas, "Measurement and prediction of dew point curves of natural gas mixtures," *Fluid Phase Equilibria*, 2012.

[24] B. Rusten, L. Gjertsen, E. Solbraa, T. Kirkerød, T. Haugum, and T. Puntervold, "Determination of the phase envelope - crucial for process design and problem solving," in *GPA conference*, (Grapevine, Texas, USA), 2012.

[25] H. Warner, E. Leamer, A. Spence, R. Bone, R. Hubbard, J. Bernos, and W. Kriel, "Hydrocarbon dewpoint determination of lean natural gases," in *Proceedings 80th Annual Convention, Gas Processors Association*, 2001.

[26] C. Cowper, "Natural gas hydrocarbon dew point; comparison of measurement and calculation methods," in *2nd Gas Analysis Symposium & Exhibition*, 2002.

[27] AMETEK, *Chandler ScanScope and Dew Point Tester [user manual]*. AMETEK Inc, Pittsburgh, PA, 2005.

[28] E. Clouet, "Modeling of nucleation processes," *arXiv preprint arXiv:1001.4131*, 2010.

[29] wiseGEEK, "What is nucleation? [internet]." Available from: `http://www.wisegeek.org/what-is-nucleation.htm`, 2014. [cited 2014 April 29].

[30] J. K. Platten, "The soret effect: a review of recent experimental results," *Journal of applied mechanics*, vol. 73, no. 1, pp. 5–15, 2006.

[31] B. E. Poling, J. M. Prausnitz, and J. P. O'Connell, *The properties of gases and liquids.* McGraw-Hill New York, 5 ed., 2001.

[32] S. Kjeldsrup, D. Bedeaux, and E. Johannessen, *Elements of irreversible thermodynamics for engineers.* tapir academic press, 2006.

[33] R. B. Bird, W. E. Stewart, and E. N. Lightfoot, *Transport phenomena.* John Wiley & Sons, 2007.

[34] COMSOL, *Introduction to COMSOL Multiphysics [user manual].* COMSOL AB, 2013.

[35] COMSOL, *Introduction to CFD Module [user manual].* COMSOL AB, 2011.

[36] F. M. White, *Fluid Mechanics.* McGraw-Hill New York, 6 ed., 2008.

[37] COMSOL, *CFD Module User's Guide [user manual].* COMSOL AB, 2013.

[38] The Engineering ToolBox, "Thermal diffusion [internet]." Available from: `http://www.engineeringtoolbox.com/reynolds-number-d_237.html`. [cited 2014 May 03].

[39] J. H. Ferziger and M. Peric, *Computational Methods for Fluid Dynamics.* Springer, 2002.

[40] J. D. Freels, R. V. Arimilli, and I. T. Bodey, "Exploiting new features of comsol version 4 on conjugate heat transfer problems," in *COMSOL Conference*, 2010.

[41] COMSOL, *Chemical Species Transport Help Guide [user manual].* COMSOL.

[42] E. Solbraa, "Neqsim [internet]." Available from: `http://folk.ntnu.no/solbraa/neqsim/NeqSim.htm`. [cited 2014 Jan 24].

[43] Tibtech innovations, "Properties table of stainless steel, metals and other conductive materials [internet]." Available from: `http://www.tibtech.com/conductivity.php`, 2011. [cited 2014 May 06].

[44] T. J. Craft, "Turbulent heat transport [lecture notes]." Available from: `http://cfd.mace.manchester.ac.uk/twiki/pub/Main/TimCraftNotes_All_Access/flmsc-rathermal.pdf`, 2010. [cited 2014 May 02].

[45] C. Vallance, "Properties of gases lecture notes [internet]." Available from: `http://vallance.chem.ox.ac.uk/pdfs/PropertiesOfGasesLectureNotes.pdf`. [cited 2014 May 30].

[46] F. P. Incropera, A. S. Lavine, and D. P. DeWitt, *Fundamentals of heat and mass transfer.* John Wiley & Sons, 2011.

[47] G. Nellis and S. Klein, *Heat transfer.* Cambridge University Press, 2008.

Appendix A

Appendix

A.1 Material properties used in COMSOL

Table A.1: Solid properties

Material	Property	Value	Unit	Name
Copper	Density	8700	kg/m^3	rho
	Thermal conductivity	400	W/(m·K)	k
	Thermal capacity at constant pressure	385	J/(kg·K)	Cp
Polyethylene	Density	930	kg/m^3	rho
	Thermal conductivity	0.38	W/(m·K)	k
	Thermal capacity at constant pressure	1900	J/(kg·K)	Cp
Stainless Steel 304	Density	7900	kg/m^3	rho
ENI1.4301	Thermal conductivity	16.3	W/(m·K)	k
	Thermal capacity at constant pressure	500	J/(kg·K)	Cp

Table A.2: Natural Gas properties

T [K]	p [bar]	ρ [kg/m^3]	Cp [kJ/(kg·K)]	ν [kg/(m·K)]	k [W/(m·K)]	γ [-]
261.15	10	9.0472E0	2.02	9.9521E-6	2.6722E-2	1.3447
268.15	22	2.0139E1	2.15	1.0294E-5	2.7597E-2	1.4042
263.15	70	7.9831E1	3.03	1.2192E-5	2.6971E-2	1.9087
253.15	85	1.1525E2	3.87	1.4244E-5	2.5734E-2	2.4080
243.15	90	1.4516E2	4.83	1.6609E-5	2.4516E-2	2.9783

Table A.3: Binary Mixture properties

T [K]	p [bar]	ρ [kg/m^3]	Cp [kJ/(kg·K)]	ν [kg/(m·K)]	k [W/(m·K)]	γ [-]
286.06	10	6.92115E0	2.27	1.06994E-5	3.19291E-2	1.34
291.73	20	1.38117E1	2.35	1.09013E-5	3.26882E-2	1.37
291.73	40	2.86632E1	2.51	1.10681E-5	3.26882E-2	1.45
288.91	60	4.51683E1	2.71	1.13569E-5	3.23098E-2	1.55
283.18	70	5.53875E1	2.85	1.15191E-5	3.15462E-2	1.63
277.30	80	6.68850E1	3.03	1.18149E-5	3.07699E-2	1.73

A.2 Mesh

A.2.1 Mesh quality

Table A.4: Mesh statistics

Domain	Mirror	Seal	Copper tap	Copper rod	Chamber
Tethrahedral elements	113204	30444	72326	67871	2091772
Pyramid elements	0	0	0	0	1519
Prism elements	0	0	0	0	237637
Number of elements	113204	30444	72326	67871	2330928
Minimum element quality	0.1273	0.1137	0.2056	0.1597	0.01825
Average element quality	0.7323	0.727	0.7703	0.7573	0.6833
Element volume ratio	4.73E-4	6.541E-4	0.0819	3.562E-4	0.01514
Mesh volume [mm^3]	162.8	159.6	3.139	680.5	1628
Maximum growth rate	4.431	4.051	3.778	3.549	11.56
Average growth rate	1.771	1.749	1.612	1.656	1.674

Table A.5: Mesh element quality histogram

Mirror	Seal	Copper tap	Copper rod	Chamber
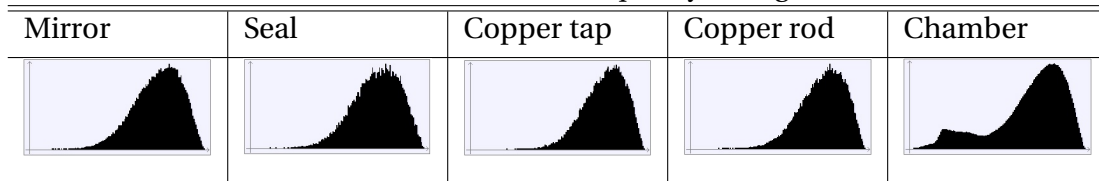
A.3 Simulation set-up

Table A.6: Global parameters

Name	Value	Description
depth_c	1.0 [cm]	Depth of cylinder
depth_cm	depth_c+1[mm]	Depth of cylinder and mirror
depth_cms	depth_cm+1[mm]	Depth of cylinder, mirror and seal
T_in	-	Inlet temperature
p	-	Inlet pressure
u_in	-	Inlet velocity
T_CO2	-	Cooling temperature

Table A.7: Geometry parameters

Object	Radius	Position (x,y,z)	Extrusion
Chamber	7.20 [mm]	(0,0,0)	depth_c
Inlet	4.25 [mm]	(0,depth_c/2,0)	3 [mm]
Outlet	4.25 [mm]	(depth_c/2,0,0)	-3 [mm]
Mirror	7.20 [mm]	(depth_c, 0, 0)	1 [mm]
Copper nib	1.00 [mm]	(depth_cm, 0, 0)	1 [mm]
Seal	7.20 [mm]	(depth_cm, 0, 0)	1 [mm]
Copper cylinder	7.20 [mm]	(depth_cms, 0, 0)	5 [mm]
Copper sphere	4.00 [mm]	(depth_cms+2+3, 0, 0)	-

A.3.1 Non-isothermal flow

Table A.8: Model parameters non-isothermal flow

Name	Settings	Value
Fluid 1	Pressure(nitf/fluid1)	p_{ref}=p
Thermal Insulation 1		
Wall 1	Boundary condition	No slip
Initial Values 1	Pressure	p=0
	Temperature	T=T_in
Inlet 1	Boundary condition	Velocity
	Normal inflow velocity	U_0=u_in
Temperature 1 inlet	Temperature	T_0=T_in
Outflow 1		
Outlet 1	Boundary condition	Pressure, no viscous stress
	Pressure	p_0=0
Heat Transfer in Solids 1 Copper		
Heat Transfer in Solids 2 Seal		
Heat Transfer in Solids 3 Mirror		
Temperature 2 Cooling temp	Temperature	T_0=T_CO2

A.3.2 Transport of concentrated species

Table A.9: Model parameters transport of concentrated species

Name	Settings	Value
Convection and diffusion 1	Velocity field(nitf/fluid1) Temperature(nitf) Pressure(nitf/fluid1) Mixture density	p_{ref}=p ideal gas
No flux 1	Overridden by inflow and outflow	
Initial values 1	Mass fraction	methane=0.994 heptane=0.006
Inflow 1	Mole fraction	heptane=0.01
Outflow 1		

A.4 Calculations

A.4.1 Velocity

Method for converting 400 cc/h to m/s:

Inlet radius = 4.25 mm

Area $= \pi \cdot r^2 = \pi \cdot (4.25mm)^2 = 56.75mm^2 = 5.675 \cdot 10^{-5} m^2$

Flow rate $= 400cc/h = 400cm^3/h = 0.000111L/s = 0.000111dm^3/s = 1.1 \cdot 10^{-7} m^3/s$

Velocity $= \frac{Flowrate}{Area} = \frac{1.1 \cdot 10^{-7} m^3/s}{5.675 \cdot 10^{-5} m^2} = 1.958 \cdot 10^{-3} m/s = 0.002 m/s$

A.4.2 Mass and mass fraction of binary gas

Table A.10: Values of the binary gas composition at the inlet

Parameter	Methane	Heptane
M_w	0.01604 $\frac{kg}{mol}$	0.10021 $\frac{kg}{mol}$
x_i	0.999	0.001

Calculation for an amount of 100 mole gives 99.9 moles of methane and 0.1 moles of n-heptane. This gives the parameter m_i which is the mass of each component in the mixture. n is here the number of moles.

$m_{methane} = M_{methane} \cdot n_{methane} = 0.01604kg/mol \cdot 99.9mol = \underline{1.602396kg}$

$m_{heptane} = M_{heptane} \cdot n_{heptane} = 0.10021kg/mol \cdot 0.1mol = \underline{0.010021kg}$

$m_{methane}$ and $m_{heptane}$ is mentioned in the thesis as m_1 and m_2 in equation 4.3.

$m_{total} = m_{methane} + m_{heptane} = 1.612417kg$

$$\omega_{methane} = \frac{m_{methane}}{m_{total}} = \underline{0.9937 = 99.4\%}$$

$$\omega_{heptane} = \frac{m_{heptane}}{m_{total}} = \underline{0.0062 = 0.6\%}$$

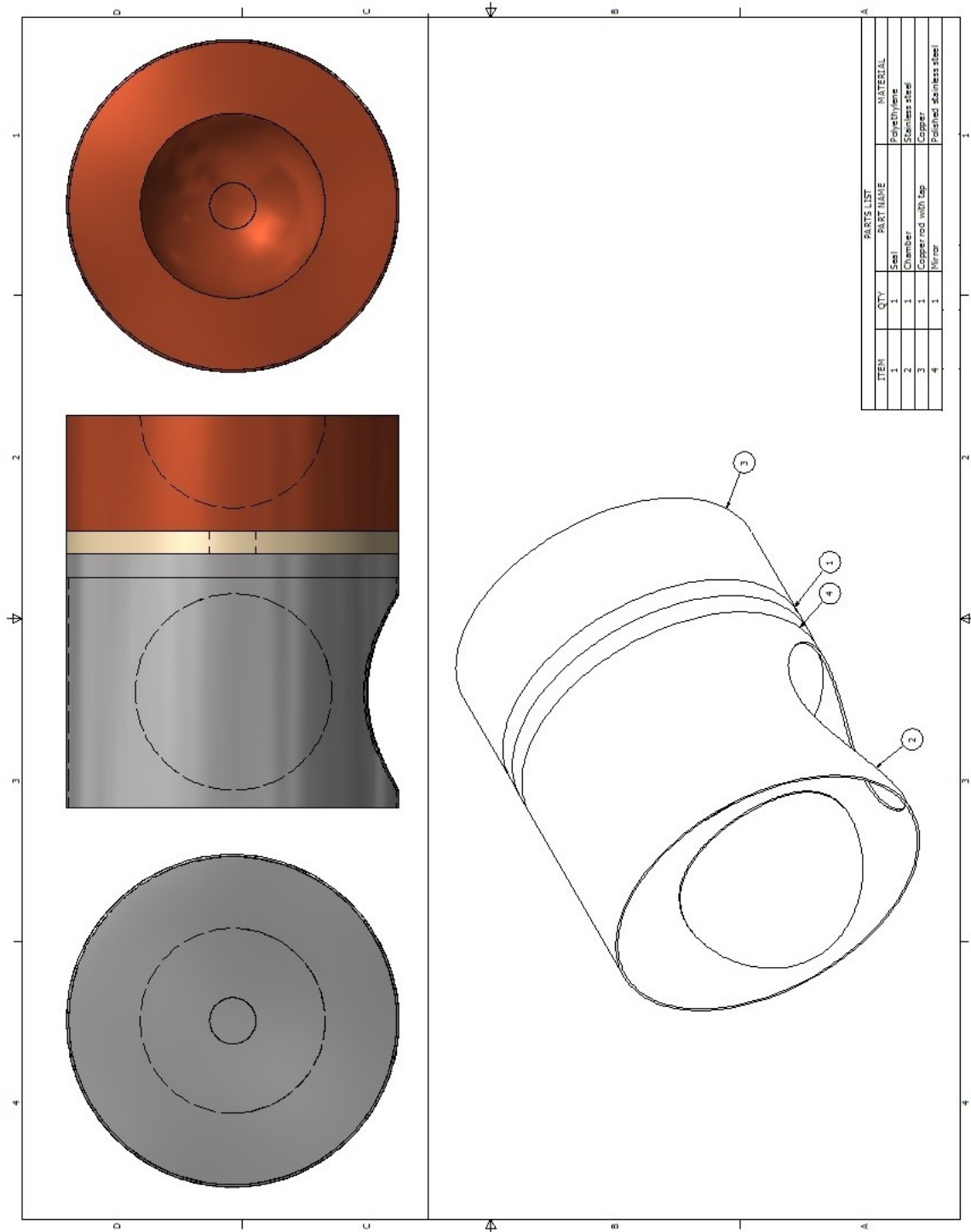## A.5 Drawings of the unit with dimensions

Figure A.1: Drawing of the model used for the simulations
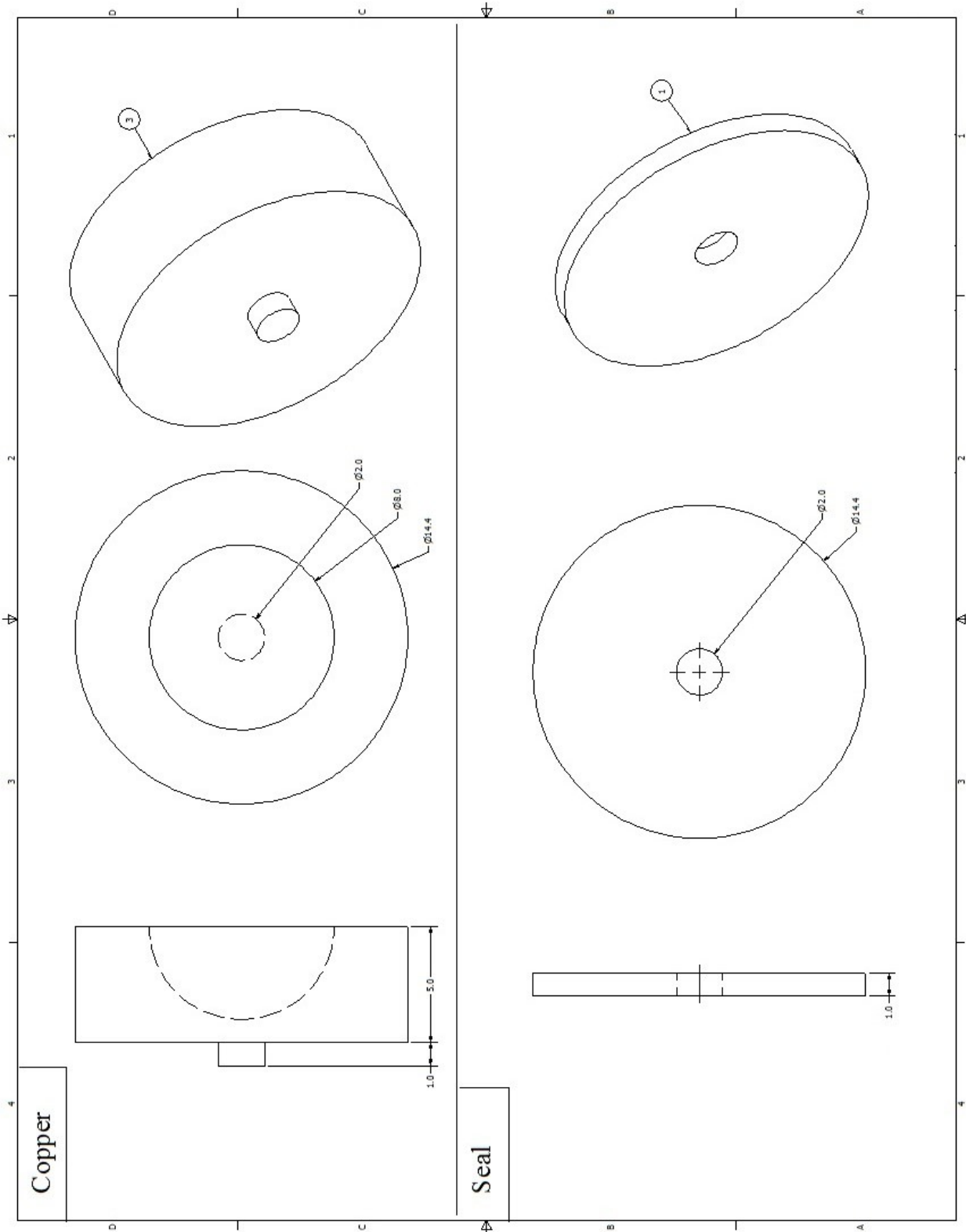
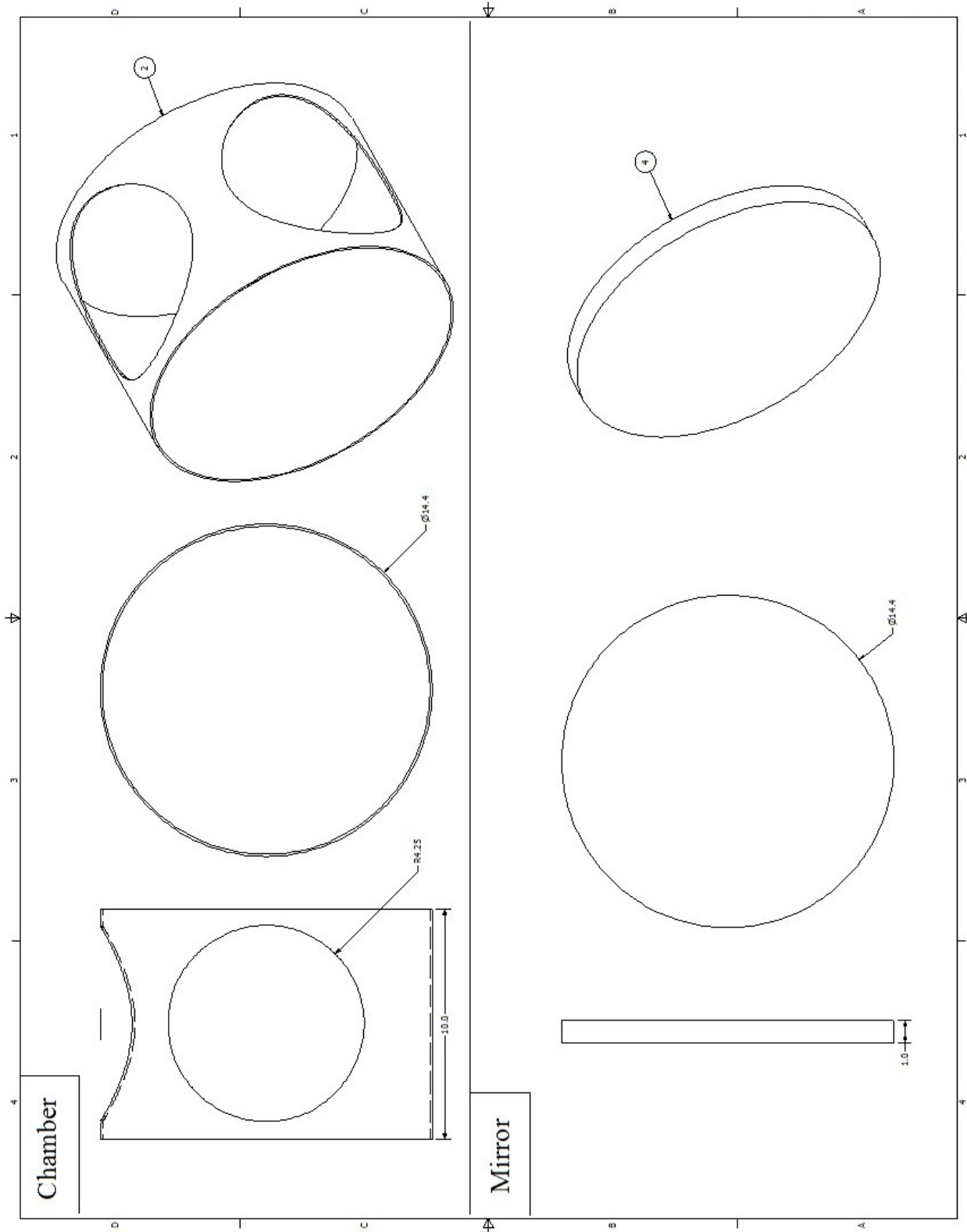Figure A.2: Drawing of the copper rod and seal
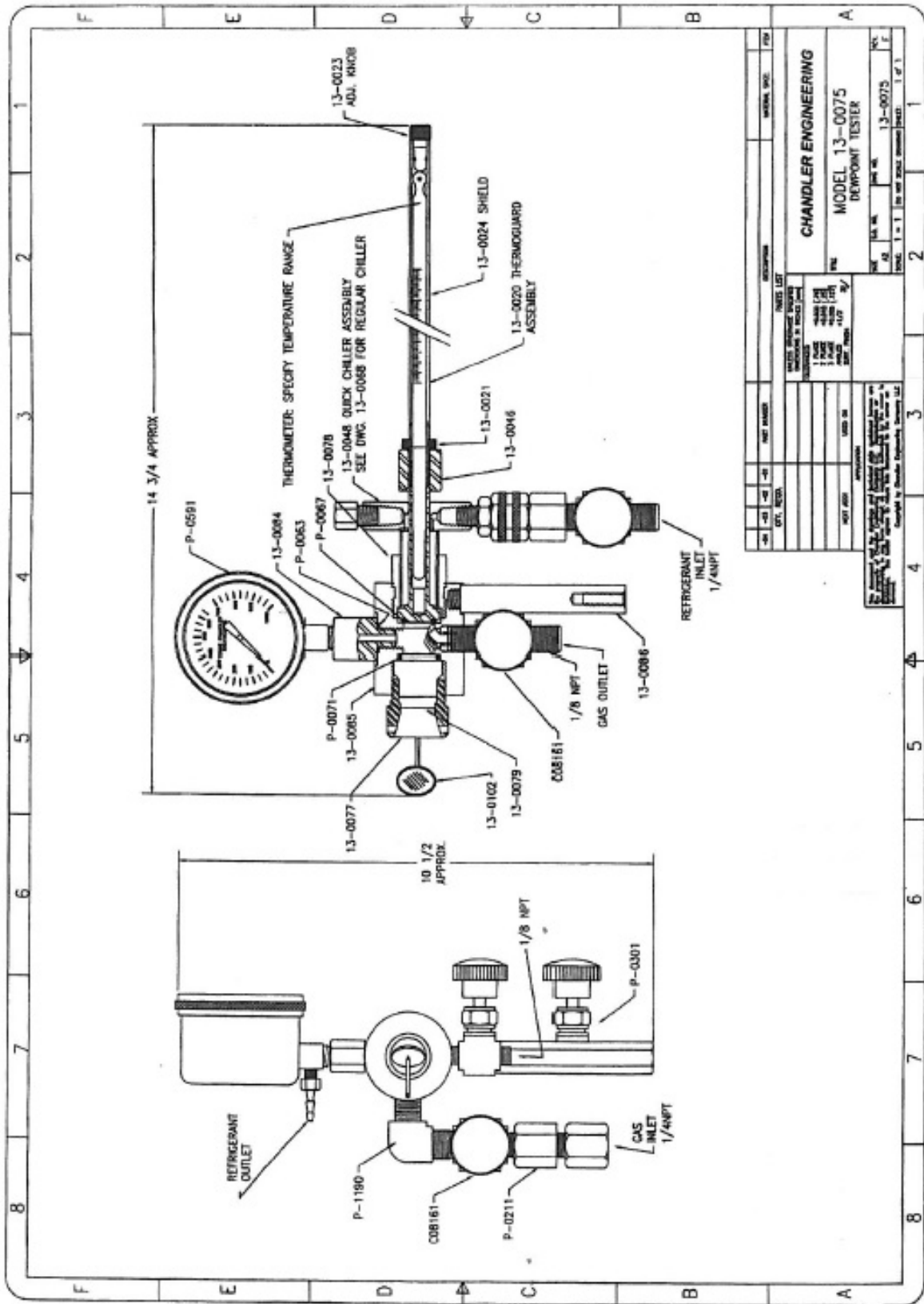
Figure A.3: Drawing of the chamber and mirror

Figure A.4: A detailed drawing of the dew point unit